UNIVERSITY OF CALIFORNIA, SAN DIEGO

MicroRNA-mediated regulation of stem cell fate decisions during reprogramming and viral infection

A dissertation submitted in partial satisfaction of the requirements for the degree

Doctor of Philosophy

in

Bioengineering

by

Jason Wai Leung Dang

Committee in charge:

Professor Shankar Subramaniam, Chair
Professor Tariq Rana, Co-Chair
Professor Albert La Spada
Professor Gabriel Silva
Professor Yingxiao Wang

The Dissertation of Jason Wai Leung Dang is approved, and it is acceptable in quality and form for publication on microfilm and electronically:

_____

_____

_____

_____

_____

Chair

University of California, San Diego

2017

TABLE OF CONTENTS

LIST OF FIGURES

LIST OF SUPPLEMENTARY FILES

ACKNOWLEDGEMENTS

I would like to thank my advisor, Dr. Tariq Rana, for his support and mentorship during my graduate studies. Your dedication to science is inspiring. I would also like to thank Dr. Rana for allowing me and encouraging me to pursue many different areas of research.

I would like to thank all past and present members of the Rana lab for their invaluable support and insight. Thank you for your help designing and executing experiments, analyzing data and, most of all, for your friendship over the last several years. I have enjoyed working with all of you.

Lastly, I would like to thank my friends and family for their love and support. Thank you for all that you have done and continue to do for me.

Chapter 2 is an adapted version of materials published as MicroRNA-mediated regulation of extracellular matrix formation modulates somatic cell reprogramming. Li Z*, Dang J*, Chang KY, Rana TM. (2014). *RNA*. 20(12):1900-15. doi: 10.1261/rna.043745.113. Epub 2014 Oct 21. PMID: 25336587. The dissertation author is the co-first author on this work with Dr. Zhonghan Li.

Chapter 3 is an adapted version of materials published as Zika Virus Depletes Neural Progenitors in Human Cerebral Organoids through Activation of the Innate Immune Receptor TLR3. Dang J*, Tiwari SK*, Lichinchi G, Qin Y, Patil VS, Eroshkin AM, Rana TM. (2016). *Cell Stem Cell*. 4;19(2):258-65. doi: 10.1016/j.stem.2016.04.014. Epub 2016 May 6. PMID: 27162029. The dissertation author is the co-first author on this work with Dr. Shashi Kante Tiwari.

Chapter 4 is an adapted version of materials that will be published in the near future with the tentative title of miR-218 regulates neuronal differentiation in Zika infected neural stem cells. Dang J, Qin Y, Tiwari, SK, Rana TM. The dissertation author is the primary researcher and author on this work.

VITA

2008 Bachelor of Science in Chemical Engineering, University of Southern California

2009 Master of Science in Chemical Engineering, University of Southern California

2017 Doctor of Philosophy in Bioengineering, University of California, San Diego

PUBLICATIONS

Dang J, Qin Y, Tiwari SK, Rana TM. (2017). Effect of methamphetamine addiction on the human brain modeled using cerebral organoids and single cell RNA-seq. (in preparation).

Tiwari SK*, **Dang J***, Lin N, Qin Y, Rana TM. (2017). Zika virus depletes neural stem cells by suppressing the Fanconi anemia protein FANCC. (in preparation).

Dang J, Qin Y, Tiwari SK, Rana TM. (2017). miRNAs regulate cell cycle and stem cell maintenance during Zika virus infection. *Cell Reports*. (under review).

Tiwari SK*, **Dang J***, Qin Y, Lichinchi G, Bansal V, Rana TM. (2017). Zika virus infection reprograms global transcription of host cells to allow sustained infection. *Emerging Microbes and Infections*. doi:10.1038/emi.2017.9 (in press).

Zhou Y, **Dang J**, Chang KY, Yau E, Aza-Blanc P, Moscat J, Rana TM. (2016). miR-1298 Inhibits Mutant KRAS-Driven Tumor Growth by Repressing FAK and LAMB3. *Cancer Res*. 1;76(19):5777-5787. PMID: 27698189

Mohammed I, Kummetha IR, Singh G, Sharova N, Lichinchi G, **Dang J**, Stevenson M, Rana TM. (2016). 1,2,3-Triazoles as Amide Bioisosteres: Discovery of a New Class of Potent HIV-1 Vif Antagonists.
J Med Chem. 25;59(16):7677-82. doi: 10.1021/acs.jmedchem.6b00247. Epub 2016 Aug 10. PMID: 27509004

Yang CS, Chang KY, **Dang J**, Rana TM. (2016). Polycomb Group Protein Pcgf6 Acts as a Master Regulator to Maintain Embryonic Stem Cell Identity.
Sci Rep. 1;6:26899. doi: 10.1038/srep26899. PMID: 27247273

Dang J*, Tiwari SK*, Lichinchi G, Qin Y, Patil VS, Eroshkin AM, Rana TM. (2016). Zika Virus Depletes Neural Progenitors in Human Cerebral Organoids through Activation of the Innate Immune Receptor TLR3. *Cell Stem Cell*. 4;19(2):258-65. doi: 10.1016/j.stem.2016.04.014. Epub 2016 May 6. PMID: 27162029

Lin N, **Dang J**, Rana TM. (2015). Haunting the HOXA Locus: Two Faces of lncRNA Regulation. *Cell Stem Cell*. 7;16(5):449-50. doi:10.1016/j.stem.2015.04.010. PMID: 25957895

Dang J, Rana TM. (2016). Enhancing Induced Pluripotent Stem Cell Generation by MicroRNA. *Methods Mol Biol*. 2016;1357:71-84. doi: 10.1007/7651_2015_201. PMID: 25687299

McCarroll JA, Dwarte T, Baigude H, **Dang J**, Yang L, Erlich RB, Kimpton K, Teo J, Sagnella SM, Akerfeldt MC, Liu J, Phillips PA, Rana TM, Kavallaris M. (2015). Therapeutic targeting of polo-like kinase 1 using RNA-interfering nanoparticles (iNOPs) for the treatment of non-small cell lung cancer. *Oncotarget*. 20;6(14):12020-34. PMID: 25557168

Li Z*, **Dang J***, Chang KY, Rana TM. (2014). MicroRNA-mediated regulation of extracellular matrix formation modulates somatic cell reprogramming. *RNA*. 20(12):1900-15. doi: 10.1261/rna.043745.113. Epub 2014 Oct 21. PMID: 25336587

Sakurai K, Talukdar I, Patil VS, **Dang J**, Li Z, Chang KY, Lu CC, Delorme-Walker V, Dermardirossian C, Anderson K, Hanein D, Yang CS, Wu D, Liu Y, Rana TM. (2014). Kinome-wide functional analysis highlights the role of cytoskeletal remodeling in somatic cell reprogramming. *Cell Stem Cell*. 3;14(4):523-34. doi: 10.1016/j.stem.2014.03.001. PMID: 24702998

Lin N, Chang KY, Li Z, Gates K, Rana ZA, **Dang J**, Zhang D, Han T, Yang CS, Cunningham TJ, Head SR, Duester G, Dong PD, Rana TM. (2014). An evolutionarily conserved long noncoding RNA TUNA controls pluripotency and neural lineage commitment. *Mol Cell.* 20;53(6):1005-19. doi:10.1016/j.molcel.2014.01.021. Epub 2014 Feb 13. Erratum in: Mol Cell. 2014 Mar 20;53(6):1067. PMID: 24530304

Henzler CM, Li Z, **Dang J**, Arcila ML, Zhou H, Liu J, Chang KY, Bassett DS, Rana TM, Kosik KS. (2013). Staged miRNA re-regulation patterns during reprogramming. *Genome Biol.* 2013 Dec 31;14(12):R149. doi: 10.1186/gb-2013-14-12-r149. PMID: 24380417

Lee CL, **Dang J**, Joo KI, Wang P. (2011). Engineered lentiviral vectors pseudotyped with a CD4 receptor and a fusogenic protein can target cells expressing HIV-1 envelope proteins. *Virus Res*. 160(1-2):340-50. doi: 10.1016/j.virusres.2011.07.010. Epub 2011 Jul 23. PMID: 21802459

* authors contributed equally

ABSTRACT OF DISSERTATION

MicroRNA-mediated regulation of stem cell fate decisions during reprogramming and viral infection

by

Jason Wai Leung Dang

Doctor of Philosophy in Bioengineering

University of California, San Diego, 2017

Professor Shankar Subramaniam, Chair

Professor Tariq Rana, Co-Chair

Zika virus (ZIKV) is an emerging arbovirus linked to an increased incidence of microcephaly. To study the potential link between ZIKV and microcephaly, stem cell-based models must be utilized to understand the effect

of ZIKV infection. The objectives of this dissertation are to analyze the somatic cell reprogramming to enhance iPSC production, generate human cerebral organoids, and utilize these models to study ZIKV-mediated neurodegeneration in vitro.

To study the stochastic nature of somatic cell reprogramming and enhance reprogramming yield, microRNAs were profiled in mouse embryonic fibroblasts (MEFs) during the early stage of cell fate decisions. miR-135b was highly upregulated and repressed expression of extracellular matrix genes including Wisp1 and Igfbp5. These data reveal a novel link between microRNA-mediated regulation of ECM formation and somatic cell reprogramming.

To investigate the link between ZIKV and microcephaly, human embryonic stem cell-derived cerebral organoids were generated and characterized to recapitulate first trimester fetal brain development. ZIKV infected organoids revealed preferential infection of neural stem cells, attenuated growth and activation of innate immune receptor Toll-Like-Receptor 3 (TLR3). Pathway analysis of differentially expressed genes during TLR3 activation highlighted 41 genes also related to neuronal development.

Lastly, meta-analyses and regulatory interaction networks integrating miRNA and mRNA expression profiling data were used to study the role of miRNA-mediated repression during ZIKV infection. These analyses identified miRNA-mediated repression of cell cycle, metabolism, stem cell maintenance and neurogenesis related genes. Moreover, miR-218 was upregulated during

ZIKV infection and directly represses a gene network governing stem cell maintenance.

CHAPTER 1: INTRODUCTION

Until recently, most of our understanding of the developing human brain has come from various animal models and post-mortem tissues. Unfortunately, many of these models are unable to fully mimic the cellular architecture and molecular mechanisms that are responsible for the uniquely human cognitive and behavioral patterns. These substantial morphological, functional and molecular differences in human and rodent brains present problems not only in understanding fundamental developmental biology but also in modeling neurodegenerative diseases, such as Zika virus-mediated microcephaly. Thus, alternative models must be developed to model the developing human brain.

Chapter 1.1: Brain development

The development of the human brain is initiated during the third week of gestation when the neural tube is formed and the radial glial cell, or neural progenitor cell, population has been positioned along the rostral-caudal midline (Stiles and Jernigan, 2010). The neural progenitors form a uniform layer around the inner side of the neural tube. As the neural progenitors symmetrical divide, the brain grows in size and complexity until the ventricular zone is formed. Through a series of transcriptomic, epigenomic, and epitranscriptomic changes, as well as temporal and spatial intercellular signals, neural progenitors differentiate and migrate radially and tangentially. Neural progenitor cells can asymmetrically divide into intermediate progenitors, which populate the

subventricular zone (SVZ) or migrate to form the various cortical layers. The SVZ can then be further subdivided into four distinct layers, each containing a distinct set of intermediate progenitor cells more characteristically associated with human brains (Fietz et al., 2010; Hansen et al., 2010; Zecevic et al., 2005). Neural progenitors differentiate into neurons from the ventricular zone and migrate to generate the preplate. From there, neurons transiently split within the PP to form the marginal zone, cortical plate and subplate. Finally, as the brain matures, both the MZ and SP disappear and six cortical layers will emerge with neurons from the CP forming cortical layer 6.

While many stages of brain development are conserved between human and rodent models, several notable aspects differ. In a recent study, Hansen et al. showed that the developing human ventricular and subventricular zones are composed of more radial glial cells and intermediate progenitor cells which may give rise to the enlarged human cerebral cortex and larger outer subventricular zone (Hansen et al., 2010). They then hypothesized that this increased population of neural progenitors in the ventricular zone may contribute to the evolutionary difference between rodent and human brains. However, others have postulated that the increased density of neuronal and non-neuronal cells in the human brain is responsible for the uniqueness of the human brain (Herculano-Houzel, 2009). Nevertheless, the molecular mechanisms which distinguish the developing human brain from other animals both morphologically and functionally have yet to be elucidated. Thus, alternative means of modeling human brain development may be required.

Chapter 1.2: Somatic Cell Reprogramming

The fields of developmental biology and disease modeling were revolutionized in 1988 when the first human blastocyst-derived embryonic stem cells were isolated by Thomson et al. (Thomson et al., 1998) and again in 2006 when Yamanaka et al. revealed that somatic cells could be reprogrammed into an embryonic stem cell-like state, thus establishing the now ubiquitously utilized field of induce pluripotent stem cells, or iPSCs (Takahashi and Yamanaka, 2006). With the expansion of regenerative medicine, high-throughput sequencing and need for advanced disease modeling, the field of iPSCs has experienced incredible growth both in terms of basic biology and application in both mouse and human modeling (Aoi et al., 2008; Giorgetti et al., 2009; Loh et al., 2009; Meissner et al., 2007; Park et al., 2008a; Park et al., 2008b; Takahashi et al., 2007; Yamanaka, 2012; Yu et al., 2007). Because of their fully reprogrammed transcriptomic and epigenetic state through the overexpression of a combination of transcription factors, iPSC are restored to an embryonic stem cell-like pluripotency state capable of differentiating into virtually any lineage and cell type including neuronal cells (Chen et al., 2014; Marchetto et al., 2010), hematopoietic cells (Hanna et al., 2007), and cardiac muscle tissue (Itzhaki et al., 2011). Thus, iPSC possess the potential to revolutionize the way we study disease pathogenesis and develop novel therapeutics.

The first iteration of iPSCs generated in Yamanaka et al. utilized a combination of core pluripotency transcription factors – octamer-binding protein 4 (OCT4), sex determining region Y-box 2 (SOX2), Kruppel-like factor 4 (KLF4) and MYC proto-oncogene (MYC) – to reprogram mouse fibroblasts (Takahashi and Yamanaka, 2006). To identify these four pluripotency factors, Yamanaka et al. introduced a βgeo cassette into the Fbx15 gene, a gene specifically expressed in embryonic stem cells which would introduce β-galactosidase and neomycin resistance, and transduced these cells with 24 hypothesized pluripotency-related genes using retroviruses. Cells which were successfully reprogrammed to an embryonic-like state were selected using G418. G418 resistant colonies were clonally selected and RT-qPCR was utilized to identify the candidate genes required for reprogramming. From these assays, Yamanaka et al. identified *Oct4*, *Sox2*, *Klf4* and *Myc*. Pluripotency of reprogrammed MEFs by OSKM was confirmed by microarray gene expression analysis, teratoma formation in which all three germ layers were observed, and chimeric mouse generation.

Subsequently, it was found that these same four factors (OSKM) could also be employed to reprogram a wide range of human cells (Lowry et al., 2008; Nakagawa et al., 2008; Park et al., 2008b; Takahashi et al., 2007; Wernig et al., 2007; Yu et al., 2007). The limiting factor for iPSC generation is low reprogramming efficiency. To generate robust reprogramming of somatic cells for regenerative medicine and disease modeling applications, studies have shown that mRNA (Warren et al., 2010); small molecules (Feng et al., 2009b; Ichida et

al., 2009b; Li and Rana, 2012b; Maherali and Hochedlinger, 2009b; Nichols et al., 2009; Silva et al., 2008; Yang et al., 2011b; Ying et al., 2008; Zhu et al., 2011); and miRNAs (Choi et al., 2011b; Judson et al., 2009a; Li and He, 2012; Li et al., 2011a; Liao et al., 2011a; Lipchina et al., 2011; Melton et al., 2010; Pfaff et al., 2011; Subramanyam et al., 2011b; Yang and Rana, 2013; Yang et al., 2011a) can be utilized to enhance reprogramming efficiency. Many of these reprogramming enhancers include pluripotency-related genes such as NANOG (Feng et al., 2009a; Picanco-Castro et al., 2011) and LIN28 (Yu et al., 2007), cell cycle-regulating genes such as those in the p53 pathway (Banito et al., 2009; Hong et al., 2009; Kawamura et al., 2009; Li et al., 2009; Utikal et al., 2009), and epigenetic modifiers (Ang et al., 2011; Kuzmichev et al., 2002; Shinagawa et al., 2014; Wang et al., 2011).

Somatic cell reprogramming is a complex and dynamic process in which cells undergo dramatic alterations to the transcriptomic, epigenomic and epitranscriptomic landscape following the introduction to OSKM core pluripotency factors. Somatic cell reprogramming can be theoretically divided into two main stages of reprogramming characterized by an initial change in the epigenome through ectopic binding of OSKM which leads to a population of partially reprogrammed cells, and a maturing later iPSC stage in which cells enter a deterministic and hierarchical late stage (Polo et al., 2012; Soufi et al., 2012).

Despite a decade of research probing the mechanisms by which cells are reprogrammed, much is still not known. Several theories have been proposed to account for the low efficiency in iPSC induction. Induced pluripotent stem cell

reprogramming is considered a stochastic and deterministic reprogramming that is dependent on many factors throughout the initial and maturation stages. Systematic analysis of the promoters targeted by overexpression of the four reprogramming factors has demonstrated that expression of the factor target genes is similar in iPSCs and mouse embryonic stem (mES) cells, and is altered in some partially reprogrammed cells (Sridharan et al., 2009). Various signaling pathways and cascades have been shown to regulate iPSC induction including TGFβ signaling (Ichida et al., 2009b) and the mesenchymal-to-epithelial transition which occurs during the initial stages of reprogramming (Li et al., 2010; Samavarchi-Tehrani et al., 2010). iPSC reprogramming is also dependent on the metabolic state (Panopoulos et al., 2012). A recent study revealed that OCT4, SOX2 and KLF4 interact with other transcription factors in a stage-specific manner to modulate the enhancer landscape by inactivating somatic enhancers and binding pluripotency enhancers (Chronis et al., 2017).

Chapter 1.3: Neural Differentiation and Organoids using Pluripotent Stem Cells

Advances in embryonic stem cell and induced pluripotent stem cell technology have opened up new avenues of disease modeling in vitro (Yamanaka, 2012). To study neurodegenerative disorders, embryonic stem cells and human derived iPSC can be differentiated towards forebrain, midbrain and hindbrain specific neuron subtypes to model various regions of the brain. A

variety of methods have been developed to facilitate neural differentiation of pluripotent stem cells. In 2001, Zhang et al. presented the first protocol for the derivation of embryonic stem cell-derived human neural rosettes which exhibit epithelial characteristics and resemble the formation of the neural tube in two dimensions (Zhang et al., 2001). A second advancement in in vitro neural differentiation was the introduction of serum free culture to induce spontaneous neural induction in embryonic stem cells (Ying et al., 2003). The combination of these two approaches introduced the now ubiquitous serum free culture of embryoid bodies, or SFEB, method (Watanabe et al., 2005). Addition of SMAD inhibitors promoted neural differentiation of embryonic stem cells without the formation of embryoid bodies (Chambers et al., 2009). Using these methods, researchers have been able to generate in vitro models for various regions of the brain including the cerebellum (Muguruma et al., 2015), forerain (Kadoshima et al., 2013), hippocampus (Sakaguchi et al., 2015) and retina (Eiraku et al., 2011).

More recently, stem cells and iPSC have been differentiated into three dimensional organoid systems to study the development of the intestine, retina, liver, kidney and even the brain (Koehler and Hashino, 2014; Lancaster and Knoblich, 2014). These organoid are able to differentiate, self-organize and form distinct, complex, biologically relevant structures, thus making them ideal in vitro models of development, disease pathogenesis and drug screening. Organoids are generated from embryonic stem cells by manipulating and mimicking the biochemical and biophysical signals resembling those during embryogenesis.

Time dependent addition of signaling molecules and extracellular matrices enable temporal and limited spatial control over the differentiation processes.

Unlike primary cell cultures, ES cell derived cerebral organoids have shown the capacity for prolonged survival in culture, reportedly at least 10 months in a bioreactor (Kadoshima et al., 2013; Lancaster et al., 2013). Moreover, the use of a bioreactor enhances the developing cerebral organoids' capacity for growth up to 4mm due to improved diffusion of nutrients, oxygen and potentially drugs or small molecule treatments (Lancaster et al., 2013). Thus, because of their ability to self-organize and recapitulate many regenerative events seen in vivo, organoids present a human relevant, easily accessible, scalable model for disease pathogenesis and drug testing.

The first prominent use of self-organizing organoid formation came in 2009 when researchers generated three-dimensional intestinal organoids from isolated Lgr5+ stem cells which exhibited crypt and villus-like structures (Sato et al., 2009). Moreover, these organoids were able to recapitulate both the stem cell, progenitor and differentiated cell types within the three-dimensional architecture. Using these technologies, van de Wetering et al. generated a "living organoid biobank" of colorectal cancer patient-derived Lgr5+ organoids for drug screening use (van de Wetering et al., 2015). Similarly, patient-derived organoids were utilized to study advanced prostate cancer (Gao et al., 2014).

Several groups have developed cerebral organoid models that generate functional cortical neurons and can recapitulate forebrain, midbrain and hindbrain regions with functional electrophysiological properties to probe the mechanisms

of neurodevelopment, autism and microcephaly (Camp et al., 2015; Eiraku et al., 2008; Lancaster et al., 2013; Mariani et al., 2015; Nowakowski et al., 2016). Previous studies have shown the use of cerebral organoid models in modeling microcephaly resulting from a heterogeneous nonsense mutation in *CDK5RAP2* from patient-derived iPSC (Lancaster et al., 2013). The nonsense mutation altered the spindle orientation of radial glial cells causing a severe decrease in overall organoid size and premature differentiation of neural progenitors in the neuroepithelium. Similarly, Mariani et al. generated autism patient-derived iPSCs and cerebral organoids to model autism spectrum disorders in vitro (Mariani et al., 2015). Through transcriptomic analyses, they observed an overexpression of transcription factor FOXG1 in patient versus proband organoids. Gain and loss of function experiments revealed that FOXG1 alters gene expression networks and shifts neuronal differentiation towards the GABAergic neuron fate.

Yet, there are still limitations to the use of organoids, primarily the timing and duration of organogenesis and the balance between organoid homogeneity and tissue complexity. Stem cell-derived organoid formation, as it relies on self-organization and differentiation, is typically a long process. Moreover, the tissue complexity and maturation of neurons and neuronal subtypes within cerebral organoids are highly time dependent. Qian et al. showed that cortical neuronal subtypes mimicking the preplate, ventricular zone, cortical plate and subventricular zone emerge overtime (Qian et al., 2016). In addition, high-throughput sequencing of whole organoids 26, 40, 54 and 100 days old showed a correlation between organoid age and fetal development (Qian et al., 2016)

and the maturation of neuronal subtypes (Dang et al., 2016). While prolonged maturation of cerebral organoids can increase complexity and formation of cortical layers, the increased heterogeneity of cell types may compromise reproducibility between organoids. Nevertheless, organoids present a powerful tool for modeling complex human tissues, such as the brain, for regenerative medicine, disease modeling and drug screening applications.

Chapter 1.4: Zika virus pathogenesis

Zika virus (ZIKV) is an arbovirus belonging to the Flaviviridae family, which includes dengue, West Nile (WNV), tickborne encephalitis, Japanese encephalitis (JEV), and yellow fever viruses (Lazear and Diamond, 2016). ZIKV is a positive single-stranded RNA virus that replicates in the cytoplasm. The polyprotein encoded by ZIKV is processed into three structural proteins; the capsid, envelope, and precursor of membrane proteins, as well as seven nonstructural proteins.

Zika virus is a mosquito-borne disease transmitted by the *Aedes* genus (Plourde and Bloch, 2016) but may also be transmitted sexually and vertically (D'Ortenzio et al., 2016; Moreira et al., 2016). ZIKV was first discovered more than 60 years ago in samples taken from a sentinel rhesus monkey in the Zika forest of Uganda, and has since been isolated from mosquitoes and humans (Dick et al., 1952; Macnamara, 1954). Various epidemiological studies have revealed a worldwide spread of ZIKV to geographic areas ranging from Asia and

the Pacific to, most recently, the Americas (Hajra et al., 2016). The rapid spread of ZIKV from Asia to the Americas has affected more than 30 countries. Due to its sporadic nature and mild symptoms, ZIKV infection was initially ignored.

The recent ZIKV outbreak in the Western hemisphere is associated with severe fetal abnormalities, including microcephaly and hydranencephaly, as well as placental insufficiency, which may cause intrauterine fetal growth restriction (Brasil et al., 2016b; Noronha et al., 2016; Sarno et al., 2016; Ventura et al., 2016). In adults, ZIKV infection can cause a self-limiting febrile illness, arthralgia, rash, and conjunctivitis; however, an estimated 80% of cases are asymptomatic (Brasil et al., 2016a; Duffy et al., 2009; Hayes, 2009).

The molecular mechanisms by which ZIKV causes microcephaly are not fully understood, but there is compelling evidence that ZIKV crosses the placenta barrier and directly damages the developing fetus (Calvet et al., 2016a; Martines et al., 2016; Mlakar et al., 2016; Oliveira Melo et al., 2016; Petersen et al., 2016b). Several in vitro and in vivo models have been described that facilitate the study of ZIKV biology. Current reports indicate that dermal fibroblasts, dendritic cells, neural progenitor cells, and epidermal keratinocytes are permissive to ZIKV infection while placental trophoblasts are resistant due to constitutive release of type III interferon (Bayer et al., 2016; Briant et al., 2014; Dang et al., 2016; Hamel et al., 2015; Tang et al., 2016). Mouse models have shown that ZIKV may be neurotropic (Cugola et al., 2016; Lazear et al., 2016; Li et al., 2016; Mlakar et al., 2016; Sarno et al., 2016). However, the pathogenesis of ZIKV infection remains poorly understood.

Chapter 1.5: Non-coding RNAs and microRNAs

MicroRNAs (miRNAs) are a class of endogenous small non-coding, single-stranded RNAs 18–24 nucleotides long associated with a protein complex termed the RNA-induced silencing complex (RISC) first discovered in *Caenorhabditis elegans*. MicroRNAs are a key post-transcriptional regulatory and function through imperfectly binding to target mRNAs, thereby facilitating degradation or destabilization of the mRNAs (Ambros, 2004a; Li and Rana, 2012a).

miRNAs are transcribed by RNA Pol II from introns of coding and non-coding gene transcripts and function to suppress gene expression by translational repression and/or mRNA degradation (Ambros, 2004b; Chu and Rana, 2006, 2007; Djuranovic et al., 2011; Huntzinger and Izaurralde, 2011; Rana, 2007). After transcription, primary miRNAs, or pri-miRNAs, contain a stem-loop structure which is cropped by the nuclear RNase III endonuclease Drosha in complex with DGCR8 to generate a ~65bp hairpin-shaped RNA known as the pre-miRNA (Lee et al., 2003). Pre-miRNAs are then exported into the cytoplasm with help from the exportin 5 and RAN-GTP transport complex (Lund et al., 2004). Within the cytoplasm, pre-miRNAs are cleaved by Dicer to generate a small double-stranded RNA duplexes (Hutvagner et al., 2001; Knight and Bass, 2001). RNA duplexes are then loaded into the RNA-induced silencing complex (RISC), during which the RNA duplex is loaded and unwinded (Kawamata and

Tomari, 2010). The RISC contains an AGO protein which is the catalytic component responsible for target mRNA cleavage (specific to only AGO2), translational repression and mRNA decay (Huntzinger and Izaurralde, 2011).

miRNA-mRNA interactions are governed by many factors including seed sequence base pairing, cooperative action between neighboring miRNA binding sites, and miRNA binding sequencing within putative mRNA target transcripts (Agarwal et al., 2015; Bartel, 2009; Grimson et al., 2007; Lewis et al., 2005) as well as non-canonical binding revealed by CLIP, PAR-CLIP and CLASH experiments, of which less is understood (Chi et al., 2012; Hafner et al., 2010; Loeb et al., 2012). In fact, miRNAs are capable of directly downregulating hundreds of target mRNAs to repress translation (Baek et al., 2008; Selbach et al., 2008).

Because miRNAs are able to potentially post-transcriptionally regulate hundreds of target transcripts, miRNAs play an important role in many diverse biological processes including stem cell biology, somatic cell reprogramming, virology, innate immunity and neurogenesis. In fact, knockout of miRNA processing components DGCR8 (Chong et al., 2010) and AGO2 (Liu et al., 2004) are embryonic lethal in mice and negatively affects stem cell proliferation and differentiation (Wang et al., 2007).

Furthermore, miRNAs have also been shown to play diverse roles in viral infections ranging form pro-viral to anti-viral, generated from RNA virus transcripts or dysregulated host miRNAs influenced by viral infection. Interestingly, RNAi is a well-known antiviral immunity mechanism in plants and

invertebrate. Previous studies have shown that that miRNAs can directly bind to the viral genome to modulate viral replication. For instance, human immunodeficiency virus (HIV) is targeted by miR-29a to enhance association with RISC and is trafficked to P bodies to post-transcriptionally repress viral replication (Nathans et al., 2009). On the other hand, the hepatitis C virus (HCV) is well known to interact with miR-122 at the 5' UTR to stabilize viral transcripts as well as act as a competitive endogenous RNA (Luna et al., 2015; Shimakami et al., 2012). The abundant HCV transcripts effectively sequester miR-122 in a sponging effect, thereby de-repressing other miR-122 targets within the host cell. Luna et al. proposed that this miR-122 sponge effect of HCV de-repressed endogenous miR-122 targets to enhance viral infection and potentiate long-term HCV-related oncogenesis (Luna et al., 2015). Thus, viruses may dysregulated host cellular miRNAs to in a pro-viral or anti-viral manner. Dengue virus and Japanese encephalitis virus, both from the flavivirus genus, for instance, upregulate miR-146a to repress the interferon response through downregulation of TRAF6 (Sharma et al., 2015; Wu et al., 2013). Thus, miRNAs are an important post-transcriptional regulatory mechanism across many biological processes.

Chapter 1.6: Goals of this dissertation

Because ZIKV is a relatively new, unknown and emerging virus, there are many foundational questions that need to be addressed. Namely, despite a correlation between ZIKV infected patients and fetal microcephaly, is there a

causal relationship? If so, which cells are targeted by ZIKV and what effect does ZIKV have on them? And, what are the appropriate model systems to study ZIKV pathogenesis? The objectives of this dissertation are to better understand the mechanisms governing somatic cell reprogramming and how they may be utilized to generate human cerebral organoid models to study Zika virus-mediated neurodegeneration in vitro.

The first aim of this dissertation was to study the molecular mechanisms which promote and enhance somatic cell reprogramming of mouse embryonic fibroblasts to iPSCs. Somatic cell reprogramming is a stochastic process with very low yield, thus to develop robust model systems using iPSCs, it is essential that iPSC reprogramming is understood and made more efficient. To do so, we hypothesized that miRNAs may regulate barriers which inhibit iPSC maturation, thus miRNAs may be used to enhance reprogramming.

Our second aim was to generate three-dimensional, self-organizing cerebral organoid models to recapitulate the developing brain and to study neurodegenerative diseases such as, in this case, the relationship between ZIKV and microcephaly. The most recent ZIKV epidemic originating in Brazil in late 2015/early 2016 saw a rise in microcephalic infants in ZIKV infected mothers, a phenomena not associated with ZIKV previously. Thus, organoids present a physiologically relevant human platform for the developing fetal brain with which to study ZIKV infection and pathogenesis. Immunohistochemistry, functional electrophysiological assays, RNA-seq, and single cell RNA-seq were utilized to

systematically characterize these organoids and study the phenotypic effect of ZIKV on brain development.

Finally, the last aim of this dissertation is to analyze the dynamic effect of ZIKV on the coding and non-coding transcriptome. It is still unclear how ZIKV replicates and how it affects cells at the transcriptomic level. We hypothesized that gene network analyses and miRNA profile would provide insight into ZIKV-mediate microcephaly.

CHAPTER 2: MicroRNAs regulate ECM during iPSC reprogramming

Chapter 2.1: Introduction

While significant progress is being made in understanding the intracellular signaling pathways governing somatic cell reprogramming, little is known about the extracellular events also associated with the reprogramming process. The extracellular matrix (ECM) is a multifunctional system that is involved in many stages of mammalian development (Adams and Watt, 1993; Rozario and DeSimone, 2010; Sanes, 1989) and human disease progressions, including tumor formation (Bissell and Hines, 2011; Kessenbrock et al., 2010). ECM is made of secreted polysaccharides and proteins that are organized into a well-defined complex structure surrounding the surface of cells that produce them. A variety of proteins and polysaccharides are involved in ECM, which could be divided into at least two groups: proteins with structural role, such as fibrous proteins and glycosaminoglycans; and proteins with regulatory role, including different growth factors (e.g., TGFβ and IGFs), matricellular proteins (CCN family proteins, IGFBPs, decorin, and biglycan), enzymes (metalloproteinases) and receptors (integrins). ECM plays a crucial role in regulating various cellular behaviors and maintaining the identity and normal function of those cells (Bissell and Hines, 2011; Kessenbrock et al., 2010).

For embryonic stem cells, ECM components are essential for establishing the proper niche for long term ES cell survival and self-renewal (Bendall et al.,

2007; Peerani et al., 2007). Moreover, recent studies have shown that culture media supplemented with FGF2 can enhance iPSC induction through the regulation of collagen gene expression, thus bringing attention to the role of the microevironment in reprogramming (Jiao et al., 2013). In fact, given the dramatic changes of both cellular morphology and functional characteristics during the course of reprogramming, potential iPSCs would need to establish their own niche for supporting their growth and colony formation. At the same time, successful iPSCs also need to exclude the effects brought by secreted ECM proteins from surrounding cells that are not reprogrammed. However, despite that iPSCs expressed a different set of ECM proteins from starting fibroblasts cells (Sridharan et al., 2009), little is known about the dynamic remodeling of ECMs during reprogramming. Understanding the molecular mechanisms that govern ECM remodeling during reprogramming would provide fundamental knowledge essential in efficiently creating and controlling various states of pluripotent stem cells.

Recent work indicates that ES-specific microRNAs can enhance iPSC induction (Judson et al., 2009b) and, specifically, that the hES miR-302 can antagonize the senescence response induced by four-factor expression in human fibroblasts (Banito et al., 2009). In addition, our recent findings suggest that the microRNA biogenesis machinery may be required for efficient reprogramming (Li et al., 2011b), and microRNAs induced by OSKM are known to regulate several key pathways affecting reprogramming efficiency, including cell cycle control, the p53 pathway, TGFβ signaling, and MET (Choi et al., 2011a;

Li et al., 2011b; Liao et al., 2011b; Subramanyam et al., 2011a; Yang et al., 2011a). Moreover, during somatic reprogramming, many microRNAs undergo small changes in expression in the early stages while only a select few microRNAs undergo large changes in expression in the later stages of reprogramming (Henzler et al., 2013; Polo et al., 2012). These data indicate a transition from a deterministic to stochastic process and suggest that microRNAs are regulated in a highly stage-dependent manner during reprogramming. Importantly, expression of microRNAs alone can fully reprogram fibroblasts to iPSCs (Anokye-Danso et al., 2011; Henzler et al., 2013; Miyoshi et al., 2011; Polo et al., 2012; Salzman, 2016). These findings clearly suggest that microRNAs play crucial roles during the reprogramming process by targeting key barrier signaling networks. However, most studies to date have focused on intracellular signaling networks regulated by microRNAs, and the ability of microRNAs to influence critical cellular interactions with the microenvironmental niche during reprogramming has not yet been investigated.

Here, we performed a systematic analysis of expression of microRNAs and their potential target genes at an early stage of reprogramming, and identified a novel link between microRNAs, ECM formation and reprogramming of MEFs. In particular, we found that microRNA-135b is highly induced and modulating its expression significantly affected the reprogramming process. Using genome-wide mRNA array analysis, we show that miR-135b controls expression of Tgfbr2, Igfbp5, and Wisp1, the latter two genes encoding components of the MEF ECM. Wisp1 was found to regulate the secretion of

several ECM proteins including TGFBI (TGF-beta induced), IGFBP5 (insulin-like growth factor binding proteins-5), NOV (nephroblastoma overexpressed gene), and DKK2 (dickkopf homolog 2) proteins. Interestingly, the effects of Wisp 1 are mediated through biglycan, a glycoprotein that is highly expressed in MEFs and is incompletely silenced in reprogramming cells. Notably, knockdown or overexpression of biglycan enhanced or suppressed MEF reprogramming, respectively. Collectively, our results have identified a novel role for microRNA-mediated regulation of ECM formation in iPSC generation, and further, demonstrate that microRNAs can be powerful tools to dissect and understand the intracellular and extracellular molecular mechanisms of somatic cell reprogramming.

Chapter 2.2: Results

Systematic identification of highly regulated microRNAs during the early stages of reprogramming

We hypothesized that at different reprogramming stages, potential iPSCs may express unique ‘marker signatures’ of microRNAs that regulate how the cells reach a fully reprogrammed stage. Previous findings indicate that reprogramming of MEFs is accompanied by sequential modulation of somatic cell and stem cell markers at different reprogramming stages (Brambrink et al., 2008; Stadtfeld et al., 2008), which can be used to track the process. These markers include the cell surface antigen Thy1, the mES markers alkaline phosphatase

Figure 2.1: Identification of highly regulated microRNAs during the early reprogramming stage

(A) Scheme of experimental design. MEFs were infected with 4F virus for 5 days, and sorted based on expression of the Thy1 surface antigen. Both $Thy1^{-}$ and Thy1+ cells were collected for microRNA expression profile analysis.
(B) Representative gating for day 5 4F-infected MEF sorting. PE-conjugated Thy1 antibody was used to detect Thy1- and Thy1+ populations.
(C) iPSCs were enriched in the Thy1- population of 4F-infected MEFs at day 5. Equal numbers of cells (10,000 cells) sorted from 4F-infected MEFs were replated into feeder plates and cultured for 14 days, then GFP^{+} colonies were counted.
(D) AP staining confirmed that iPSCs generated in (C) were enriched in the Thy1- population. Cells were harvested for AP staining at day 14 post-infection.
(E) Representative image of AP+ colonies from replated Thy1- and Thy1+ cells.
(F) Induced or repressed microRNAs were identified in Thy1- cells. Both Thy1- and Thy1+ cells were harvested for microRNA expression profiling. Data from the $Thy1^{-}$ population was compared with the original MEFs and microRNAs showing a 2-fold change and $p<0.05$ were identified using a volcano map. Hits are labeled as red dots.
(G) Set of significantly induced microRNAs. MicroRNAs induced by at least 2-fold are shown. (H) Set of significantly repressed microRNAs. MicroRNAs repressed by at least 2-fold are shown.

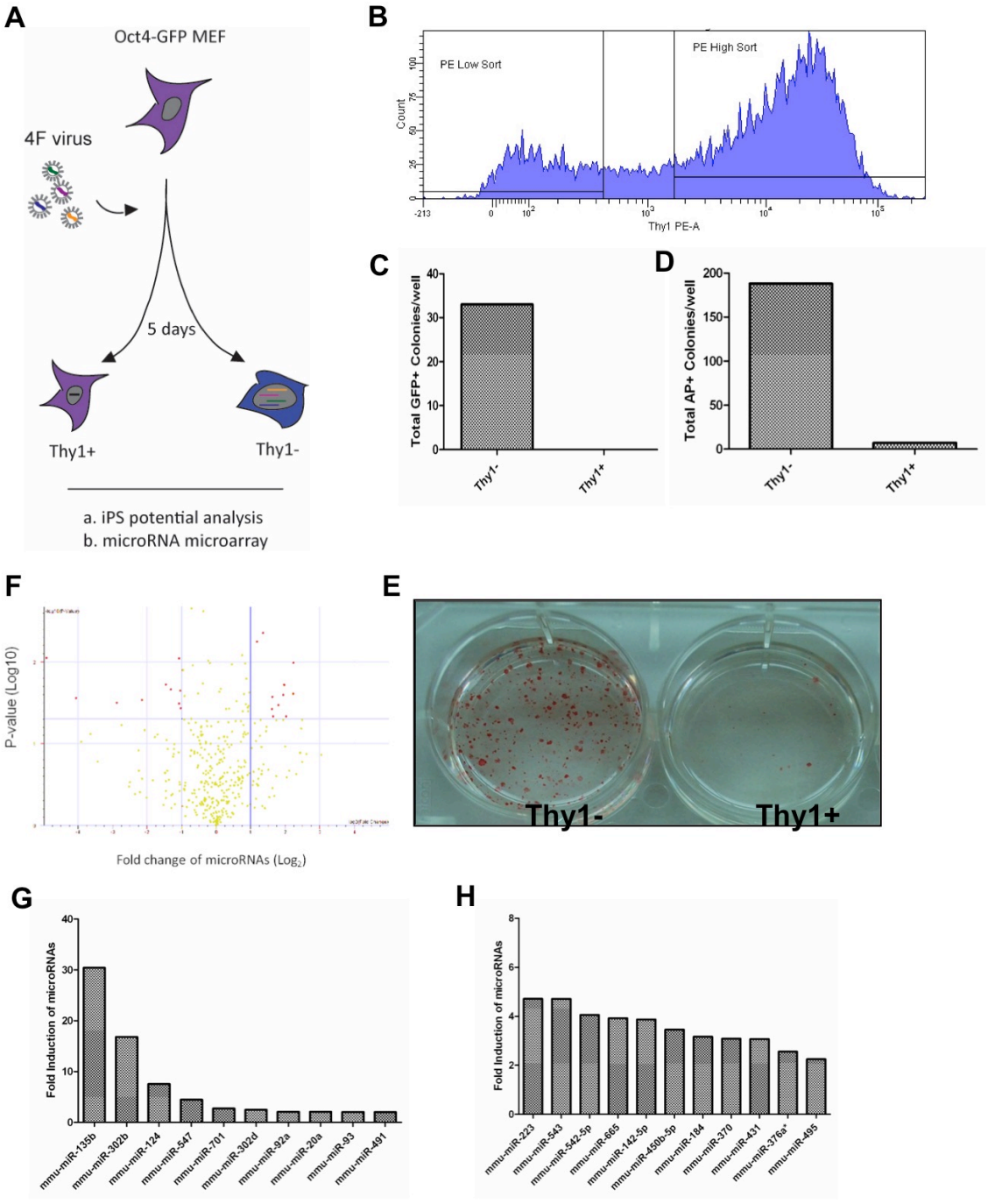
A
Oct4-GFP MEF
4F virus
5 days
Thy1+
Thy1-
a. iPS potential analysis
b. microRNA microarray
B
PE Low Sort
PE High Sort
Count
Thy1 PE-A
C
Total GFP+ Colonies/well
Thy1-
Thy1+
D
Total AP+ Colonies/well
Thy1-
Thy1+
F
P-value (Log10)
Fold change of microRNAs (Log2)
E
Thy1-
Thy1+
G
Fold Induction of microRNAs
mmu-miR-135b
mmu-miR-302b
mmu-miR-124
mmu-miR-547
mmu-miR-701
mmu-miR-302d
mmu-miR-92a
mmu-miR-20a
mmu-miR-93
mmu-miR-491
H
Fold Induction of microRNAs
mmu-miR-223
mmu-miR-543
mmu-miR-542-5p
mmu-miR-665
mmu-miR-142-5p
mmu-miR-450b-5p
mmu-miR-184
mmu-miR-370
mmu-miR-431
mmu-miR-376a*
mmu-miR-495

Figure 2.2: miR-135b enhances reprogramming of MEFs to iPSCs

(A) miR-135b enhances Oct4-GFP+ colony formation. The indicated microRNA mimics were transfected at a final concentration of 50 nM into MEFs on day 0 and again on day 5 after 4F transduction. GFP+ colonies were counted at day 11-12. Data represents two independent experiments with triplicate wells. Let-7a was used as a control. *p<0.05.
(B) miR-135b increases the percentage of Oct4-GFP+ cells. Cells from the indicated treatments were harvested at day 14 post-infection with 4F and paraformaldehyde-fixed prior to FACS analysis to determine the percentage of GFP+ cells. Data represents two independent experiments with triplicate wells. *p<0.05.
(C) Blocking of miR-135b compromises reprogramming. MicroRNA inhibitors were transfected into MEFs on days 0 and 5 post-infection with 4F. GFP+ colonies were counted at day 11-12 post-infection. Data represents two independent experiments with triplicate wells. *p<0.05.
(D) miR-135b iPSCs reach a fully reprogrammed state. miR-135b–transfected iPSCs were fixed with paraformaldehyde and stained for alkaline phosphatase, Nanog, and SSEA1 expression. Endogenous Oct4 expression was monitored by GFP expression.
(E) Teratoma formation confirms the pluripotency of miR-135b iPSCs. $1x10^6$ iPSCs were injected into athymic nude mice and tumors were harvested for H&E staining 3–4 weeks later.
(F) miR-135b iPSCs show expression profiles similar to mES cells. Total RNA from miR-135b iPSCs was used for mRNA expression profile analysis and compared with original MEFs and with mES cells. The three tested miR-135b iPSC clones (clones 1, 3, and N1) showed similar expression patterns to mES cells, which were quite different from the expression profile of the original starting MEFs.
(G) Chimeric mouse from miR-135b iPSC clone 4.
(H) miR-135b iPSC could contribute to the germline of recipient embryos (miR-135b iPSC clone 4)

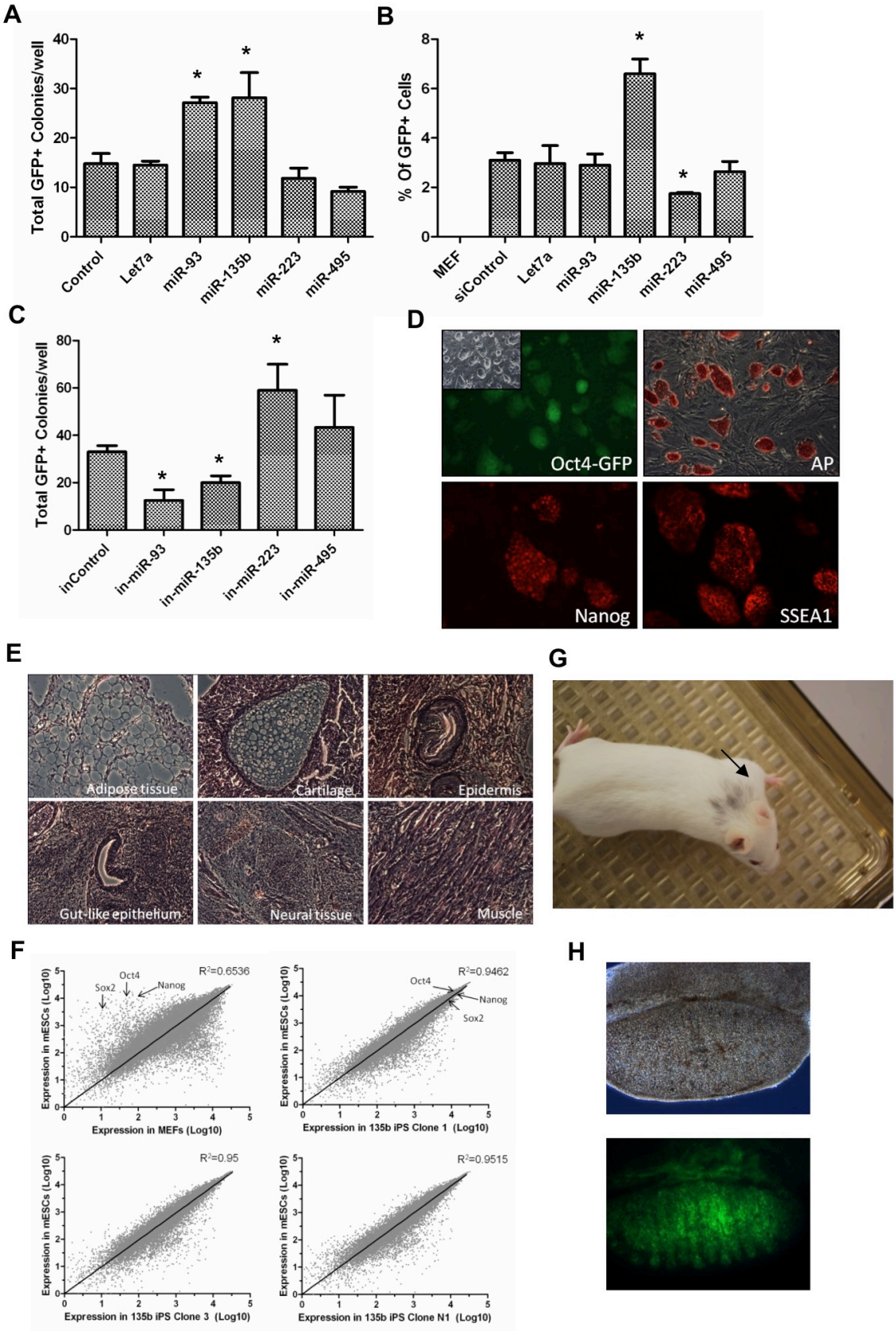
A
Total GFP+ Colonies/well
Control
Let7a
miR-93
miR-135b
miR-223
miR-495
B
% Of GFP+ Cells
MEF
siControl
Let7a
miR-93
miR-135b
miR-223
miR-495
C
Total GFP+ Colonies/well
inControl
in-miR-93
in-miR-135b
in-miR-223
in-miR-495
D
Oct4-GFP
AP
Nanog
SSEA1
E
Adipose tissue
Cartilage
Epidermis
Gut-like epithelium
Neural tissue
Muscle
G
F
Expression in mESCs (Log10)
Expression in MEFs (Log10)
Oct4
Sox2
Nanog
R²=0.6536
Expression in 135b iPS Clone 1 (Log10)
R²=0.9462
Expression in 135b iPS Clone 3 (Log10)
R²=0.95
Expression in 135b iPS Clone N1 (Log10)
R²=0.9515
H

(AP) and SSEA1, and the self-renewal genes Nanog and Oct4. Thy1 is highly expressed in MEFs but its expression is repressed at the initiation of reprogramming. Conversely, AP and SSEA1 expression is upregulated, followed by upregulation of Nanog and endogenous Oct4. Thus, MEFs expressing GFP under control of Oct4 are often used as the starting somatic cells because GFP expression then identifies cells that have been fully reprogrammed to the iPSC stage. To identify key microRNAs in reprogramming, we focused on the early reprogramming stage in the first 5 days after transduction of MEFs with the four factors (4F; OSKM) in what is reported to be the first stage of major transcriptional changes in the biphasic reprogramming process (Polo et al., 2012). To determine whether the fate of 4F-transduced cells is set at that stage, Oct4-GFP MEFs were infected with 4F virus and then harvested five days later for cell sorting (Figure 2.1A). PE-conjugated Thy1 antibody was used to isolate pure Thy1+ and Thy1- populations, with gates set to exclude cells expressing intermediate Thy1 levels (Figure 2.1B). Equal numbers (10,000 cells) of Thy1+ and $Thy1^-$ cells were reseeded in 12-well plates on CF1-MEF feeders and their potential for iPSC induction was evaluated based on GFP and marker expression. Potential iPSCs were enriched mainly in the Thy1- population, as determined by counting of colonies expressing GFP or AP (Figure 2.1C, D). We detected no GFP^+ colonies and only a few AP^+ colonies in the Thy1+ population at day14 post 4F infection (Figure 2.1C, E). These results suggest that the fate of 4F-infected MEFs is determined before day 5 post-infection and that potential iPSCs are enriched in the Thy1- population. We therefore collected total RNA

from sorted Thy1- cells at day 5 post-transduction to analyze overall microRNA expression changes by microarray. To identify microRNAs whose expression is significantly altered relative to that seen in starting MEFs, we filtered the data by setting a gate of at least a 2-fold change in expression with $p<0.05$ (Figure 2.1F). We identified a set of microRNAs in the Thy1- $^{-}$ population that were significantly induced by 4F transduction (Figure 2.1G). Among them, miR-135b was the most highly induced and showed a statistically significant change in expression (Table 2.2, Fig S2.1A), and was thus selected for further analysis of its role, and that of its direct gene targets, in the reprogramming process. We observed that other microRNAs, such as miR-93 which belongs to miR-25~106b cluster, miR-92a which belongs to miR-17~92 cluster, and miR-302b which belongs miR-302 cluster, were also highly induced at the early stage of reprogramming, confirming previous findings (Li et al., 2011b; Liao et al., 2011b; Subramanyam et al., 2011a). Our analysis also revealed a set of microRNAs that were significantly repressed (Figure 2.1H), suggesting that they may serve as reprogramming barriers. Of these, we chose to evaluate the potential barrier function of miR-223 and miR-495, because they are highly expressed in MEFs.

Reprogramming is enhanced by miR-135b and inhibited by miR-223 and miR-495

To determine how miR-135b affects reprogramming, miR-135b microRNA mimic was transfected into Oct4-GFP MEFs infected with 4F virus, and GFP^{+} colonies were counted at day 11–12 post-transduction. Transfection of the miR-

135b mimic increased the number of Oct4-GFP$^+$ colonies by ~ 2-fold, as did transfection with miR-93, which was previously characterized as an enhancer of reprogramming (Anokye-Danso et al., 2011) (Figure 2.2A). In similar experiments, cells were transfected with miR-223 or miR-495 mimics, which had minor inhibitory effects on reprogramming (Figure 2.2A). This observation is potentially due to the saturation effect of endogenous miRs as these miRs already have high expression in MEFs. We then analyzed the percentage of GFP$^+$ cells in the miR-transfected reprogrammed cells and found that although both miR-93 and miR-135b increased GFP$^+$ colony formation, only miR-135b increased the overall percentage of GFP+ cells by ~2 fold (Figure 2.2B, Figure S2.1B). In the same assay, miR-223 transfection significantly decreased the GFP+ population (Figure 2.2B), supporting the possibility that it serves as a reprogramming barrier. To confirm our findings, we used microRNA inhibitors. As expected, blocking miR-135b compromised reprogramming efficiency, while inhibiting miR-223 resulted in a significant increase in the number of Oct4-GFP+ colonies (Figure 2.2C). Following transfection with miR-135b mimics or inhibitors, miR-135b expression levels were quantified by RT-qPCR to confirm overexpression or downregulation, respectively (Figure S2.2A). Overall, these data demonstrate that miR-135b enhances reprogramming, consistent with its high induction by the 4F factors, while miR-223, which our analysis showed to be the most highly repressed microRNA, serves as a barrier.

Because GFP expression by putative iPSC could result from inappropriate reactivation of the Oct4 locus, we asked whether miR-135b–

transfected iPSCs reached a fully reprogrammed state, both phenotypically and functionally. Analysis of miR-135b–transfected iPSCs indicated that they expressed appropriate markers, including AP, SSEA1, Nanog, and endogenous Oct4 (Figure 2.2D). Moreover, these cells had the full capacity to differentiate into three germ layers as indicated by marker analysis (Figure S2.2B), and to form heterogeneous teratomas when injected into athymic nude mice (Figure 2.2E). Genome-wide mRNA profiling also confirmed that gene expression in miR-135b–transfected iPSCs resembled mES cells and differed significantly from MEFs (Figure 2.2F), and these cells contributed to chimeric mice and showed germline transmission (Figure 2.2G, H) which clearly indicated that a fully reprogrammed state has been achieved in these cells. These data demonstrated that miR-135b transfection in iPSCs did not adversely affect their pluripotency.

Identification of miR-135b-regulated genes

We next sought to identify genes that are directly regulated by miR-135b. Initially, microRNAs were thought to simply repress mRNA translation. However, recent findings suggest that microRNA-induced degradation of mRNA is a major mechanism of mRNA repression in animals (Djuranovic et al., 2011; Huntzinger and Izaurralde, 2011). Thus, we performed a genome-wide mRNA expression analysis to detect potential miR-135b targets. miR-135b or control siRNA were transfected into Oct4-GFP MEFs, and total RNAs were harvested 48 hr later for array analysis. The raw data was filtered to detect at least 2-fold changes in gene expression, (either increased or decreased) with $p<0.05$ (Figure 2.3A). Candidate

genes were then compared with published mESC, iPSC, and MEF expression profiles (Sridharan et al., 2009) and segregated into genes induced (group 1) or repressed (group 2) after miR-135b transfection, the latter being considered more likely to contain direct targets. Notably, we found that over 80% of the genes repressed by miR-135b transfection (group 2) were genes that are silenced as MEFs are reprogrammed to iPS/mES cells (correlated) (Figure 2.3B). This was not observed in genes that were induced by miR-135b transfection (group 1), of which approximately half are normally suppressed during reprogramming (uncorrelated), and the other half are increased (correlated). This data suggests that miR-135b targets a subset of genes that are normally repressed during reprogramming.

To identify the targets of miR-135b, the “correlated” genes in group 1 (Figure 2.3C) were analyzed using both miRanda (Enright et al., 2003) and Targetscan (Lewis et al., 2005). Potential target sites were identified based on seed region matches and overall predicted binding energy. Of 27 genes repressed by miR-135b by at least 2-fold, 14 contained at least one predicted miR-135b target site (Figure S2.3A and Table 2.1). Among them, Wisp1, Tgfbr2, and Igfbp5 showed high expression intensity detected by microarray and appeared to have direct miR-135b target sites. Therefore, they were chosen for further validation.

Figure 2.3: Genome-wide identification of potential miR-135b target genes

(A) Volcano maps from miR-135b–transfected MEFs. MEFs were transfected with siControl and miR-135b for two days and analyzed by mRNA expression array. Hits (red dots) were gated for at least 2-fold expression change and $p<0.05$.
(B) miR-135b–repressed genes are enriched for genes suppressed in ES/iPS cells. miR-135b–regulated genes were separated into two groups (induced or repressed) and then compared with existing iPS/ES/MEF expression profiles. "Correlated genes" indicates that genes changed upon miR-135b transfection showed similar changes from MEFs to iPS/mES cells. "Uncorrelated genes" indicates a group of genes that were changed upon miR-135b transfection but had a different (reversed) change in expression pattern from MEFs to iPS/mES cells.
(C) List of correlated miR-135b–repressed genes.
(D) Representative miR-135b–regulated genes from microarray.
(E) Expression of miR-135b–regulated genes was confirmed by RT-qPCR. MEFs were transfected with microRNA mimics for two days before harvesting for RT-qPCR analysis. Error bar represents two independent experiments with duplicate samples.
(F) TGFBR2 protein expression is suppressed by miR-93 and miR-135b. Total proteins were harvested for western blotting analysis at day 2 post-transfection with miR mimic.
(G) IGFBP5 protein expression is suppressed by miR-135b. A miR-93-transfected sample was included as a negative control. RT-qPCR data was analyzed using the Wilcoxon rank-sum test. * $P<0.05$; ** $P<0.01$; *** $P<0.001$

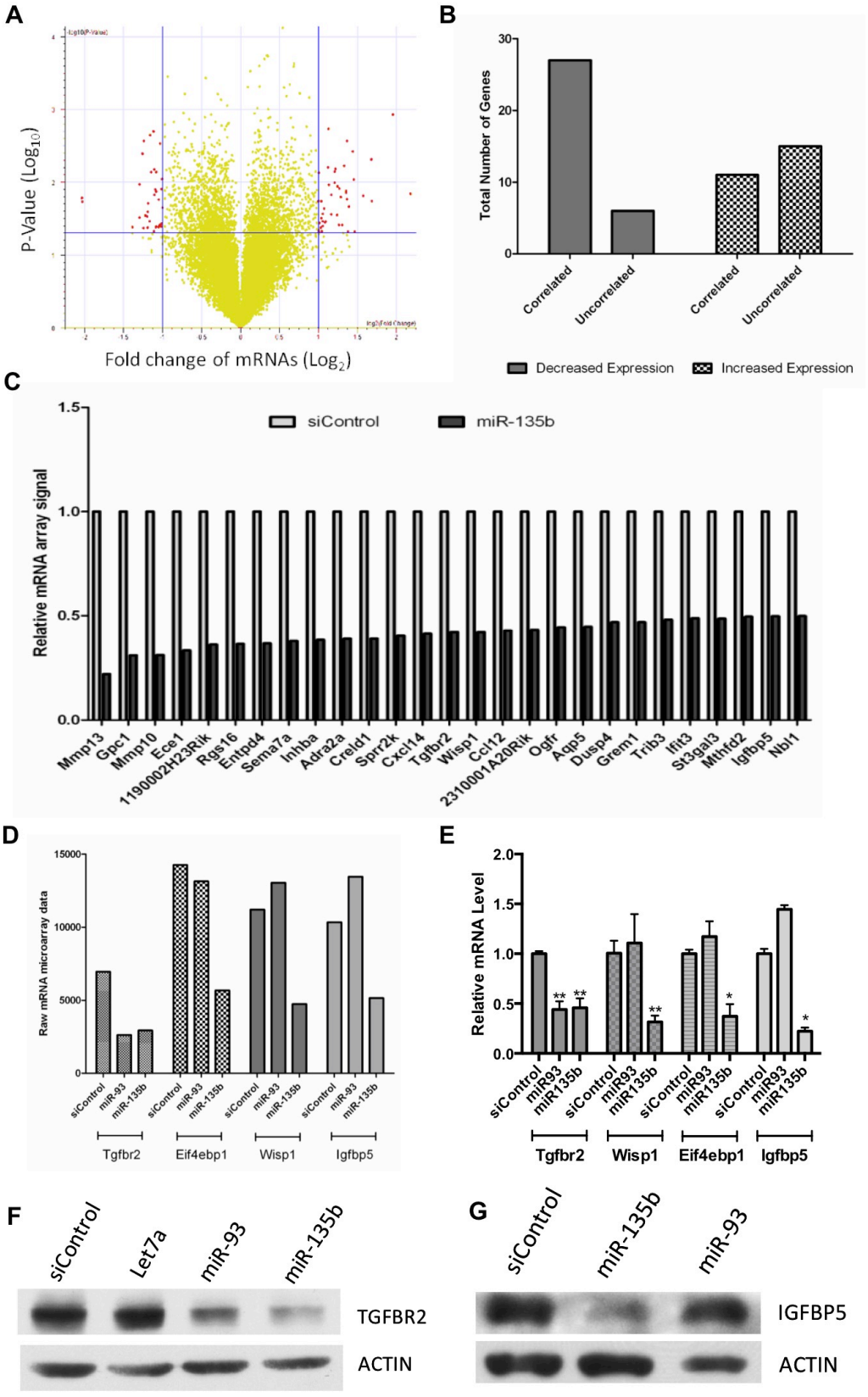
A
P-Value (Log10)
Fold change of mRNAs (Log2)
B
Total Number of Genes
Correlated
Uncorrelated
Correlated
Uncorrelated
Decreased Expression
Increased Expression
C
siControl
miR-135b
Relative mRNA array signal
Mmp13
Gpc1
Mmp10
Ece1
1190002H23Rik
Rgs16
Entpd4
Sema7a
Inhba
Adra2a
Creld1
Sprr2k
Cxcl14
Tgfbr2
Wisp1
Ccl12
2310001A20Rik
Ogfr
Aqp5
Dusp4
Grem1
Trib3
Ifit3
St3gal3
Mthfd2
Igfbp5
Nbl1
D
Raw mRNA microarray data
siControl
miR-93
miR-135b
Tgfbr2
Eif4ebp1
Wisp1
Igfbp5
E
Relative mRNA Level
siControl
miR93
miR135b
Tgfbr2
Wisp1
Eif4ebp1
Igfbp5
F
siControl
Let7a
miR-93
miR-135b
TGFBR2
ACTIN
G
siControl
miR-135b
miR-93
IGFBP5
ACTIN

To confirm our mRNA microarray analysis, total RNAs were harvested from miR-135b-transfected Oct4-GFP MEFs in an independent experiment, and RT-qPCR was used to quantify the representative mRNAs. Indeed, we detected decreases in mRNA levels upon miR-135b transfection that were in good agreement with the mRNA array data (Figure 2.3D, E). Tgfbr2 and Igfbp5 mRNA levels were decreased ~70% upon miR-135b transfection, and western analysis confirmed that this was accompanied by a dramatic decrease in Tgfbr2 and Igfbp5 protein expression (Figure 2.3F, G). Although expression of Wisp1 mRNA was also markedly reduced by miR-135b expression (Figure 2.3D, E), no Wisp1 antibodies are currently available, which prevented us from analyzing Wisp1 protein expression. We cloned the 3'UTR of these potential targets into the pGL3 luciferase reporter vector and co-transfected the reporters plus the pRL-TK plasmid into HeLa cells. Indeed, miR-135b decreased luciferase activity of Tgfbr2 and Wisp1 reporters by ~80%, and the Igfbp5 reporter by ~30% (Figure S2.3B). We also noticed that the combination of miR-93 and 135b showed additive effects on Tgfbr2 repression (Figure S2.3C). These data strongly suggest that Tgfbr2, Wisp1, and Igfbp5 are direct targets of miR-135b, of which the latter two are key component of extracellular matrix proteins. To further validate Wisp1 as a target of miR-135b, RT-qPCR was utilized to assess the Wisp1 mRNA level after transfecting cells with miR-135b mimic, mutant mimic or miR-135b inhibitors. Wisp1 mRNA decreased by ~50% during miR mimic transfection, increased by ~25% upon inhibition and remained consistent with the non-targeting siRNA control when transfected with the mutant miR mimic (Figure S2.3D). In

conjunction with the dual luciferase reporter assay, this data indicates a direct sequence specific interaction between miR-135b and Wisp1.

Wisp1 has dual roles during reprogramming and is a key regulator of ECM proteins

We next asked whether the potential miR-135b targets Tgfbr2, Wisp1, and Igfbp5 function as reprogramming barriers. Tgfbr2 was previously reported to be a reprogramming barrier and a potential target of miR-93 and its family of microRNAs (Li et al., 2011b). In addition to Tgfbr2, Wisp1, and Igfbp5, we chose to investigate several other genes that might be indirectly regulated by miR-135b, such as Eif4ebp1 and Cxcl14 as they do not have predicted miR-135b target sites. Before using siRNAs for these experiments, we confirmed by RT-qPCR that each mRNA was efficiently knocked down by at least 60% by its cognate siRNA (Figure 2.4A).

To determine whether knockdown of the candidate barrier genes increased reprogramming efficiency, we transfected siRNAs into Oct4-MEFs on the same day as 4F transduction (day 0), then again on day 5 post-infection, and counted GFP^+ iPSC colonies on day 11–12. We detected a significant increase in the number of GFP+ colonies after transfection of siRNA targeting Igfbp5 and Tgfbr2, consistent with their possible function as barrier genes (Figure 2.4B). Interestingly, a dramatic decrease in reprogramming efficiency was observed in cells transfected with siWisp1 on days 0 and 5 post-4F infection. However, if

Figure 2.4: Wisp1 plays a dual role during reprogramming, while Tgfbr2 and Igfbp5 knockdown enhances reprogramming

(A) Potential target genes are efficiently knocked down by siRNAs. Smartpool siRNAs at a final concentration of 50 nM were used to transfect MEFs. Total RNAs were harvested at day 2 for RT-qPCR to evaluate knockdown efficiency of each siRNA.
(B) Knockdown of Tgfbr2 or Igfbp5 enhances Oct4-GFP+ colony formation, while knockdown of Eif4ebp1 and Cxcl14 had no effect. MEFs were transfected with siRNAs on days 0 and 5 at the same time as 4F infection. GFP+ colonies were counted at day 11-12 post-infection. Error bars represent three independent experiments with triplicate wells. The p value was calculated using Student's *t*-test. **p<0.01.
(C) Knockdown of Wisp1 shows stage-specific effects on reprogramming. Knockdown of Wisp1 on the same days as 4F transduction (day 0) decreased the reprogramming efficiency by ~70% percent, while knockdown on day 5 enhanced reprogramming by ~3 fold. Error bars represent three independent experiments with triplicate wells. **p<0.01.
(D) Wisp1 is efficiently knocked down by siRNAs during both procedures. siWisp1 was transfected at a final concentration of 50 nM on day 0 or day 5. Total RNAs were harvested at day 2 post-transfection for RT-qPCR analysis of Wisp1 expression.
(E) Knockdown of Wisp1 is able to rescue iPS reprogramming after inhibition of miR-135b at day 5. Error bars represent three independent experiments with duplicate wells.
(F) Knockdown of Wisp1 at day 0 inhibits mesenchymal-to-epithelial transition (MET). MEFs were infected with 4F and transfected with siRNA on the same day (day 0). Total RNAs were harvested 2 days later. Expression of several MET markers was evaluated.
(G) Knockdown of Wisp1 at day 5 does not affect MET. MEFs were transduced with 4F at day 0 and transfected with siRNA at day 5 post-4F infection. Total RNAs were harvested 2 days after transfection and expression of the MET markers was evaluated.
(H) Overexpression of Wisp1 inhibits iPS induction. MEF were transduced with a Wisp1 HA tagged retroviral vector along with OSKM and GFP colonies were quantified on day 12-14. RT-qPCR data was analyzed using the Wilcoxon rank-sum test. * P<0.05; ** P<0.01; *** P<0.001

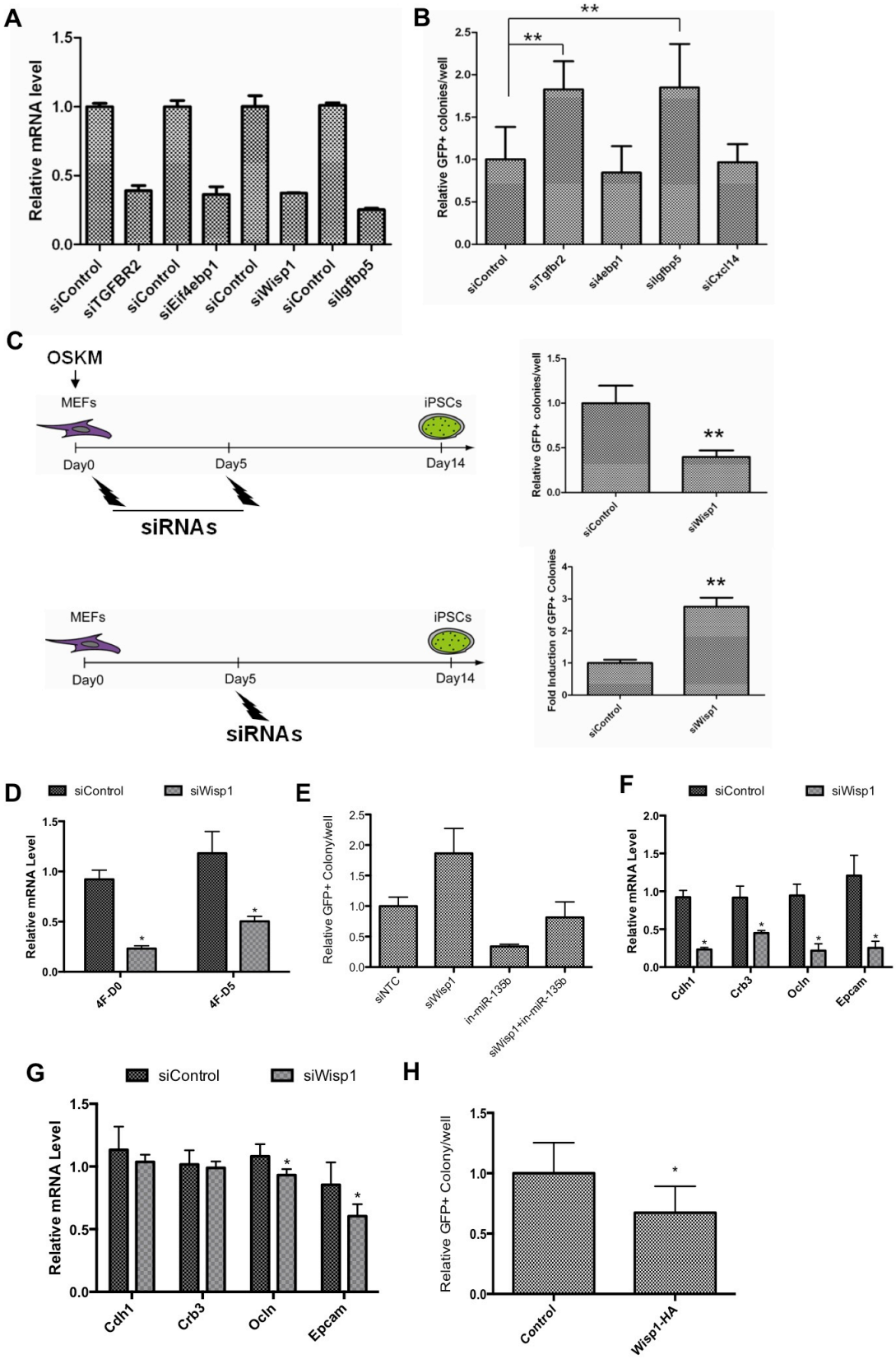
A
Relative mRNA level
siControl
siTGFBR2
siControl
siEif4ebp1
siControl
siWisp1
siControl
siIgfbp5
B
Relative GFP+ colonies/well
siControl
siTgfbr2
si4ebp1
siIgfbp5
siCxcl14
C
OSKM
MEFs
iPSCs
Day0
Day5
Day14
siRNAs
Relative GFP+ colonies/well
siControl
siWisp1
Fold Induction of GFP+ Colonies
D
siControl
siWisp1
Relative mRNA Level
4F-D0
4F-D5
E
Relative GFP+ Colony/well
siNTC
siWisp1
in-miR-135b
siWisp1+in-miR-135b
F
siControl
siWisp1
Relative mRNA Level
Cdh1
Crb3
Ocln
Epcam
G
siControl
siWisp1
Relative mRNA Level
Cdh1
Crb3
Ocln
Epcam
H
Relative GFP+ Colony/well
Control
Wisp1-HA

siWisp1 was transfected on day 5 only, there was a 3-fold increase in the number of GFP^+ colonies (Figure 2.4C), suggesting that Wisp1 can play temporally distinct roles during reprogramming. This effect was not due to a difference in siRNA transfection efficiency, because Wisp1 mRNA knockdown was equivalent under both protocols (Figure 2.4D). We observed that Wisp1 mRNA expression was sharply reduced by 4F initially and then maintained at a steady level during the rest course of the reprogramming process (Figure S2.4A) while Wisp1 protein levels showed a decline between days 4 and 6 (Figure S2.4B). To analyze the significance of Wisp1 in the context of miR-135b reprogramming, MEF were reprogrammed while simultaneously knocking down the endogenous Wisp1 and inhibiting miR-135b using an antisense oligo five days post OSKM transduction. Wisp1 knockdown and miR-135b inhibition at day 5 of iPS reprogramming showed an increase and a decrease in GFP+ iPS colonies, respectively. However, when both were simultaneously inhibited during reprogramming, a rescuing effect in iPS Oct4 GFP positive colonies was observed (Figure 2.4E). This data suggests that Wisp1 contributes significantly to miR-135b reprogramming and acts as a barrier to iPSC generation.

To prove this observation further, we next analyzed the effect of Wisp1 siRNA transfection on markers of MET, which is believed to be the initial step of the reprogramming process (Li et al., 2010; Samavarchi-Tehrani et al., 2010). Remarkably, knockdown of Wisp1 on day 0 dramatically decreased mRNA expression of each of the MET markers tested, suggesting a significant delay or suppression of MET by siWisp1 (Figure 2.4F). In contrast, Wisp1 knockdown on

day 5 had little effect on MET marker mRNA levels, except a small and insignificant decrease in Epcam expression (Figure 2.4G). In addition, constant overexpression of HA tagged Wisp1 showed inhibitory effects on reprogramming (Figure 2.4H) with HA-tagged Wisp1 overexpression verified by western blot (Figure S2.4C). Together, these data show that the role of Wisp1 is temporally dependent, and suggests a dual role of Wisp1 in which it acts as a positive regulator of reprogramming in the early stages and a negative regulate later.

To identify the mechanism by which Wisp1 affects reprogramming, we next investigated the downstream targets of Wisp1. Wisp1 is a member of CCN family proteins, the function of which usually includes two aspects: (1) binding of scaffold of extracellular matrix proteins; (2) binding receptors and transcriptionally regulating signaling events mediated by biological active molecules such as growth factors and cytokines (Jun and Lau, 2011). We reasoned that since somatic cell reprogramming is an *in vitro* process, it is more likely that Wisp1 functions through transcriptional regulation of downstream genes. To identify the downstream targets of Wisp1, we utilized mRNA microarrays to search for genes significantly changed upon Wisp1 knockdown in control, non-infected and 4F-transduced MEFs (Table 2.4). The microarray experiments identified a panel of ECM genes, including Dkk2, Igfbp5, Nov, and Tgfbi, that showed profoundly decreased expression upon Wisp1 knockdown, which was confirmed by RT-qPCR (Figure 2.5A). Moreover, expression of Dkk2, Igfbp5, Nov, and Tgfbi was suppressed by 4F transduction. In addition, Wisp1 knockdown increased expression of Ccl20 (Figure 2.5A), which was also induced in MEFs by

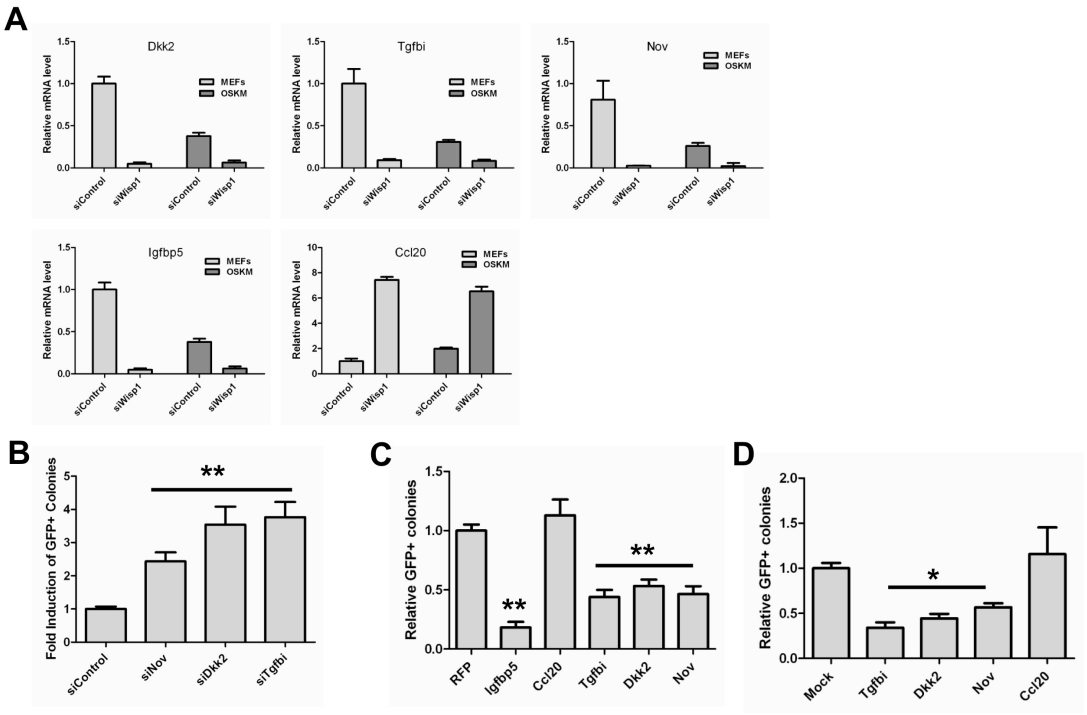

Figure 2.5: Wisp1 is a key regulator of extracellular matrix genes

(A) Wisp1 regulates expression of several ECM genes. Expression of Tgfbi, Igfbp5, Dkk2 , Nov, and Ccl20 were dramatically changed upon Wisp1 knockdown. Uninfected and 4F-infected MEFs were transfected with siWisp1 for 2 days and total RNAs were harvested for RT-qPCR analysis of different ECM genes. Error bars represent two independent experiments with duplicate wells.
(B) Knockdown of Nov, Dkk2, and Tgfbi significantly enhances iPSC generation. MEFs were transduced with 4F at day 0 and transfected with siRNAs at day 5 post-infection. GFP+ colonies were quantified at around day 11-13. Error bars represent three independent experiments with triplicate wells. **p<0.01.
(C) Overexpression of Wisp1-regulated ECM genes compromises reprogramming. The indicated ECM genes were cloned into pMX retroviral vectors. MEFs were transduced with 4F plus the indicated ECM genes and GFP+ colonies were quantified at around day 11-13. Data was normalized to pMX-RFP–transduced cells. Error bars represent three independent experiments with triplicate wells. **p<0.01.
(D) Addition of recombinant ECM proteins compromises reprogramming. Purified recombinant TGFBI, DKK2, NOV, and CCL20 were added at a final concentration of 100 ng/ml to cultures of 4F-MEFs undergoing reprogramming. GFP+ colonies were quantified at day 11-13. Error bars represent two independent experiments with triplicate wells. *p<0.05.

4F transduction alone. To rule out the possibility of off-target effects of the Wisp1 siRNA, two additional shRNAs were tested. These shRNAs efficiently suppressed Wisp1 expression, and had the same inhibitory effects on expression of Wisp1 target genes (Figure S2.5A). To confirm that the miR-135b effects on MEFs was at least partially mediated through Wisp1, we transfected MEFs with an miR-135b mimic, and found decreased expression of Dkk2, Igfbp5, Nov, and Tgfbi (Figure S2.5B). We only observed modest upregulation of Wisp1 target genes with miR-135b inhibitor transfection (Figure S2.5C), possibly due to indirect targeting effects. In addition, overexpression of Wisp1 target genes did not affect Wisp1 expression, indicating a lack of feedback regulation (Figure S.5D). Together, these data suggest that Wisp1 may serve as a key regulator of ECM genes in MEFs.

To determine if expression of Wisp1-regulated ECM genes could affect reprogramming, Oct4-GFP MEFs were infected with 4F and on day 5 were transfected with siRNAs targeting Dkk2, Igfbp5, Nov, and Tgfbi. Indeed, knockdown of each of these genes at day 5 only significantly increased reprogramming efficiency (Figure 2.4B, Figure 2.5B), while similar biphasic effects were observed for Tgfbi and Nov when they were knocked down at day 0 and 5 (Figure S2.6A). We also detected an increase in mES marker gene expression in the siRNA-transfected cells (Figure S2.6B). Conversely, overexpression of these genes in MEFs strongly reduced GFP+ colony formation, particularly with Igfbp5, which reduced reprogramming by ~70% (Figure 2.5C). Interestingly, addition of recombinant DKK2, TGFBI, and NOV proteins to the 4F-

transfected MEF cultures from day5 post infection had similar effects on the cells as overexpression of the genes (Figure 2.5D), demonstrating that the effects of Wisp1 were mediated by secretion of the protein products of its target genes, and confirming that the Wisp1-regulated ECM genes do indeed act as barriers to the reprogramming process.

Based on the results described above, we propose a model of how Wisp1 may have a biphasic effect on MEF reprogramming (Figure 2.6A). Wisp1 is highly and specifically expressed in MEFs compared with iPSCs (Sridharan et al., 2009), and through its effects on the downstream ECM genes, plays a crucial role in maintaining normal MEF growth. This is supported by our finding that persistent knockdown of Wisp1 and NOV (Figure S.7A) by shRNAs in MEFs compromises their proliferation (Figure S2.7B). shRNA mediated knockdown of Wisp1 also confirms a similar biphasic effect on reprogramming (Figure S.7C). siRNA mediated knockdown of Nov also showed impaired cell proliferation (Figure S.7E). Upon 4F transduction and reprogramming, infected MEFs would have two regulatory networks, one established by the four reprogramming factors, and the other being endogenous. The ability of a cell to become fully reprogrammed would depend on whether the 4F-induced network could silence the existing MEF regulatory network. In these cells, although MEF-specific genes such as Wisp1 and its potential receptors are being down-regulated, the remaining receptors could still be stimulated by signals secreted by surrounding cells that are not reprogrammed. This constant stimulation of original MEF

Figure 2.6: Target gene regulation by Wisp1 through biglycan

(A) Proposed model for Wisp1 dual role during reprogramming. In wild type MEFs (fibroblast state), normal proliferation and function of the cells are dependent on a MEF-specific regulation network, where Wisp1 is one of the most important ECM components and regulates the expression of several other ECM genes. In 4F-transduced MEFs (intermediate state), two systems co-exist; one from the MEF-specific network and the other from the four transcription factors. ECM signals from the MEF-specific network interfere with the cells becoming fully reprogrammed. In fully reprogrammed cells (ES cell state), ECM receptors are no longer expressed, and the cells are thus resistant to interfering signals from surrounding MEFs.
(B) Biglycan and decorin are specifically expressed in MEFs. Expression of biglycan and decorin was analyzed by RT-qPCR in sorted cells.
(C) Biglycan and decorin are efficiently knocked down by siRNAs. MEFs were transfected with siRNAs for 2 days and total RNAs were harvested for RT-qPCR analysis.
(D) Knockdown of biglycan decreases expression of Wisp1-regulated ECM genes. Expression of Wisp1-regulated ECM genes was analyzed in MEFs subjected to knockdown of biglycan or decorin. Error bars represent two independent experiments with duplicate wells. **$p<0.01$.
(E) Overexpression of biglycan inhibits reprogramming. Flag-tagged biglycan was cloned into pMX vector and transduced into MEFs together with 4F. GFP+ colonies were quantified at day 11-13. Error bar represents two independent experiments with triplicate wells. *$p<0.05$.
(F) Knockdown of biglycan enhances reprogramming. Biglycan siRNAs were transfected into MEFs at day 5 post-4F transduction. GFP+ colonies were quantified at day 11-13. Error bar represents two independent experiments with triplicate wells. RT-qPCR data was analyzed using the Wilcoxon rank-sum test. * $P<0.05$; ** $P<0.01$; *** $P<0.001$

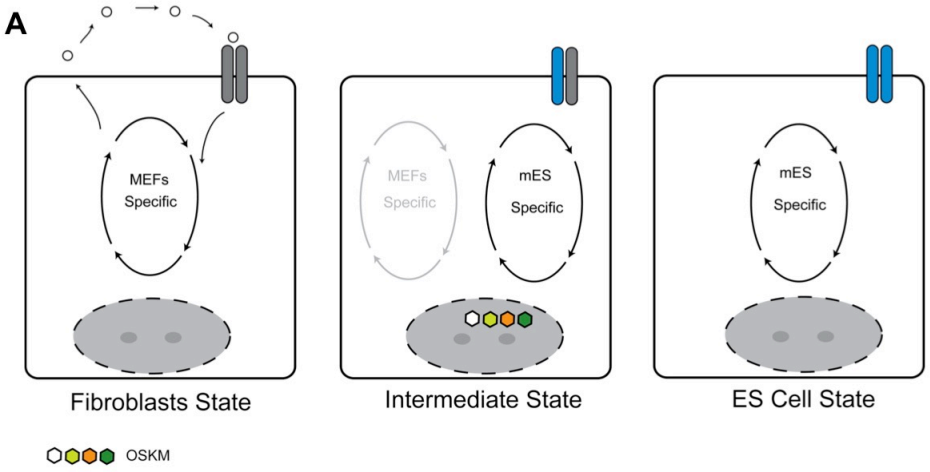
A
MEFs Specific
MEFs Specific
mES Specific
mES Specific
Fibroblasts State
Intermediate State
ES Cell State
OSKM

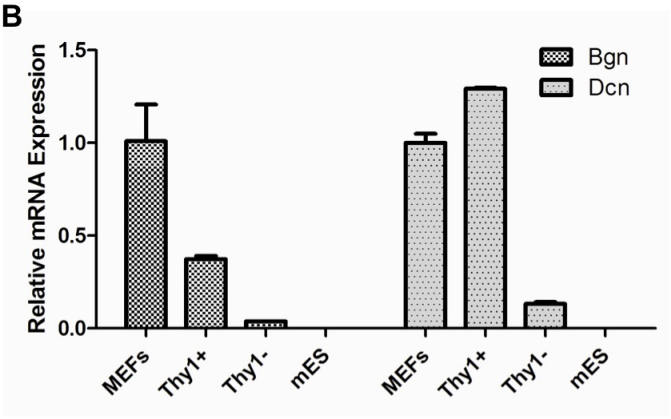
B
Relative mRNA Expression
Bgn
Dcn
MEFs
Thy1+
Thy1-
mES
MEFs
Thy1+
Thy1-
mES

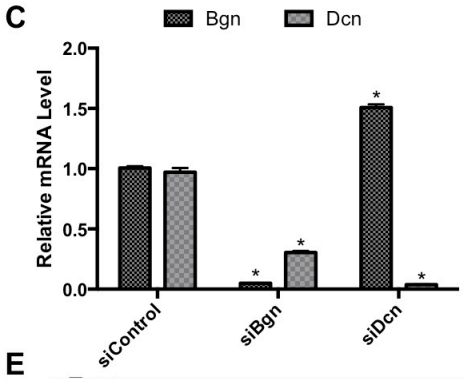
C
Bgn
Dcn
Relative mRNA Level
siControl
siBgn
siDcn

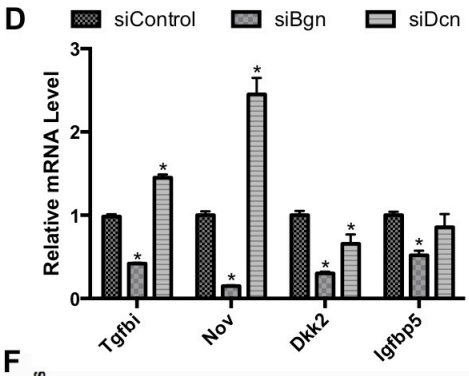
D
siControl
siBgn
siDcn
Relative mRNA Level
Tgfbi
Nov
Dkk2
Igfbp5

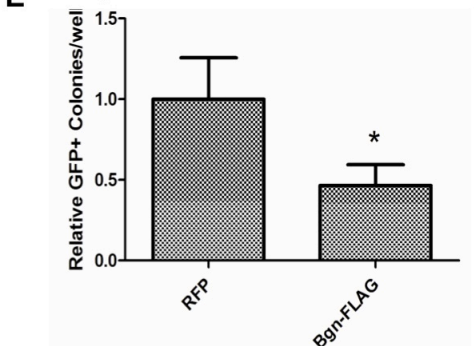
E
Relative GFP+ Colonies/well
RFP
Bgn-FLAG

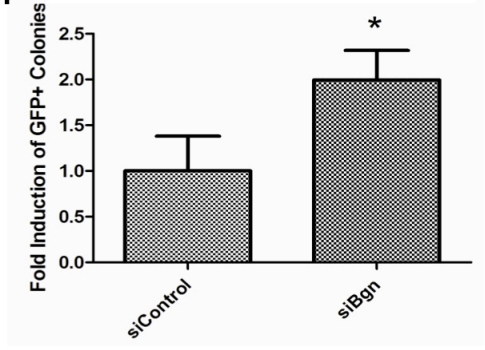
F
Fold Induction of GFP+ Colonies
siControl
siBgn

network would compete with 4F-mediated ES regulatory network and resulted in a low efficiency for cells to become fully reprogrammed. Thus, knocking down Wisp1 in these cells could reduce the MEF signaling stimulation, significantly break the balance and push them toward a fully reprogrammed state. Once the cells become mES-like cells, MEF ECM genes and receptors are completely shut down and they become resistant to the signals from nearby feeder cells.

Wisp1 may regulate ECM genes through its interaction with biglycan

To test our model (Figure 2.6A), we searched the literature for known factors that could interact with Wisp1. If our model is correct, we predict we will see high expression of these genes in the starting population of MEFs, whereas cells undergoing reprogramming will downregulate but not extinguish their expression, and expression will be silenced in fully reprogrammed iPSCs/mES cells. Interestingly, Wisp1 has been reported to bind the proteoglycans decorin and biglycan on the surface of human skin fibroblasts (Desnoyers et al., 2001) and both are highly expressed in MEFs (Sridharan et al., 2009). To determine if decorin and biglycan might be involved in Wisp1 regulation in MEFs, we first examined their gene expression in the starting MEFs, the sorted Thy1^{+}/$^{-}$ cells, and in mES populations. The two genes were highly expressed in MEFs but undetectable in mES cells (Figure 2.6B). They were highly expressed in Thy1+ cells and showed strongly reduced but detectable expression in Thy1- cells (Figure 2.6B), which are enriched in potential iPSCs (Figure 2.1C-E). We then transfected MEFs with siRNAs targeting these two genes and confirmed the

knockdown efficiency by RT-qPCR (Figure 2.6C). Of interest, knockdown of biglycan also decreased decorin expression, suggesting possible cross regulation of the two genes. Knockdown of biglycan also decreased the expression of the Wisp1 target genes Dkk2, Igfbp5, Nov, and Tgfbi, to a similar level to that seen with Wisp1 knockdown (Figure 2.6D). Consistent with these observations, overexpression of biglycan strongly suppressed reprogramming, and conversely, knockdown significantly enhanced reprogramming (Figure 2.6E, F). In addition, we also observed similar phenotype with decorin knockdown and overexpression (Figure S2.8). Therefore, we conclude that biglycan may be an intermediate for Wisp1-mediated regulation of its target ECM genes.

Chapter 2.3: Discussion

Since the discovery that MEFS can be directly reprogrammed to iPSCs, considerable effort has been made to understand how the four reprogramming transcription factors extinguish endogenous MEF gene expression and gradually re-establish mES-like regulatory networks. Understanding the critical barriers to reprogramming is essential to allow development of novel technologies and compounds to improve the efficiency and to elucidate the underlying transcriptional and epigenetic changes associated with the pluripotent state.

Here, we used microRNAs as powerful tools to dissect the molecular mechanisms that elicit successful reprogramming. We analyzed a Thy1– cell population enriched in potential iPSCs to identify its microRNA expression profile

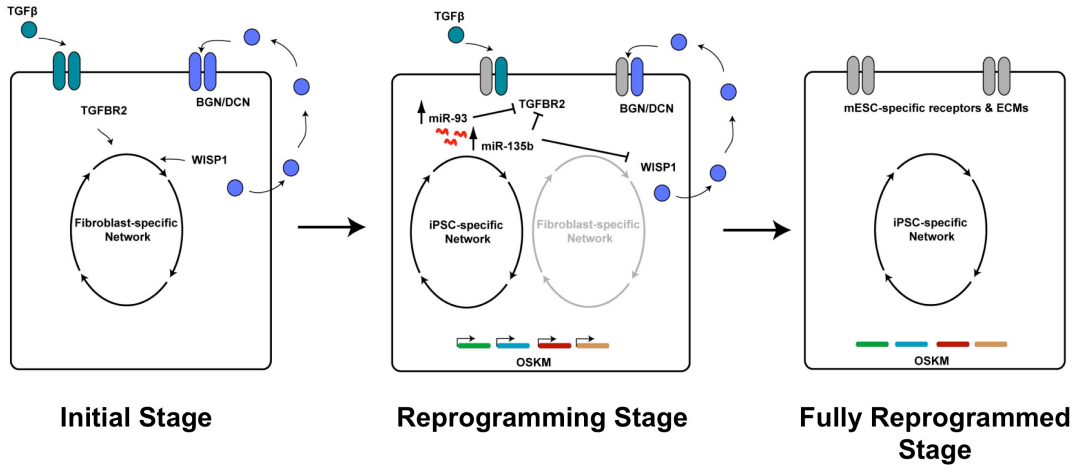

Figure 2.7: Model for roles of microRNAs during the reprogramming process

MicroRNAs induced by the four factors regulate intracellular and extracellular processes involved in cell fate decisions. Intracellularly, microRNAs target signaling pathways that are barriers for iPSC generation, such as TGFβ signaling, the p53-p21 pathway, and cell cycle control. Meanwhile, some microRNAs, such as miR-135b, regulate expression of ECM genes to establish a growth environment that promotes the fully reprogrammed state. Both groups of microRNAs work collaboratively following 4F transduction to reprogram MEFs to iPSCs.

during the early stages of reprogramming. From these experiments, we identified sets of microRNAs that were induced or repressed during the process, and showed that manipulating their expression with miR mimics or inhibitors dramatically altered the efficiency of iPSC induction. Among the microRNAs analyzed, miR-135b was the most highly induced by the four factors, and was shown to enhance iPSC generation. Moreover, by mining genome-wide mRNA expression data for potential miR-135b target genes, we showed that Wisp1 and its downstream ECM genes could compromise the efficiency of the reprogramming process. Therefore, our approach has not only identified a novel ECM network that is involved in modulating the reprogramming process, but we have also shown that using microRNAs as probes could be an efficient method to study both the intracellular and extracellular molecular mechanisms of reprogramming.

Somatic cell reprogramming is believed to be a stochastic process in which extensive gene network rewiring happens within the reprogramming cells (Hanna et al., 2009). According to the previous report on molecular cornerstones of the reprogramming process (Stadtfeld et al. 2008), the reprogramming factors are only needed during the initial 8 days for cells to become fully reprogrammed. One of the most notable changes in the transition from somatic to embryonic stem cell-like identity is the modulated expression of cell surface antigens. According to previous reports and our own studies, the transition from Thy1+ to Thy1- represents an important early step, where most of the potential iPSCs are present in Thy1- population and significant transcriptional changes occur (Polo et

al., 2012). In this study, we identified miR-135b to be among the most highly induced microRNAs during this key Thy1+ to Thy1- transitional stage and showed that its putative extracellular matrix targets, particularly Wisp1, act as barriers to the reprogramming process.

Wisp1 was first described as a Wnt1-inducible protein (Pennica et al., 1998). It belongs to the CCN gene family that encodes six 30–40 KDa secreted proteins (Berschneider and Konigshoff, 2011; Chen and Lau, 2009). CCN proteins have four conserved structural domains with sequences homologous to insulin-like growth factor binding proteins (IGFBPs), von Willebrand factor type C repeat (VWC), thrombospondin type I repeat (TSP), and carboxyl-terminal (CT) domain. These domains determine the function of CCN member proteins during development and in human diseases. Although Wisp1 has been linked to oncogenic transformation (Pennica et al., 1998; Xu et al., 2000), proliferation and cell survival (Venkatachalam et al., 2009; Venkatesan et al., 2010), and epithelial-to-mesenchymal transition (Konigshoff et al., 2009), little is known about its downstream genes or how it regulates their expression. In this study, we identified several downstream ECM components that were regulated by Wisp1, likely through its interaction with biglycan. These include Tgfbi, Dkk2, Igfbp5, and Nov. These findings provide some new insights into Wisp1 function. For example, TGFBI is a known downstream gene induced by TGFβ signaling and has profound tumor suppressive effects (Ahmed et al., 2007; Zhang et al., 2009). The TGFβ signaling pathway has itself been identified as a barrier for somatic reprogramming (Ichida et al., 2009a; Maherali and Hochedlinger,

2009a). Our finding thus indicates there may be crosstalk between Wisp1 and TGFβ signaling in regulating expression of the ECM protein TGFBI. Knockdown of Wisp1 decreases Tgfbi expression, which might compromise TGFβ signaling and allow cells to become fully reprogrammed. Two other Wisp1 target genes we identified are DKK2 and IGFBP5. DKK2 is known as a Wnt signaling antagonist (Kawano and Kypta, 2003) and IGFBP5 could regulate IGF signaling by binding to IGF-1/2 (Beattie et al., 2006). We found that knockdown of Wisp1 decreased expression of Dkk2 and Igfbp5, which would derepress Wnt and IGF signaling. Consistent with this, previous studies have indicated that Wnt signaling could promote somatic reprogramming (Marson et al., 2008). It was recently shown that IGFBP5 overexpression induces cell senescence in a p53-dependent manner (Kim et al., 2007). This protein is highly expressed in fibroblasts, and its expression is further increased upon senescence (Yoon et al., 2004). Thus, decreased expression of IGFBP5 and DKK2 is likely to be beneficial to iPSC generation. Furthermore, it was recently reported that Wnt signaling also regulates iPSC reprogramming in a stage specific manner in which Wnt inhibits early stage reprogramming but enhances it later (Ho et al. 2013). Our findings are consistent with this biphasic effect and suggest that the Wnt signally pathway may be an underlying or overlapping mechanism in our proposed extracellular matrix regulated model.

Over the past few years much progress has been made in understanding the molecular mechanisms of somatic reprogramming and several important barrier pathways have been discovered. However, these efforts have mainly

focused on intracellular signaling networks, and the effect of the extracellular environment on reprogramming has not been fully explored. In our study, biglycan, a surface glycoprotein that binds Wisp1, is expressed in MEFs but decreases in reprogramming cells, as shown in Thy1$^-$ cells that are enriched with potential iPSCs. These cells will still be stimulated by Wisp1 and presumably other ECM proteins secreted by surrounding feeder MEF cells or unreprogrammed cells, as they still express the receptors such as biglycan, although at much lower level compared with original MEFs. These stimulations would prevent the cells from shutting down MEF-specific regulation networks and compete with four factors-mediated regulatory networks to determine the fate of target cells. Meanwhile, our discovery that microRNAs induced by the four factors can regulate ECM genes reveals some new insights into how the four factors manage to reprogram a small percentage of cells. Down-regulation of MEF-specific ECM proteins seems to be part of the entire reprogramming process and is mediated at least in part by 4F-mediated induction of microRNAs such as miR-135b. Together with previous findings, it is clear that microRNAs are important regulators of reprogramming, both through intracellular and extracellular mechanisms (Figure 2.7).

In summary, we have identified a novel microRNA-mediated pathway of ECM gene regulation that is involved in iPSC generation. Our results indicate that 4F-induced miR-135b expression in turn regulates expression of Wisp1 and Igfbp5. Wisp1 is a key regulator of several ECM proteins, which may be mediated through Wisp1 interaction with biglycan. Our findings not only identify a

novel role for ECM components in somatic cell reprogramming, but also demonstrate that microRNAs can be powerful tools to dissect the intracellular and extracellular molecular mechanisms of iPSC generation.

Chapter 2.4: Materials and Methods

Cell culture, vectors, and virus transduction

Oct4-GFP MEFs were derived from mouse embryos harboring an IRES-EGFP fusion cassette downstream of the stop codon of *pou5f1* (Jackson lab, Stock#008214) at E13.5. MEFs were cultured in DMEM (Invitrogen, 11995-065) with 10% FBS (Invitrogen) plus glutamine and nonessential amino acids (NEAA). Only MEFs at passage 0 to 4 were used for iPSC induction. pMXs-Oct4, Sox2, Klf4, and cMyc were purchased from Addgene. Tgfbi, Dkk2, Igfbp5, Nov, and biglycan overexpression vectors were constructed by inserting cDNA coding sequences into the pMX vector. To generate retrovirus, PLAT-E cells were seeded in 10 cm plates. The next day, the cells were transfected with 9 μg of each vector using Lipofectamine (Invitrogen, 18324-012) and PLUS (Invitrogen, 11514-015). Viruses were harvested and combined 2 days later. For iPSC induction, MEFs were seeded in 12-well plates and the next day were transduced with “four factor” (4F) virus with 4 μg/ml Polybrene. One day later, the medium was changed to fresh MEF medium, and 3 days later it was changed to mES culture medium supplemented with LIF (Millipore, ESG1107). GFP^+ colonies were picked at day 14 post-transduction, and expanded clones were cultured in DMEM with 15% FBS (Hyclone) plus LIF, thioglycerol, glutamine, and NEAA. Irradiated CF1 MEFs served as feeder cells to culture mES and derived iPSC clones.

Recombinant proteins were obtained from commercial sources as follows: mouse Dkk2 (R&D systems, 2435DK/CF), human NOV/CCN3 (R&D systems, 1640NV), human TGFBI (Prospec, #PRO-568), CCL20 (R&D systems, 760-M3)

MicroRNAs, siRNAs, and MEF transfection

microRNA mimics and inhibitory siRNAs were purchased from Dharmacon. To transfect MEFs, microRNA mimics were diluted in Opti-MEM (Invitrogen, 11058-021) to the desired final concentration. Lipofectamine 2000 (Invitrogen, 11668-019) (2 μl/well) was added and the mixture was incubated for 20 min at RT. For 12-well plate transfections, 80 μl of the miR mixture was added to each well with 320 μl of Opti-MEM. Three hours later, 0.8 ml of the virus mixture (for iPSC) or fresh medium was added to each well, and the medium was changed to fresh MEF medium the next day.

Western blotting

Total cell lysates were prepared using M-PER buffer (PIERCE, 78503), incubated on ice for 20 min, and cleared by centrifuging at 13,000 rpm for 10 min. Equal amounts of lysate were loaded onto 10% SDS-PAGE gels. Proteins were transferred to PVDF membranes (Bio-Rad, 1620177) using the semi-dry system (Bio-Rad) and then blocked with 5% milk in Tris-buffered saline–Tween 20 (TBST: 50mM Tris, 150mM NaCl, 0.05% Tween20) for at least 1 hr at room temp or overnight at 4°C. The following antibodies were used: anti-mNanog (R&D Systems, AF2729), anti-h/mSSEA1 (R&D Systems, MAB2156),

anti-TGFBR2 (Cell Signaling, #3713), anti-IGFBP5 (R&D Systems, AF578), anti-actin (Thermo, MS1295P0), anti-AFP (Abcam, ab7751), anti-beta III tubulin (R&D Systems, MAB1368), anti-WISP1 (Santa Cruz Biotechnology, sc-25441) and anti-alpha actinin (Sigma, A7811).

Expression data analysis

Illumina Mouse_miRNA-12 v2 and Illumina Mouse-6 v2 Expression BeadChips were analyzed using the manufacturers BeadArray Reader and primary data was collected using the supplied Scanner software. Data analysis was done in three stages. First, expression intensities were calculated for each gene probed on the array for all hybridizations using illumina's Beadstudio3 software. Second, intensity values were quality controlled and normalized using the Illumina Beadstudio detection with a P-value threshold set to <0.05, thus removing genes which were effectively absent from the array. The initial 379 miRNAs were reduced to 368 following this step. All the arrays were then normalized using the normalize.quantiles routine from the Affy package in Bioconductor. This procedure accounted for any variation in hybridization intensity between the individual arrays. An assessment of several different normalization techniques using the Bioconductor maCorrPlot routine suggested that normalize.quantiles was the most appropriate for the data.

Finally, these normalized data were imported into GeneSpring and analyzed for differentially expressed miRNAs. The groups of biological replicates were included in the analysis and significantly differentially expressed genes

determined on the basis of t-tests and fold difference changes in expression level.

The initial comparison was between the MEF samples (2 biological replicates) and the Thy1- samples (2 biological replicates). Differentially expressed miRNAs were determined by searching for miRNAs with statistically significant differences between the groups based on the results of the Welch t-test (parametric test, variances not assumed equal; p-value cutoff 0.05). This yielded a list of 9-22 genes out of the initial 379. To find the genes with the most robust changes in expression, the data was plotted as a “Volcano Plot” (see Figure 1), which allows statistical significance to be measured along with the extent of fold change in expression. Hence, the outliers are those genes with the highest fold change which is also statistically significant.

mRNA and microRNA RT and quantitative PCR

Total RNAs were extracted using Trizol (Invitrogen), and then 1 μg total RNA was used for RT using Superscript II (Invitrogen). Quantitative PCR was performed using a Roche LightCycler480 II and the SYBR Green mixture from Abgene (Ab-4166). Mouse Ago2, Dicer, Drosha, Gapdh, and p21 primers are defined in Table 2.2. Other primers were described previously (Takahashi and Yamanaka, 2006). For microRNA quantitative analysis, total RNA was extracted using the method described above. Between ~1.5 and 3 μg of total RNA was used for microRNA reverse transcription using QuantiMir kit following the manufacturer’s protocol (System BioSciences, RA420A-1). RT products were

then used for quantitative PCR using the mature microRNA sequence as a forward primer and the universal primer provided with the kit. RT-qPCR data was analyzed using the non-parametric Wilcoxon rank-sum test. * $P<0.05$; ** $P<0.01$; *** $P<0.001$.

Immunostaining

Cells were washed twice with PBS and fixed with 4% paraformaldehyde at room temperature for 20 min. Fixed cells were permeabilized with 0.1% Triton X-100 for 5 min, and then blocked in 5% BSA in PBS containing 0.1% Triton X-100 for 1 hr at room temperature. Primary antibody was diluted at 1:100 to 1:400 in 2.5% BSA PBS containing 0.1% Triton X-100, according to the manufacturer's protocol. Cells were stained with primary antibody for 1 hr and then washed three times with PBS. Secondary antibody was diluted 1:400 and cells were stained for 45 min at room temperature.

Embryoid body formation and differentiation assay

iPSCs were trypsinized to a single cell suspension, and the hanging drop method was used to generate embryoid bodies (EB). For each drop, 4000 iPSCs in 20 µl EB differentiation medium were used. EBs were cultured in hanging drops for 3 days before being reseeded onto gelatin-coated plates. After reseeding, cells were cultured until day 14, when apparent beating areas could be identified.

Teratoma formation

To generate teratomas, iPSCs were trypsinized and resuspended at a concentration of $1x10^7$ cells/ml. Athymic nude mice were anesthetized with Avertin, and 150 µl of iPSCs were injected into each mouse. Tumors were monitored every week for ~3–4 weeks. Tumors were then harvested and fixed in Z-Fix solution for 24 hrs at room temperature, before paraffin embedding, sectioning, and H&E staining. To further evaluate pluripotency of derived iPSC clones, iPSCs were injected into C57BL/6J-Tyr(C-2J)/J (albino) blastocysts. Generally, each blastocyst received 12–18 iPSCs. ICR recipient females were used for embryo transfer.

Chapter 2 is an adapted version of materials published as MicroRNA-mediated regulation of extracellular matrix formation modulates somatic cell reprogramming. Li Z*, Dang J*, Chang KY, Rana TM. (2014). *RNA*. 20(12):1900-15. doi: 10.1261/rna.043745.113. Epub 2014 Oct 21. PMID: 25336587. The dissertation author is the co-first author on this work with Dr. Zhonghan Li.

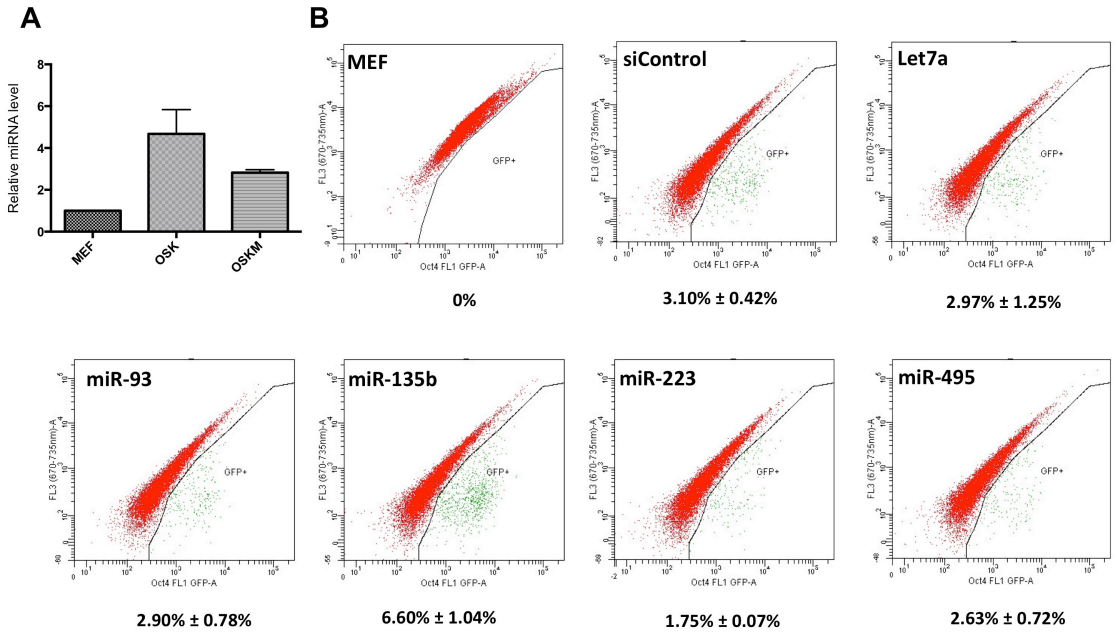

Figure S2.1: miR-135b enhances the overall percentage of Oct4-GFP+ cells during reprogramming

(A) To determine the contribution of Myc to miR-135b induction, RNA was collected 6 days post-transduction in OSKM and OSK infected MEFs and analyzed by RT-qPCR for miR-135b expression.
(B) MEFs were transfected with the indicated microRNA mimics 3 hrs before infection with 4F, and cells were trypsinized on day 14 for FACS analysis. Single cells were collected by filtering through a cell strainer. Non-transduced MEFs served as negative controls.

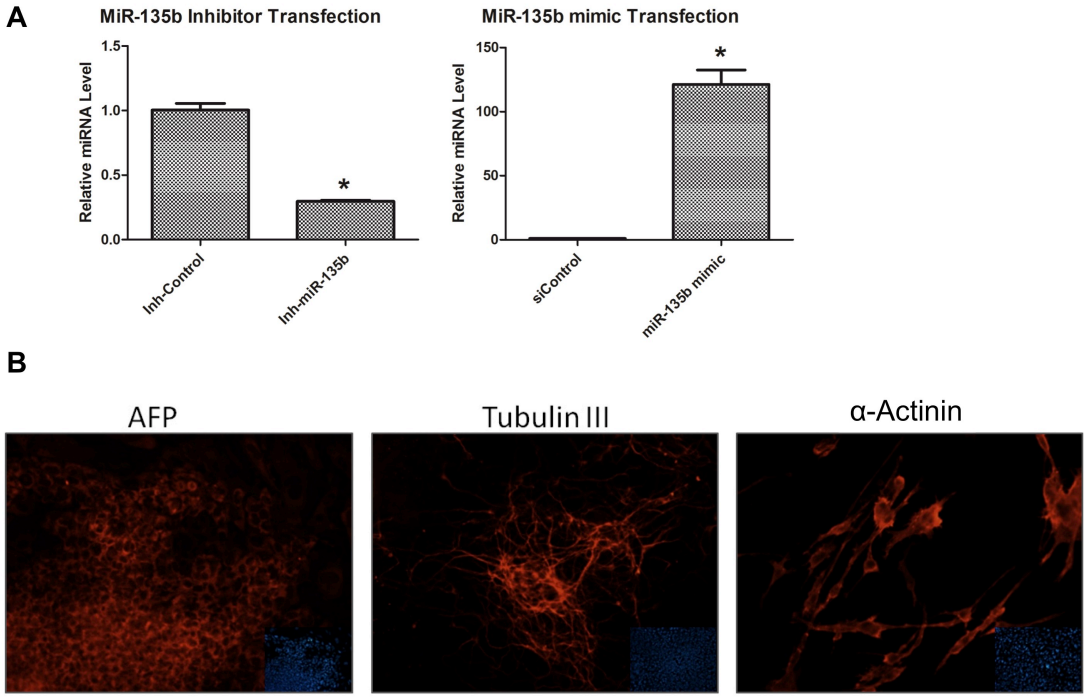

Figure S2.2: miR-135b iPSCs show full differentiation capacity

(A) RT-qPCR analysis of miR-135b levels post-transfection with miR-135b inhibitors or mimics. Error bar represents two independent experiments with duplicate wells. * $p<0.05$.
(B) miR-135b Lineage markers are expressed in differentiated EBs from miR-135b–induced iPSCs. EBs were formed using the hanging drop method for two days and replated onto gelatin-coated plates until day 12-14. Cells were then fixed and stained for AFP (endoderm), tubulin III (ectoderm), and α-actin (mesoderm) expression. DAPI was used for nuclear staining.

A

Gene Names	# of Predicted Sites (miRanda/TargetScan)	Representative Sites	Predicted Energy
Tgfbr2	0/1	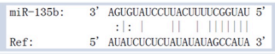	N/A
Wisp1	3/1	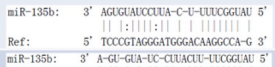	-24.7kcal/mol
Igfbp5	1/0	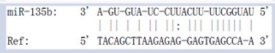	-16.8kcal/mol

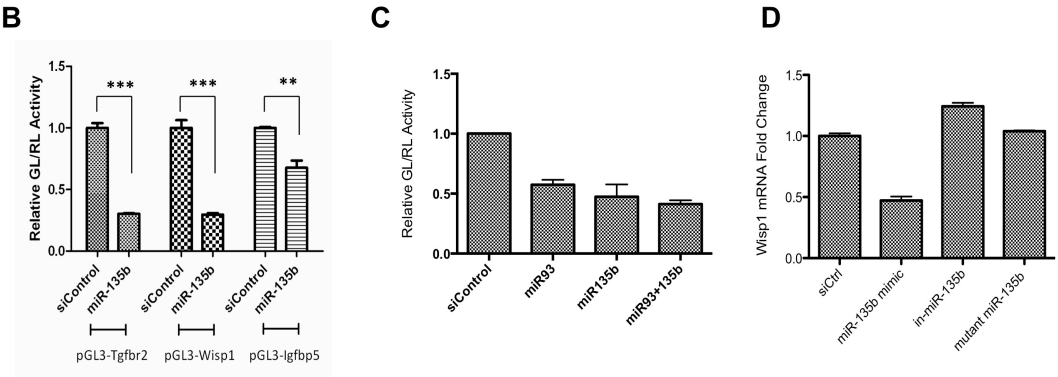

Figure S2.3: Tgfbr2, Wisp1, and Igfbp5 are directly regulated by miR-135b

(A) List of predicted miR-135b target sites identified by both miRanda software and Targetscan in Tgfbr2, Wisp1, and Igfbp5 3'UTRs.
(B) Dual luciferase assay supported direct regulation by miR-135b. The full length Tgfbr2 3'UTR, a Wisp1 fragment, and the Igfbp5 3'UTR were cloned into pGL3 luciferase reporters and transfected into HeLa cells together with pRL-TK. Relative luciferase activity was calculated by the GL/RL signal and normalized to siControl-transfected cells. p values were calculated using Student's *t*-test from at least two independent experiments with duplicate wells.
(C) miR-93 and 135b both targets Tgfbr2. Dual luciferase assays were performed in Hela cells and microRNAs were transfected at 50nM final concentration.
(D) MEFs were transfected with non-targeting siRNA control, miR-135b mimic, miR-135b inhibitor or mutant miR-135b mimic at a final concentration of 50nM for 4 days to verify the direct sequence specificity of the miR-135b and Wisp1 relationship. Total RNAs were extracted for RT-qPCR analysis of Wisp1 mRNA level. Error bar represents experiment with triplicate wells.

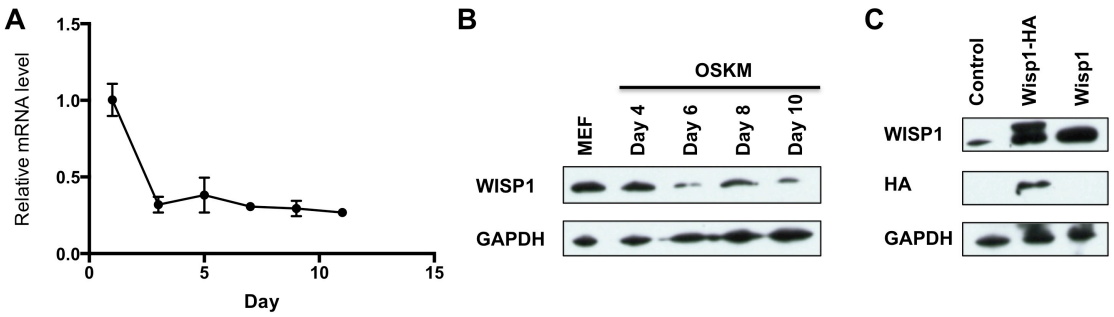

Figure S2.4: Wisp1 kinetics during iPS induction

(A) RNA was isolated from MEF during iPS induction on days 1, 3, 5, 7, 9 and 11. RT-qPCR was performed to analyze Wisp1 mRNA over time course.
(B) Wisp protein levels in MEFs transduced with 4F over the reprogramming time course were analyzed by immunoblotting.
(C) To verify the expression of the HA-tagged Wisp1 construct, immunoblotting was performed to analyze Wisp1 protein and HA expression levels. GAPDH serves as an internal control.

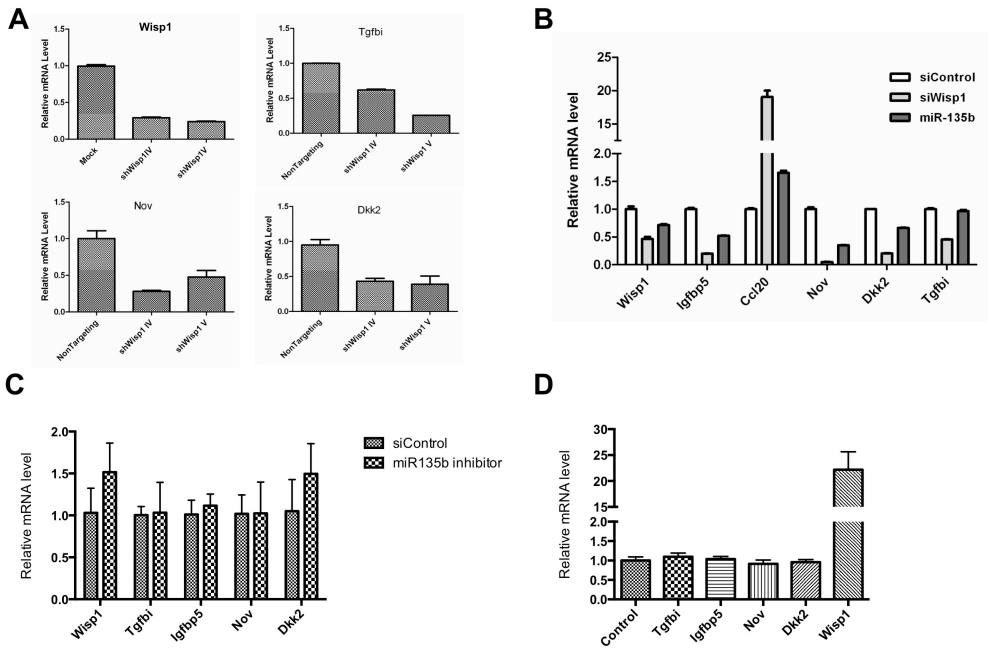

Figure S2.5: Wisp1 regulates ECM gene expression

(A) Wisp1 regulates expression of several ECM genes. Wisp1 was knocked down in MEFs by two shRNAs. Expression of representative ECM genes was examined 4 days post-infection. Expression of Tgfbi, Nov, and Dkk2 were strongly decreased upon Wisp1 knockdown, similar to results from siRNAs transfection (Figure 5A).
(B) Wisp1 ECM target genes are regulated by miR-135b in MEFs. MEFs were transfected with miR-135b mimic at a final concentration of 50 nM for 4 days. Total RNAs were harvested for RT-qPCR analysis of the indicated Wisp1-regulated ECM genes. Error bar represents experiment with duplicate wells.
(C) miR135b indirectly affects Wisp1 regulated ECM genes. Relative MEF mRNA expression of Wisp1, Tgfbi, Igfbp5, Nov and Dkk2 two days after miR-135b hairpin inhibitor transfection.
(D) PCR analysis of Wisp1 mRNA after overexpression of Tgfbi, Igfbp5, Nov, Dkk2 and Wisp1 in MEF

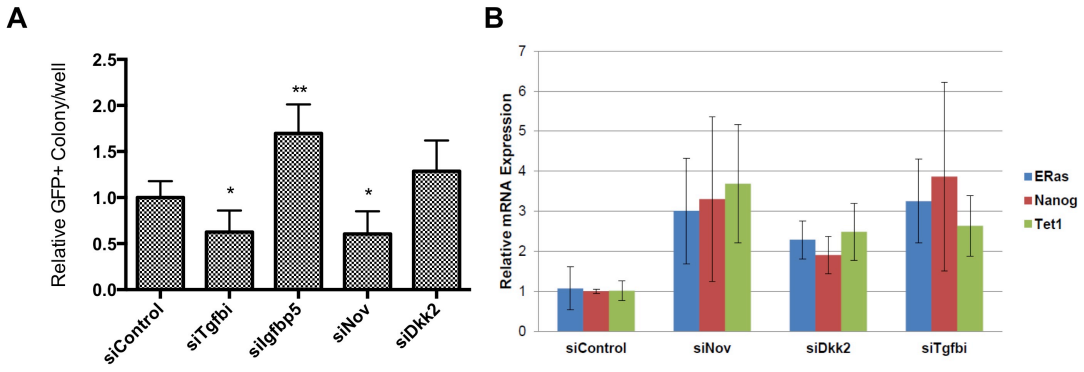

Figure S2.6: Knockdown of Wisp1 target genes promote reprogramming.

(A) Dual role of Wisp1 regulated ECM genes. MEF were transfected with siRNAs on days 0 and 5, and GFP+ colonies were counted from day 12-14. (B) Knockdown of Wisp1 target genes enhances iPSC marker expression. Nov, Dkk2, and Tgfbi were knocked down in 4F-transduced MEFs at day 5 post-transduction. Cells from each well were harvested at around day 14 and total RNAs were extracted for RT-qPCR analysis of the representative mES markers, E-Ras, Nanog, and Tet1. Error bars represent data from three independent wells.

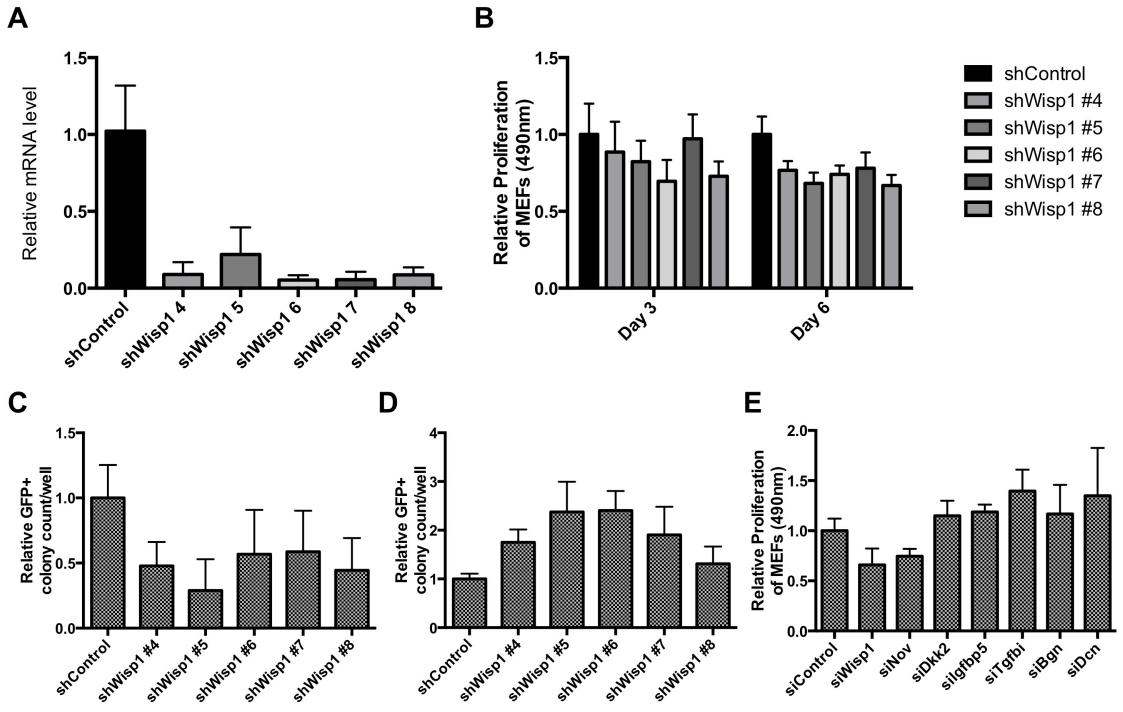

Figure S2.7: Knockdown of Wisp1 compromises proliferation of normal MEFs

(A) Wisp1 was efficiently knocked down by five different shRNAs. Five shRNAs targeting mouse Wisp1 were transduced into MEFs. Knockdown efficiency was evaluated at day 4 post-transduction.
(B) Consistent knockdown of Wisp1 compromised proliferation of MEFs. MEFs were transduced with shRNAs and then reseeded into 96-well plates. Proliferation of MEFs was measured on days 3 and 6 using Celltiter 96 One Solution assay (Promega, G3582).
(C and D) iPSC induction was evaluated for MEFs transduced with shRNAs targeting Wisp1 on day 0 (C) or day 5 (D).
(E) The effect of siRNA mediated knockdown of Wisp1 interacting proteins Nov, Dkk2, Igfbp5, Tgfbi, Bgn and Dcn on MEF proliferation was assessed on day 6 post-transfection by Celltiter 96 One Solution assay.

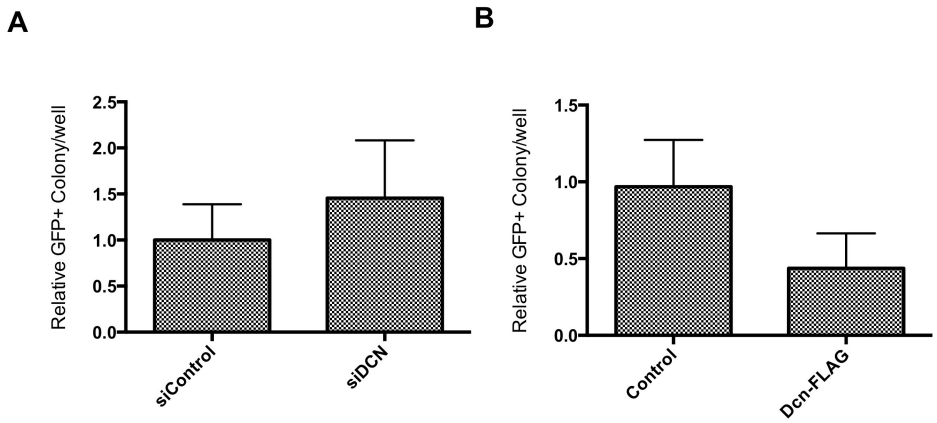

Figure S2.8: Role of decorin knockdown and overexpression in iPS induction
(A) Decorin was knockdown or (B) overexpressed at day 5 and GFP+ colonies were counted on day 12-14 post OSKM transduction.

Table 2.1: miR-135b target site analysis
Genes showing significantly repressed expression upon miR-135b transfection were analyzed with miRanda and TargetScan to identify potential miR-135b target sites in their 3'UTR regions. Sites with good seed match and significant predicted energy are listed.

Table 2.2: Original microRNA expression profile data
List of microRNAs significantly (2-fold, $p<0.05$) altered at reprogramming day 5 in Thy1- cells.

Table 2.3: mRNA expression profile upon miR-135b transfection
Significantly altered mRNAs upon miR-135b mimic transfection are listed.

Table 2.4: mRNA microarray data upon Wisp1 knockdown
Significantly altered mRNAs upon siWisp1 transfection are listed.

CHAPTER 3: Modeling ZIKV pathogenesis using cerebral organoids

Chapter 3.1: Introduction

Zika virus (ZIKV) of the Flaviviridae family is an emerging mosquito-borne virus originally identified in Uganda in 1947 (Driggers et al., 2016b). Outbreaks of the virus have been previously recognized in regions within Asia and Africa, including Malaysia, Thailand, Vietnam and as far as Micronesia (Driggers et al., 2016b; Hamel et al., 2015). ZIKV infects human skin and over 80% of ZIKV cases are asymptomatic or go unnoticed while the remaining cases typically exhibit mild fever, rash and joint pain for a period of 7 days (Hamel et al., 2015; Petersen et al., 2016a). However, with the increased incidence due to the current outbreak of ZIKV in Brazil and throughout Latin America, new data suggests a positive correlation between cases of infection and the rise of microcephaly, characterized by abnormally small brains (Driggers et al., 2016a; Mlakar et al., 2016; Petersen et al., 2016a).

In fact, ZIKV was detected by electron microscopy and RT-qPCR in brains and amniotic fluid of microcephalic fetuses, strengthening the causal link between ZIKV and increased incidence of microcephaly (Calvet et al., 2016b; Mlakar et al., 2016). Furthermore, recent studies show that ZIKV can infect human iPSC-derived neural progenitors in vitro, resulting in dysregulation of cell cycle related pathways and increased cell death (Tang et al., 2016). Evidence thus far suggests a strong causal relationship between ZIKV and microcephaly.

To investigate the mechanisms by which ZIKV induces microcephaly and other neurological disorders, it is essential to use scalable, reproducible in vitro models capable of recapitulating complex neurodevelopmental events during early embryogenesis. Because of the lack of outer subventricular zone (OSVZ) in mice and unknown relevance of ZIKV in mice, here we used human embryonic stem cell-derived cerebral organoids to investigate the role of ZIKV in microcephaly. Here we show that cerebral organoids generated from human embryonic stem cells mimic the developing fetal brain and develop malformations and severely inhibited growth following ZIKV inoculation. By analyzing the transcriptomic profile of developing organoids, we draw parallels between the stunted development of ZIKV infected organoids and TLR3-mediated dysregulation of neurogenesis and axon guidance.

Chapter 3.2: Results

Cerebral Organoids Display Regionalization and Cortical Differentiation

To model ZIKV infection in vitro in physiologically relevant models, cerebral organoids were generated from H9 human embryonic stem cells using published protocols (Lancaster et al., 2013) with slight modifications described in the Methods section. To generate cerebral organoids, embryoid bodies were formed from embryonic stem cells using the hanging drop method and differentiated to form neuroectodermal tissue in three-dimensions (Figure 3.1A). Cerebral organoids display complex, self-organized internal morphology with

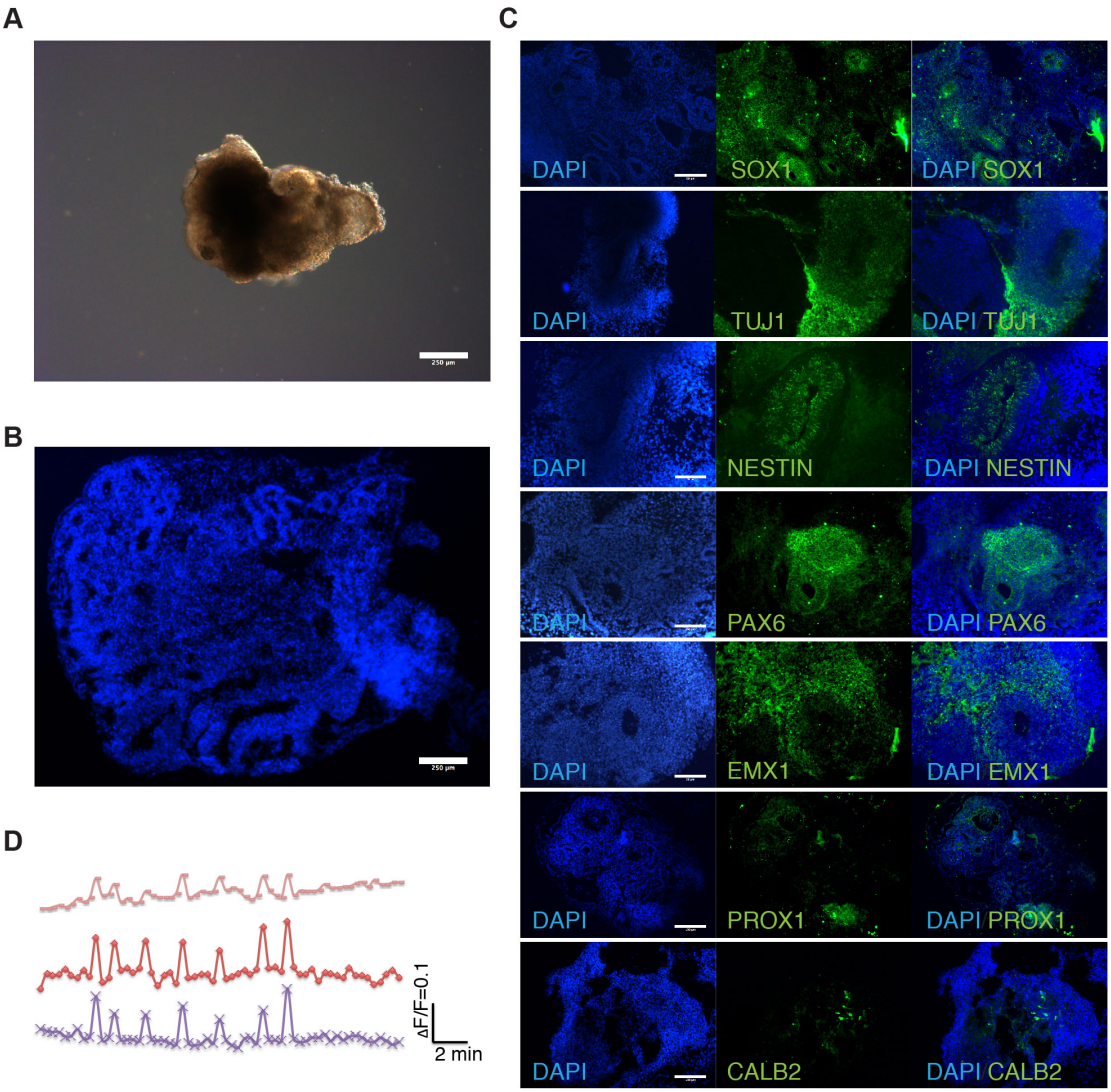

Figure 3.1: Characterization of cerebral organoids reveals recapitulation of fetal brain regions.

(A) Bright-field image of representative organoids show development of neuroepithelial layer. Scale bar: 250μm.
(B) DAPI stained organoid shows complex inner morphology including ventricle-like structures from 30-day-old organoids. Scale bar: 250μm.
(C) Organoids immunostained for neuronal (TUJ1+) and neural progenitor cells (SOX1+) cells. TUJ1 shows generalized neuronal differentiation while neural progenitors are localized near inner ventricle-like structures in 30-day-old organoids. Immunostaining for forebrain (PAX6), dorsal cortex (EMX1), hippocampus (PROX1) and interneurons (CALB2) show differentiation of organoids into discrete brain regions 30-day-old organoids. Also see Figure S1. Scale bar: 100μm.
(D) Calcium dye imaging of cerebral organoids using Fluo-4 shows functional neural activity.

fluid-filled ventricle-like structures similar to the developing cerebral cortex (Figure 3.1A, B). Immunohistochemistry for TUJ1 and SOX1 identify regional specificity of neuronal and neural progenitor populations, respectively (Figure 3.1C and S3.1). NESTIN positive cells exhibit elongated morphology around cavities. TUJ1 staining shows broad neuronal expression throughout the organoid tissue while SOX1 neural progenitors (NPCs) are localized in internal cavities, thereby emulating the intricate radially outward migratory pattern of differentiating neurons from the inner multiplication zone of the fetal brain.

To determine the regionalization and extent of cortical differentiation and expansion, organoids were immunostained for markers of early forebrain, hippocampus dorsal cortex and interneurons (Figure 3.1C). PAX6 and FOXG1 expression highlight the discrete organization of early forebrain tissue formation and specification to the ventral telencephalon. In addition, EMX1 expression shows subregionalization of dorsal cortex regions around cavities and throughout the intermediate zone. PROX1 indicates differentiation of a portion of cerebral organoid tissue to the hippocampus while CALB2 signifies the maturation of organoid neural progenitor cells into hippocampal calretinin expressing interneurons. To confirm functional neural activity in cerebral organoids, fluctuations in cytosolic calcium content were analyzed by calcium dye imaging in response to glutamate (Figure 3.1D).

Figure 3.2: RNA map of Cerebral Organoids development

(A) Heat map of transcriptome analysis from human embryonic stem cells (Group 1) and cerebral organoids after 1 month (Group 2) and 2 months (Group 3) in culture show 3226 and 3357 significantly differentially expressed genes with fold change >2, p-value <0.05. See also Figure S2A. See Table 3.1.
(B) Gene ontology analysis show top 10 more enriched terms for upregulated (top) and downregulated (bottom) genes during cerebral organoid differentiation.
(C) Grouped functional pathway analysis of differentially expressed genes during organoid formation.
(D) Heat map of differentially expressed genes between organoids 1 month (Group 2) and 2 months (Group 3) in culture. Group 1 represents human embryonic stem cells.
(E) Gene ontology analysis of differentially expressed genes in organoids 1 and 2 months old suggest formation of retinal tissue.
(F-G) Spearman's correlation heat map of cerebral organoid transcriptomes compared with regions of the fetal brain and age post conception weeks (pcw). See Table 3.2 for heat map brain region legend. Also see Figure S2B and S2C.

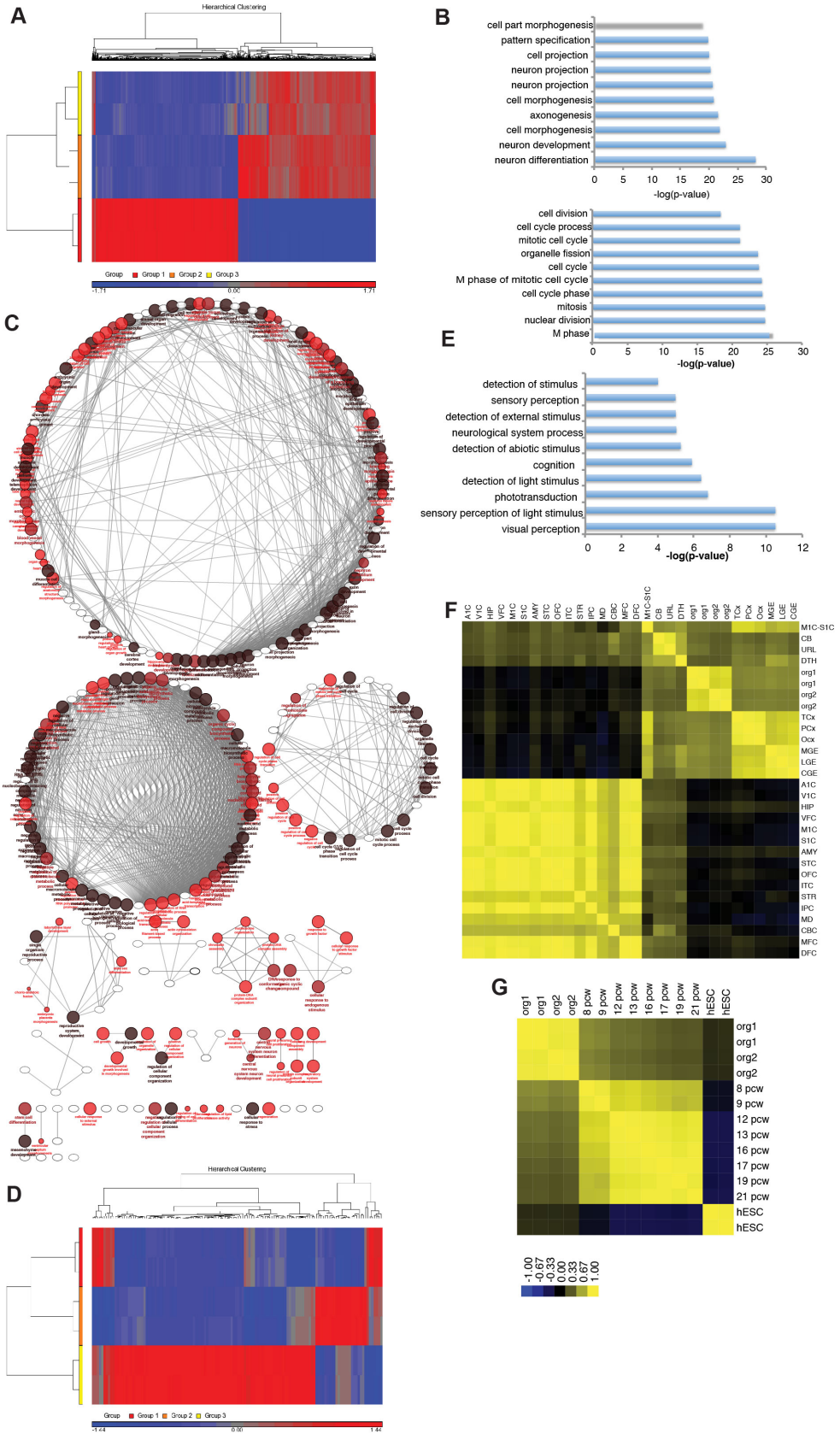
A
Hierarchical Clustering
Group Group 1 Group 2 Group 3
B
cell part morphogenesis
pattern specification
cell projection
neuron projection
neuron projection
cell morphogenesis
axonogenesis
cell morphogenesis
neuron development
neuron differentiation
0 5 10 15 20 25 30
-log(p-value)
cell division
cell cycle process
mitotic cell cycle
organelle fission
cell cycle
M phase of mitotic cell cycle
cell cycle phase
mitosis
nuclear division
M phase
0 5 10 15 20 25 30
-log(p-value)
C
E
detection of stimulus
sensory perception
detection of external stimulus
neurological system process
detection of abiotic stimulus
cognition
detection of light stimulus
phototransduction
sensory perception of light stimulus
visual perception
0 2 4 6 8 10 12
-log(p-value)
F
A1C V1C HIP VFC M1C S1C AMY STC OFC ITC STR IPC MD CBC MFC DFC M1C-S1C CB URL DTH org1 org1 org2 org2 TCx PCx Ocx MGE LGE CGE
M1C-S1C
CB
URL
DTH
org1
org1
org2
org2
TCx
PCx
Ocx
MGE
LGE
CGE
A1C
V1C
HIP
VFC
M1C
S1C
AMY
STC
OFC
ITC
STR
IPC
MD
CBC
MFC
DFC
G
org1 org1 org2 org2 8 pcw 9 pcw 12 pcw 13 pcw 16 pcw 17 pcw 19 pcw 21 pcw hESC hESC
org1
org1
org2
org2
8 pcw
9 pcw
12 pcw
13 pcw
16 pcw
17 pcw
19 pcw
21 pcw
hESC
hESC
-1.00 -0.67 -0.33 0.00 0.33 0.67 1.00
D
Hierarchical Clustering
Group Group 1 Group 2 Group 3

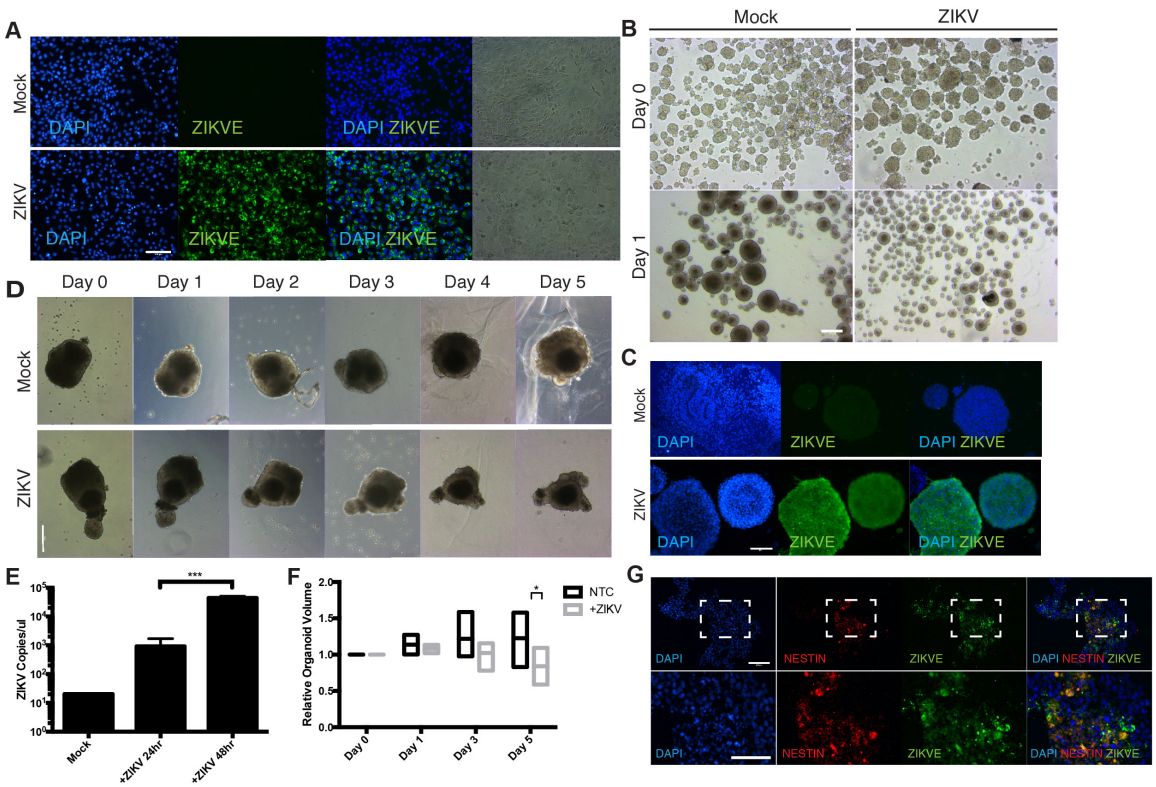

Figure 3.3: ZIKV results in attenuated organoid growth in cerebral organoids and neurospheres through activation of TLR3

(A) ZIKV infected Vero cells for virus expansion. Vero cells were seeded and infected at MOI of 1 and viral supernatant was collected 48 hours post inoculation. Scale bar 100μm.
(B) Bright-field images of mouse neurospheres at Day 0 and Day 1 post-inoculation with ZIKV. Scale bar: 250μm.
(C) Immunohistochemistry shows ZIKV can robustly infect mouse neurospheres. Scale bar: 50μm.
(D) Representative bright-field images of individual human cerebral organoids treated with ZIKV over time. Scale bar: 250μm.
(E) ZIKV viral copy count in organoid supernatant quantified by one-step RT-qPCR after ZIKV infection shows organoid susceptibility and viral permissiveness. *** p-value<0.001, Student's t-test.
(F) Quantification of organoid size over time with and without ZIKV infection. Bars represent the min, average and max relative organoid size. Individual organoids were measured over time relative to their respective Day 0 size from n=5 organoid samples * p-value<0.05, Student's t-test.
(G) Representative images of ZIKV treated organoids stained for ZIKV envelope protein and Nestin. Scale bar: 100μm.

Cerebral Organoids Recapitulate Early Fetal Brain Development

Next, we compared the coding and non-coding transcriptome of H9 human embryonic stem cells and their derived cerebral organoids to further characterize the cerebral organoid models. 3226 and 3357 significantly differentially expressed genes with fold change >2 were identified in one month and two month old organoids when compared with undifferentiated H9 cells (Figure 3.2A and S3.2A). Gene ontology analysis of the 1642 differentially upregulated genes between organoids and embryonic stem cells show significant enrichment of genes related to neuron differentiation, development, cell morphogenesis, cell projection, axonogenesis, pattern specification and regionalization, confirming the previously shown immunostaining results (Figure 3.2B). On the other hand, RNA-seq analysis shows enrichment of cell cycle and mitosis related pathways in the 1584 differentially expressed downregulated genes during organoid formation, as expected. Pathway analysis of differentially expressed genes showed functionally grouped networks of developmental, neurogenesis, transcriptional, metabolic, cell cycle and cytoskeletal genes in cerebral organoid development (Figure 3.2C). In addition, transcriptome analysis of organoids 1 month and 2 months in culture reveal an increase in genes related to visual perception, sensory and stimulus perception, phototransduction and cognition, indicating the early formation of immature retinal tissue as cerebral organoids further develop (Figure 3.2D, E).

RNA-seq transcriptome data was then analyzed to contextualize cerebral organoids in terms of fetal brain development. Using the BrainSpan database of

human brain transcriptomes, we calculated the Spearman's correlation between in vitro differentiated cerebral organoids with post-mortem human fetal brain tissues to further assess their age and regionalization (Figure 3.2F, G and S3.2B) (Kang et al., 2011). Based on these analyses, organoids showed significant correlation great than 0.5 between post-mortem neocortex (temporal, parietal and occipital), ganglionic eminence (medial, lateral and caudal), cerebellum, primary motor sensory cortex, upper rhombic lip and dorsal thalamus. In addition, organoids were correlated with post-mortem fetal tissues ranging in age from 8 weeks post-conception to 21 weeks post-conception. These data indicate that the organoid tissues most resemble early trimester fetal brain tissues 8-9 weeks post-conception (Figure 3.2G and S3.2C). In all, immunohistochemistry and transcriptome analyses suggest that human embryonic stem cell-derived cerebral organoids robustly and reproducibly model early trimester fetal brains.

ZIKV Infection Abrogates Organoid Growth

To determine the effect of ZIKV on fetal brain tissue in vitro, mouse neurospheres and early day 10 human cerebral organoids were infected with the prototype MR766 ZIKV strain originating from Uganda, isolated from monkeys and expanded in Vero cells (Figure 3.3A). Mouse neurospheres were utilized because of the large sample size and previous data suggesting robust reservoirs of ZIKV viral infection, ZIKV production in mouse brain tissues and the ability to recapitulate neurodegenerative phenotypes in vivo (Lazear et al., 2016; Rossi et

al., 2016). ZIKV infected neurospheres exhibited significantly attenuated growth relative to control mocked treated samples (Figure 3.3B, C).

To further confirm the negative effect of ZIKV on neurodevelopment, immature day 10 human organoids were utilized for ZIKV infection because it coincides with the emergence of the neuroepithelial layer and transition from embryoid body to cerebral organoid. Cerebral organoid growth was tracked over 5 days post-infection to monitor organoid growth and development. At day 5 post-infection, healthy mock treated cerebral organoids showed an average of 22.6% increase in growth while ZIKV infected organoids significantly decreased by 16%, thus resulting in a net 45.9% difference in size on average (Figure 3.3D, F). The viral kinetics indicate a significant increase in viral copy number two days post-infection, which is reflected in the rate of change in organoid size after day 2 post-infection (Figure 3.3E, F).

To probe the effect of ZIKV in fetal brain development and in neural progenitor cells, we cryosectioned and immunostained cerebral organoids for markers of neural progenitor cells (NESTIN) and ZIKV envelope (ZIKVE) expression. We observed strong co-localization of ZIKVE in NESTIN+ cell populations compared to NESTIN- cells indicating that ZIKV infects NPCs in organoid models (Figure 3.3G) (Tang et al., 2016). The non-elongated cell morphology of ZIKV infected NESTIN+ cells suggests an unhealthy state and activation of apoptotic processes. Since neural progenitors and radial glial cells may be susceptible to ZIKV and infection, RT-qPCR of organoid supernatant reveals ZIKV replication and permissiveness of organoid tissues (Figure 3.3E).

Taken together, these results demonstrate that ZIKV abrogates neurodevelopment by targeting the neural progenitor population.

ZIKV attenuates organoid growth by TLR3 activation and regulation of apoptosis and neurogenesis pathways

Previous studies have shown that ZIKV and other flaviviruses activate TLR3 in human skin fibroblasts (Hamel et al., 2015; Tsai et al., 2009). Interestingly, TLR3 has been implicated in many neuroinflammatory and neurodegenerative disorders, including in NPCs (Cameron et al., 2007; Lathia et al., 2008; Okun et al., 2010; Okun et al., 2011). *TLR3* is upregulated in cerebral organoids and neurospheres after ZIKV infection as shown by RT-qPCR analysis (Figure 3.3E and S3.3C). To investigate the link between ZIKV-mediated TLR3 activation and dysregulation of neurogenesis and apoptosis, we investigated the effect of TLR3 agonist poly(I:C) and a thiophenecarboxamidopropionate compound that acts as a direct, competitive and high affinity inhibitor of TLR3 inhibitor on mouse neurospheres and human organoids. To determine the effect of TLR3 activation, neurospheres were challenged with poly(I:C) and exhibited a statistically significant decrease in overall neurosphere size relative to mock treated organoids (n>100 neurospheres per group) (Figure 3.4A, B and S3.3A). To further reinforce the idea that TLR3 plays a key role in ZIKV-mediated microcephaly, neurospheres were inoculated with ZIKV with TLR3 competitive inhibitor (Figure 3.4B and S3.3B). We observed a statistically significant difference between ZIKV treated neurospheres with and without

Figure 3.4: ZIKV induces TLR3 and regulates pathways involved in apoptosis and neurogenesis

(A) Bright-field images of mouse neurospheres at Day 0 and Day 1 post-inoculation with ZIKV with or without TLR3 competitive inhibitor, or TLR3 agonist poly(I:C). Scale bar: 250μm.
(B) Neurospheres show significant change in size 1 day post-inoculation with ZIKV with or without TLR3 competitive inhibitor, or TLR3 agonist poly(I:C) as quantified by ImageJ. Box and whiskers plot show 10-90 percentile. * p-value<0.05. *** p-value<0.001. n.s. = not significant, Student's t-test.
(C) Representative bright-field images of individual human cerebral organoids treated with ZIKV with or without TLR3 competitive inhibitor. Scale bar: 250μm.
(D) Schematic of target selection for RT-qPCR analyses. Differentially genes involved in organoid formation (from Figure 2A) and TLR regulated genes (data not shown) were analyzed to identify common pathways activated upon ZIKV infection. The two significantly enriched pathways from this dataset were "positive regulation of nervous system development" and "regulation of synapse structure or activity."
(E) RT-qPCR analysis of *TLR3* upregulation in organoids mock and ZIKV treated. Error bars represent SEM.
(F) RT-qPCR analysis of differentially expressed genes, *NTN1* and *EPHB2*, involved in TLR3 activation and neurogenesis in organoids treated with TLR3 agonist poly(I:C). Error bars represent SEM. * p-value<0.05. ** p-value<0.01, Student's t-test.
(G) RT-qPCR analysis of *NTN1* and *EPHB2* expression in human organoids upon ZIKV and ZIKV+ TLR3 competitive inhibitor. * p-value<0.05. *** p-value<0.001, Student's t-test.
(H) Model for ZIKV infection and TLR3 mediated downregulation of regulators of neurogenesis and upregulation of pro-apoptotic pathways in NPCs.

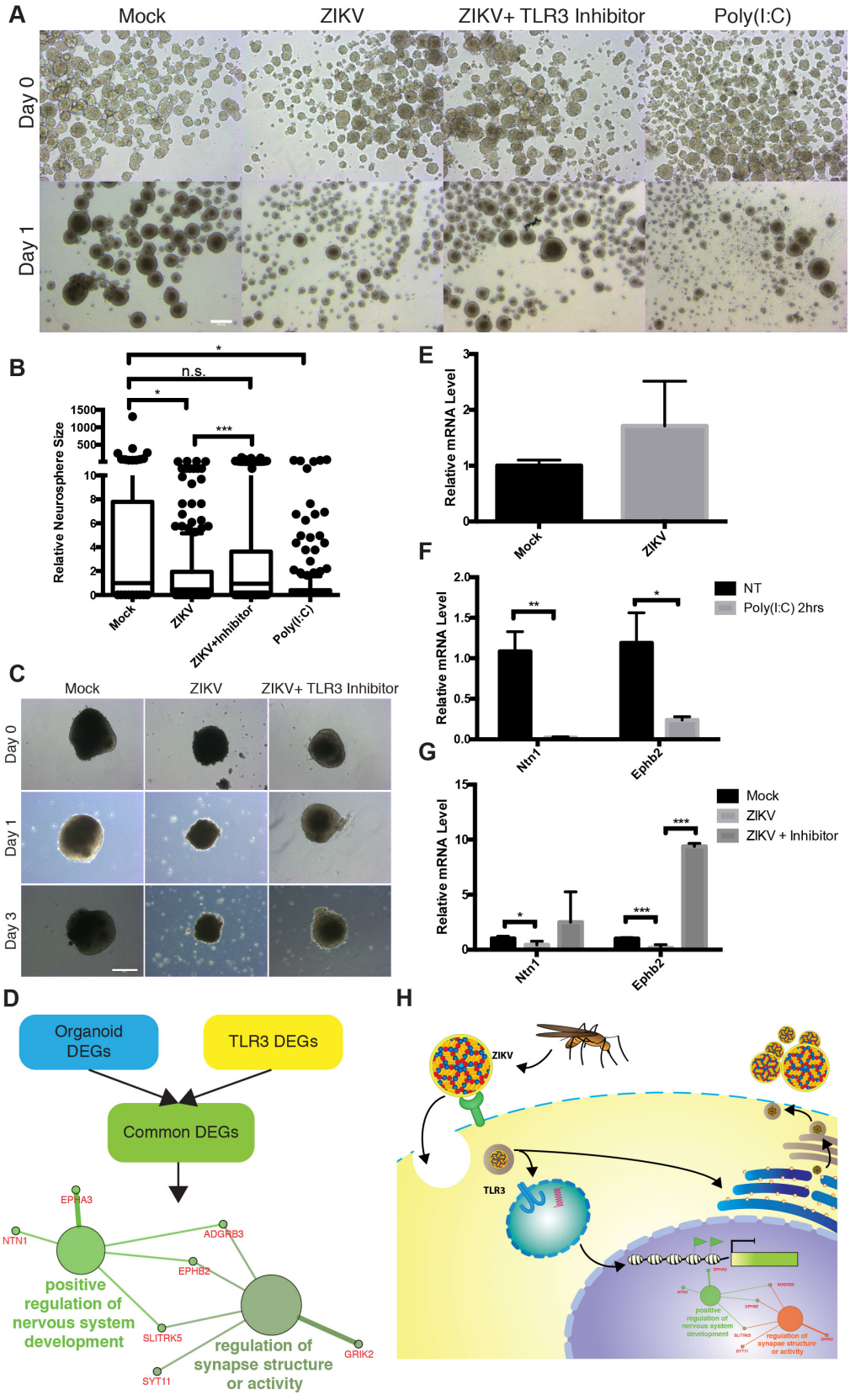
A
Mock
ZIKV
ZIKV+ TLR3 Inhibitor
Poly(I:C)
Day 0
Day 1
B
n.s.
*
***
Relative Neurosphere Size
1500
1000
500
10
8
6
4
2
0
Mock
ZIKV
ZIKV+Inhibitor
Poly(I:C)
C
Mock
ZIKV
ZIKV+ TLR3 Inhibitor
Day 0
Day 1
Day 3
D
Organoid DEGs
TLR3 DEGs
Common DEGs
EPHA3
NTN1
ADGRB3
EPHB2
SLITRK5
SYT11
GRIK2
positive regulation of nervous system development
regulation of synapse structure or activity
E
Relative mRNA Level
3
2
1
0
Mock
ZIKV
F
Relative mRNA Level
2.0
1.5
1.0
0.5
0.0
**
*
NT
Poly(I:C) 2hrs
Ntn1
Ephb2
G
Relative mRNA Level
15
10
5
0
*
***
***
Mock
ZIKV
ZIKV + Inhibitor
Ntn1
Ephb2
H
ZIKV
TLR3

TLR3 inhibitor but no statistical significance between mock and ZIKV+inhibitor groups.

To validate our hypothesized link between ZIKV-mediated TLR3 activation and dysregulation of neurogenesis and apoptosis in an orthogonal human model, organoids were treated with TLR3 competitive inhibitor in the presences of ZIKV. Although there still appears to be cell death and disruption of the developing neuroepithelium characterized by the non-smooth outer surface of the organoid, but the TLR3 competitive inhibitor attenuated the severe ZIKV-mediated apoptosis and organoid shrinkage see in ZIKV only treated organoids (Figure 3.4C). These data strongly suggest that TLR3 may play a pivotal role in the ZIKV associated phenotype.

To determine the role of TLR3 activation in neurodegeneration, we compared differentially expressed genes involved in cerebral organoid formation identified by RNA-seq with differentially expressed genes following poly(I:C)-challenged TLR3 activation (data not shown) and found 41 genes in common (Figure 3.4D). Pathway analysis was performed to identify potential pathways by which ZIKV may regulate neurogenesis. Intriguingly, from these 41 genes, only networks relating to positive regulation of nervous system development and regulation of synapse structure or activity were significantly enriched (Figure 3.4D). To validate the proposed genes regulated by TLR3 that modulate neurogenesis and apoptosis in organoid development, *NTN1* and *EPHB2* expression levels were analyzed by RT-qPCR with ZIKV+/-inhibitor or poly(I:C) stimulation (Figure 3.4E, F and G). Consistent with ZIKV infection, poly(I:C)

treatment of organoids reduced *NTN1* and *EPHB2* expression (Figure 4F). In addition, TLR3 competitive inhibitor reversed the downregulation of *NTN1* and *EPHB2* by ZIKV infection (Figure 3.4G). Altogether, these data suggest that ZIKV perturbs a TLR3 regulated network controlling neurogenesis and apoptotic pathways (Figure 3.4H).

Chapter 3.3: Discussion

Here we report the generation and application of human embryonic stem cell-derived cerebral organoids for modeling and analyzing the relationship between ZIKV and microcephaly. To properly model the complexities of the fetal brain, we employed three-dimensional organoid models capable of recapitulating regions of the developing neocortex, ganglionic eminence and retinal tissue as evidenced by immunohistochemistry and transcriptomic analyses. These in vitro cerebral organoid models present a scalable and reproducible platform for neurodevelopmental and neurodegenerative studies. Organoids were then treated with prototype MR766 ZIKV to understand the phenotypic and transcriptomic response during early stage neural development. Organoids treated with ZIKV showed significant decrease in the neuroepithelium and overall organoid size.

Neurological manifestations, such as viral encephalitis, have previously been linked to other viruses of the Flaviviruses genus (Sips et al., 2012). TLR3 has been linked to neurodegenerative disorders and negative regulation of

axonogenesis, as well as dengue and ZIKV infection, so we hypothesized that ZIKV activates the TLR3 pathway in neural progenitor cells, thereby leading to pro-apoptotic pathway activation and/or dysregulation of cell fate decisions (Cameron et al., 2007; Hamel et al., 2015; Okun et al., 2010; Okun et al., 2011; Tsai et al., 2009; Yaddanapudi et al., 2011). As seen in microcephaly, dysregulated cell fate, self-renewal and apoptotic pathways in NPCs may contribute to the microcephaly phenotype. TLR3 is highly expressed in early brain development and decreases as the NPC population differentiations and the brain matures (Lathia et al., 2008). This temporally sensitive expression of TLR3 during early brain development may contribute to the trimester-specific response of fetal brains to ZIKV infection. Induction of TLR3 has been shown to trigger apoptosis by inhibiting Sonic Hedgehog and Ras-ERK signaling in NPCs and plays a role in retinopathy (Shiose et al., 2011; Yaddanapudi et al., 2011). Moreover, TLR3 has been connected to the elevated risk of neuropathological dysfunction resulting from maternal infection using TLR3-deficient mouse models (De Miranda et al., 2010). Based on these data, TLR3 likely plays a dual role that is cell type specific in which potent downstream anti-viral responses are activated in addition to tangential dysregulation of signaling networks directing apoptosis and neurogenesis.

By comparing changes in the transcriptomic profiles during cerebral organoid formation and after TLR3 activation by poly(I:C), we identified several candidate genes (*NTN1*, *EPHA3*, *ADGRB3*, *EPHB2*, *SLITRK5*, *SYT11* and *GRIK2*) that may be responsible for depletion of the neural progenitor population

and the subsequent microcephaly phenotype through pathway analysis. Many of these TLR3 activated genes have been implicated in early brain cell fate decisions. Netrin1 is a secreted protein that works in conjunction with its dependence receptor DCC (Deleted in Colorectal Carcinoma) to regulate various pathways involved in axon guidance, apoptosis, neural cell death and cellular reprogramming (Bin et al., 2015; Furne et al., 2008; Ozmadenci et al., 2015). The role of NTN1 has been shown in vivo in floxed and null NTN1 mice. Complete loss of the gene results in severe axon guidance defects and death shortly after birth (Bin et al., 2015). Evidence suggests that NTN1 interacts with DCC to limit apoptosis but additional data has shown that the absence of NTN1 can also upregulate DCC, thus additionally triggering a pro-apoptotic cascade (Bin et al., 2015). In addition to NTN1, the membrane-bound receptor tyrosine kinase EPHB2 has been shown to be integral to fetal brain development by regulating angiogenesis, vasculogenesis and neurogenesis. EPHB2 modulates radial migration, proliferation and cell fate of neural progenitor cell in the subventricular zone (Chumley et al., 2007; Katakowski et al., 2005). Interestingly, NTN1 and EPHB2 have been shown to work synergistically through the Src family kinase-signaling pathway during neural circuit assembly (Poliak et al., 2015). However, further mechanistic studies will be required to validate the significance and underlying molecular mechanisms by which these putative genes potentially cause viral-mediated microcephaly. Nonetheless, our results present evidence that TLR3 activation of multiple genetic hubs regulating axonogenesis, cell proliferation and anti-apoptotic pathways within NPCs may strongly contribute to

the ZIKV mediated microcephaly phenotype using robustly reproducible and scalable human cerebral organoid models.

Chapter 3.4: Materials and Methods

Cerebral organoid differentiation

H9 human embryonic stem cell (hESCs) (WA09) from WiCell was cultured on a feeder layer of irradiated mouse embryonic fibroblasts following previously established protocols. All studies were conducted in accordance with approved IRB protocols by the University of California, San Diego. All animal work was approved by the Institutional Review Board at the University of California, San Diego and was performed in accordance with Institutional Animal Care and Use Committee guidelines. H9 hESCs were detached from their feeder layer using 1mg/ml collagenase for 15-20 minutes and 0.5mg/ml dispase for an additional 15 minutes. Wells were washed with media to collect floating undifferentiated hESCs and colonies were dissociated using Accumax at 37°C for 10 minutes to generate a single cell suspension. At day 0, embryoid bodies were formed using the hanging drop method with 4500 cells/drop in DMEM/F12 media supplemented with 20% knockout serum replacement, 4ng/ml bFGF, NEAA and glutamine. After 2 days of hanging drop culture, embryoid bodies were transferred to sterile petri dishes with refreshed media. After 6 days in culture, embryoid bodies were transferred to new petri dishes containing neural induction media consisting of DMEM/F12, 1:100 N2 supplement, NEAA, glutamine and 1ug/ml heparin until day 11. At day 11, organoids were transferred to Matrigel droplets and cultured in 1:1 mixture of DMEM/F12 and Neurobasal medium supplemented with 1:100 B27 without vitamin A, 1:200 N2, NEAA, insulin, beta-mercaptoethanol and glutamine. Organoids were then transferred to stir flask

bioreactors for long term growth on day 15 in the same differentiation media except with the addition of retinoic acid and vitamin A. Media was changed every 3 days.

ZIKV expansion and infection

To expand prototype MR766 virus, Vero cells were inoculated with virus at MOI of 1 in E-MEM 10% FBS medium. Media was changed 24 hours after inoculation and viral supernatant was collected at 48 hours post-inoculation. Viral titer was assessed using iScript One Step RT-PCR kit (Bio-Rad) and viral copy number was calculated based on a standard curve of in vitro transcribe viral transcripts. Organoids were inoculated with ZIKV at MOI of 1.

Neurosphere Culture

Briefly, hippocampal single cells were plated in 12-well plates in suspension at a density of 5x104 cells/well in neurobasal medium containing B27, N2, bFGF and EGF. Media was changed following viral inoculation and TLR3 inhibition and activation. Images were acquired on a Leica DMI 3000B. Neurosphere sizes were estimated using ImageJ to by adjusting the color threshold and using the “Analyze Particle” tool.

Immunohistochemistry

To section and stain organoids, organoids were washed with PBS and incubated in cell recovery solution for 30 minutes to dissolve the surrounding

Matrigel. Organoids were washed with PBS and then fixed with 4% paraformaldehyde for 1 hour. Fixed organoids were washed three times with PBS, stained with hematoxylin for 5 minutes and incubated in 30% sucrose overnight. Sucrose solution was removed, organoids were washed with PBS and embedded in OCT for cryosectioning. Cryosections were blocked in 5% BSA in PBS for 1 hours, washed three times with PBS+0.1% Triton X-100, and incubated with primary antibody at 4°C overnight. Cryosections were washed three times with PBST to remove primary antibody before 1 hour secondary antibody incubation. Cryosections were washed three more times to remove secondary antibody before being mounted with Vectashield hardset mounting medium with DAPI following manufacturer's instructions. The dilutions for primary antibodies are as follows: TUJ1 (1:100, mouse, abcam ab7751-100), SOX1 (1:100, goat, Santa Cruz Biotechnology sc-17318), PAX6 (1:100, mouse, Santa Cruz Biotechnology sc-53106), FOXG1 (1:100, rabbit, abcam ab18259), EMX1 (1:100, rabbit, Santa Cruz Biotechnology sc-28220), PROX1 (1:100, rabbit, abcam ab37128), NESTIN (1:100, mouse, rat, Millipore MAB353), CALB2 (1:100, rabbit, abcam ab702) and ZIKVE/Anti-Flavivirus Group Antigen (1:500, mouse, Millipore MAB10216). Images were acquired on a Leica DMI 3000B.

Organoid and neurosphere sizes were estimated using ImageJ to by adjusting the color threshold and using the "Analyze Particle" tool. Because of the large population of neurospheres, low magnification images of wells representative of each condition were taken and analyzed by ImageJ as mentioned (n>100 per group). To assess changes in organoids overtime,

individual organoids were placed in wells and growth was tracked daily. Organoid change was estimated relative to their respective Day 0 measurements.

RNA Extraction and RT-qPCR

For RT-qPCR, Total RNA was isolated using TRIzol reagent following manufacturer's instructions. cDNA was generated from 500ng total RNA using iScript Mastermix according to manufacturer's instructions. qPCR was performed with SYBR Green PCR Master Mix (Bio-Rad) using a Roche Lightcycler 480.

Transcriptome analysis by RNA-seq

For RNA-seq analysis, RNA was extracted from 10-20 organoids per sample using RNeasy Mini Kit (Qiagen) following manufacturer's instructions. RNA was ribo-depleted and RNA sequencing was performed using an Illumina NextSeq 500 with an average of 50M reads per sample at the Scripps Research Institute NGS Core. Reads were mapped using BWA to human hg19-Ensembl transcripts release 75(Li and Durbin, 2009). Genes with RPKM<=0.5 for all samples were removed, data log transformed and normalized (quantile). Differentially expressed genes were identified by ANOVA with absolute fold change >=2 and adjusted p-value <=0.05.

Gene ontology analyses on biological processes was performed using The Database for Annotation, Visualization and Integrated Discovery (DAVID) (Huang da et al., 2009). Spearman's correlation coefficients between transcriptomes of organoids and brain regions and ages from the BrainSpan database were

calculated between log transformed expression levels with filtered genes having a standard deviation greater than 1 across all brain regions or ages (Mariani et al., 2015). Grouped functional pathway/gene ontology network analyses were performed using Cytoscape with the ClueGo add-on (Bindea et al., 2009; Shannon et al., 2003).

Calcium dye imaging

Calcium dye imaging was performed to assess the functionality of neural activity using Fluo-4 AM cell permeant dye following manufacturer's instructions with an incubation of 1 hour at 37°C. Time-lapse images were taken at 15 second intervals for 20 minutes using a Leica DMI 3000B and fluorescent intensity was quantified by ImageJ.

TLR3 activation and inhibition

To activate TLR3, cells were transfected with poly(I:C) at 5ug/ml using Lipofectamine 2000 following manufacturer's instructions. Media was changed 6 hours post-transfection. TLR3 competitive inhibitor (EMD-Millipore 614310) was reconstituted in DMSO and cells were treated with a final concentration of 10uM in media.

ACCESSION NUMBERS

The GEO accession number for the RNA-seq data reported in this paper is GEO number GSE80264.

Chapter 3 is an adapted version of materials published as Zika Virus Depletes Neural Progenitors in Human Cerebral Organoids through Activation of the Innate Immune Receptor TLR3. Dang J*****, Tiwari SK***, Lichinchi G, Qin Y, Patil VS, Eroshkin AM, Rana TM. (2016). *Cell Stem Cell*. 4;19(2):258-65. doi: 10.1016/j.stem.2016.04.014. Epub 2016 May 6. PMID: 27162029. The dissertation author is the co-first author on this work with Dr. Shashi Kante Tiwari.

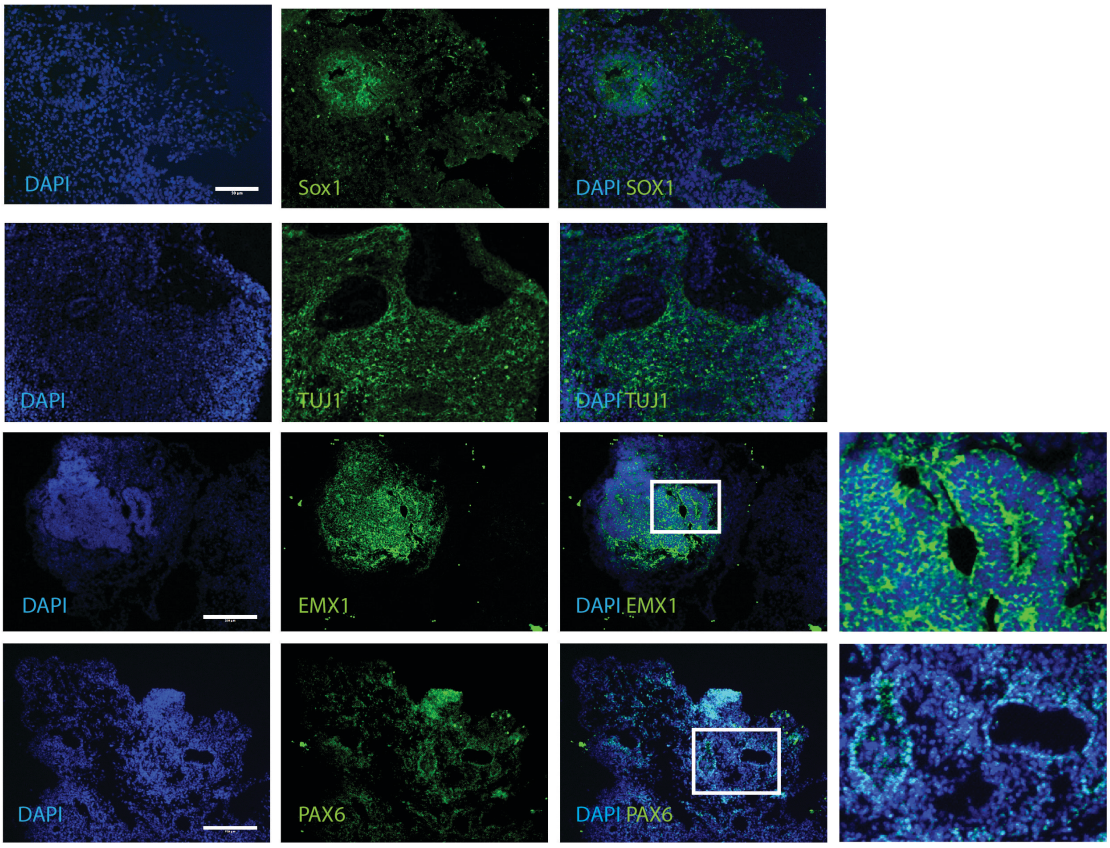

Figure S3.1: Characterization of cerebral organoids by immunohistochemistry

SOX1 neural progenitor cells and EMX1 and PAX6 forebrain marker localize around cavities while TUJ1 neuronal cells appear radially outward. Scale bar: 100um.

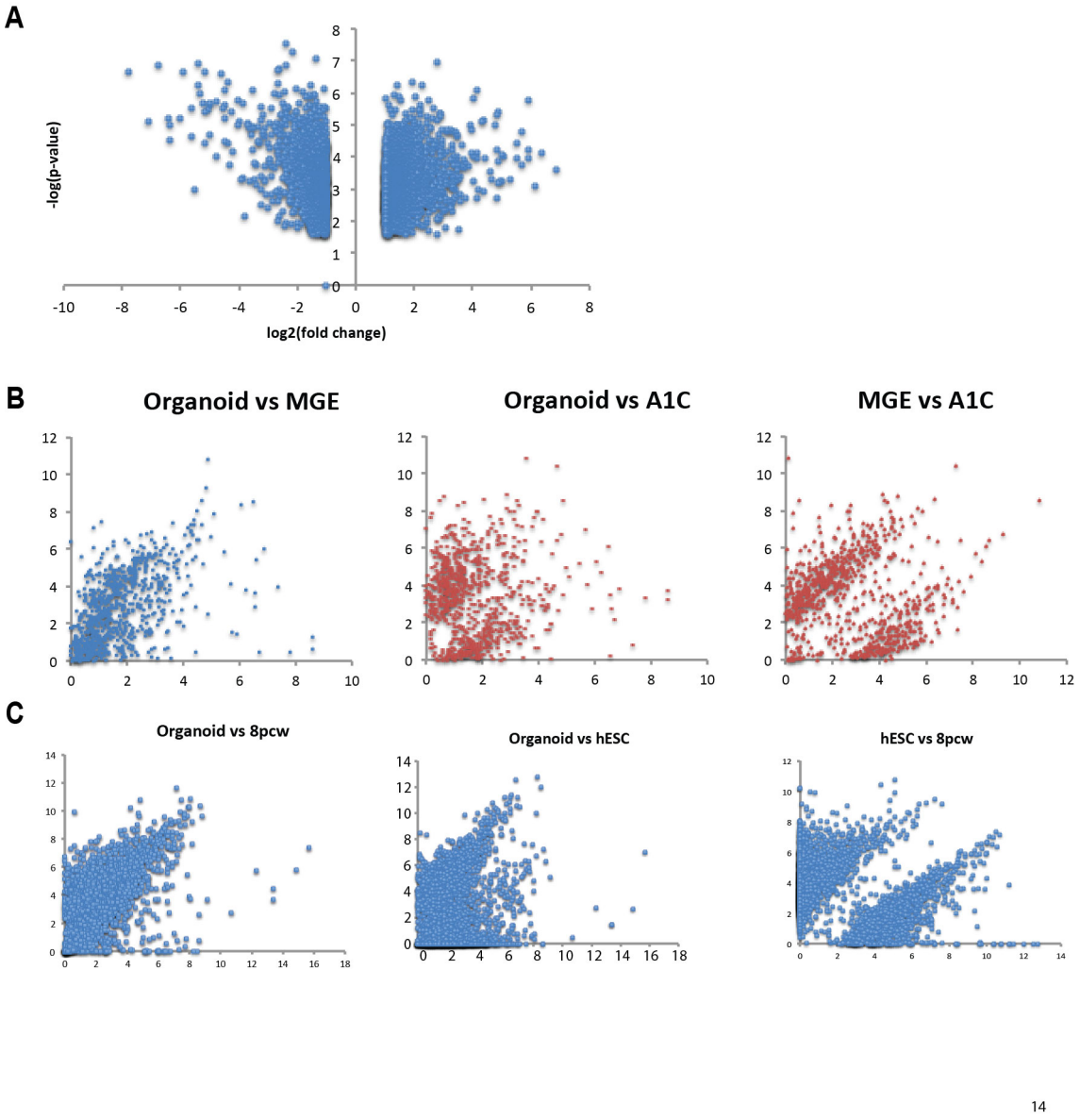

14

Figure S3.2: Transcriptome analysis of cerebral organoids

(A) Volcano plot of differentially expressed genes in organoids with fold change >2, p-value<0.05 and RPKM>0.5 from organoids 1 month old vs hESC. Also see heat map from Figure 2A.
(B and C) Representative scatter plot of cerebral organoid transcriptome compared to various regions of the fetal brain and brain ages, respectively. Organoids shows strong correlation with the medial ganglionic eminence (MGE) and poor correlation with the primary auditory cortex (A1C). MGE and A1C are poorly correlated as well. Also see Figure 2F and G.

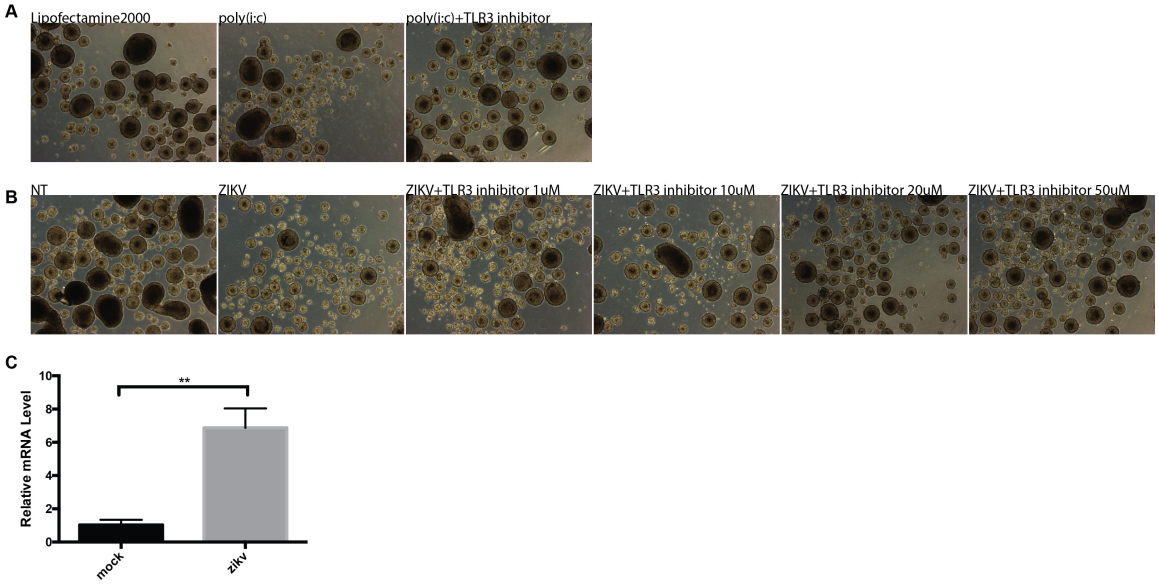

Figure S3.3: Neurosphere growth is attenuated by TLR3 activation

(A) Neurosphere treated with TLR3 agonist poly(I:C) show decreased growth 24 hours post-treatment while addition of TLR3 competitive inhibitor results in a rescue effect.
(B) Bright-field images of neurospheres show dosage dependent (1uM to 50uM) rescue effect of TLR3 competitive inhibitor in neurospheres treated with ZIKV.
(C) RT-qPCR analysis of TLR3 mRNA in mock and ZIKV inoculated neurospheres. ** p-value<0.01, Student's t-test.

Table 3.1: Transcriptomic Analyses of Organoids
Table shows differentially expressed genes between human embryonic stem cells (Group 1) and organoids 1 month (Group 2) and 2 months old (Group 3) and gene ontology analyses.

Table 3.2: Legend for Brain Region Acronyms, Related to Figure 2F.

CHAPTER 4: Dynamic Transcriptome of ZIKV infected hNSCs

Chapter 4.1: Introduction

Zika virus (ZIKV) is a re-emerging arbovirus belonging to the Flaviviridae family that has recently been linked to severe fetal abnormalities, including microcephaly and fetal growth restriction(Brasil et al., 2016b; Lazear and Diamond, 2016; Noronha et al., 2016; Sarno et al., 2016; Ventura et al., 2016). In vitro and in vivo studies have shown that ZIKV preferentially infects neural stem/progenitor cells and immature neurons in the developing brain and dysregulates processes involved in cell cycle progression, differentiation, apoptosis, autophagy, and immune activation(Cugola et al., 2016; Dang et al., 2016; Li et al., 2016; Liang et al., 2016; Tang et al., 2016). However, the molecular mechanisms by which ZIKV perturbs the transcriptomic landscape and leads to microcephaly are not well understood.

MicroRNAs (miRNAs) are a class of endogenous small non-coding RNAs ~22 nucleotides in length that play critical roles in regulating protein expression. miRNAs act post-transcriptionally by binding to partially complementary sites in the 3′-UTR of target messenger RNAs (mRNAs). This sequence-specific interaction leads to translational repression or mRNA degradation through catalytic Argonaute proteins within the RNA-induced silencing complex, which cleave the mRNA and recruit other proteins that repress translation or promote degradation. The mRNA targeting specificity of miRNAs is controlled by many

factors, including base pairing between the miRNA 5′ seed sequence and mRNA 3′-UTR sequence, cooperativity between multiple miRNA-binding sites, and the position of miRNA-binding sites in the targeted mRNA(Agarwal et al., 2015; Bartel, 2009; Grimson et al., 2007; Lewis et al., 2005). This flexibility means that individual miRNAs are capable of repressing the translation of hundreds of target mRNAs(Baek et al., 2008; Selbach et al., 2008). As a result, miRNAs are known to play pivotal roles in post-transcriptional regulation of numerous biological processes.

Given the documented roles of miRNAs in regulating neurodegeneration, viral infection, and innate immunity (Eacker et al., 2009; Lanford et al., 2010; Liu et al., 2012; O'Connell et al., 2010; Sullivan and Ganem, 2005; Taganov et al., 2006; Wang et al., 2006), we hypothesized that they may play a significant role in ZIKV pathogenesis, particularly the effects on the developing brain. In addition, the role of miRNAs in ZIKV pathogenesis and microcephaly remains unknown. Here, we report that ZIKV infection dysregulates both coding gene and miRNA transcriptomes in a strain specific manner. Meta-analyses and regulatory interaction networks integrate miRNA and mRNA expression data to investigate the role of miRNA-mediated repression during ZIKV infection. Furthermore, validation of two miRNAs, miR-188-3p and miR-218-3p, reveal miRNA-mediated suppression of gene networks involved in cell cycle progression and stem cell maintenance, respectively. Collectively, our data provide novel insight into understanding the importance of miRNA-regulated networks in ZIKV-induced pathogenesis, particularly microcephaly.

Chapter 4.2: Results

ZIKV MR766 and Paraiba have strain-specific effects on the mRNA transcriptome of neural stem cells

To determine whether the effects of ZIKV on the mRNA and miRNA transcriptomes of human neural stem cells (hNSCs) are strain specific, we employed the two most commonly studied strains, MR766 (African origin) and Paraiba (Brazilian origin), which have been shown to differ in their neural infectivity profiles(Cugola et al., 2016; Simonin et al., 2016). Consistent with these reports, we found that inoculation of hNSCs at a MOI of 1 resulted in ~10-fold higher infection by strain MR766 than by strain Paraiba, as demonstrated by RT-qPCR analysis of ZIKV mRNA (Figure 4.1A) and immunostaining of ZIKV envelope protein (ZIKVE) in hNSCs (Figure 4.1B) on the first 3 days post-infection.

To investigate whether ZIKV MR766 and Paraiba also had strain-specific effects on hNSC mRNA and miRNA transcriptomes, total RNAs were extracted from mock- or ZIKV-infected hNSCs 3 days after infection and analyzed by next-generation sequencing (Figure 4.1C). As expected, the more infectious MR766 strain had a greater effect on coding gene expression than did Paraiba (Figure 4.1D). ZIKV MR766 significantly upregulated 1159 genes and downregulated 1120 genes (Figure 4.1D, E, Table 4.1) compared with only 112 and 178 genes significantly upregulated and downregulated, respectively, in ZIKV Paraiba-infected hNSCs (Figure 4.1D, F, Table 4.2). In addition, 52 and 52 genes were

Figure 4.1: ZIKV modulates the transcriptomic profile of hNSCs in a strain-specific manner

(A) RT-qPCR analysis of ZIKV MR766 and ZIKV Paraiba mRNA levels on days 1, 2, and 3 post-inoculation of hNSCs at a MOI of 1. Mean ± SEM of biological triplicates.
(B) Fluorescence immunostaining of ZIKV envelope protein (ZIKVE) in hNSCs on days 1, 2, and 3 post-infection with ZIKV MR766 or Paraiba. Nuclei were stained with DAPI. Scale bar, 100 μm.
(C) Experimental design. hNSCs were infected with ZIKV MR766 or Paraiba for 3 days at a MOI of 1. Total RNA was analyzed by RNA-seq or miR-seq to identify miRNA-regulated networks of genes implicated in ZIKV pathogenesis. DE, differentially expressed.
(D) Venn diagram of differentially expressed genes in ZIKV MR766- and Paraiba-infected hNSCs. Up, upregulated; down, downregulated.
(E and F) Volcano plots of differentially expressed coding genes in (e) MR766- and (f) Paraiba-infected hNSCs at 3 days post-infection. Blue circles represent significantly (adjusted $p<0.05$) differentially expressed genes. The size of each circle is proportional to the square root of the base mean expression of the gene.
(G) Comparative dot plot of differentially expressed genes in MR766- and Paraiba-infected hNSCs. Blue circles represent significantly (adjusted $p<0.05$) differentially expressed genes. The size of each circle is proportional to the square root of the base mean expression of the gene.

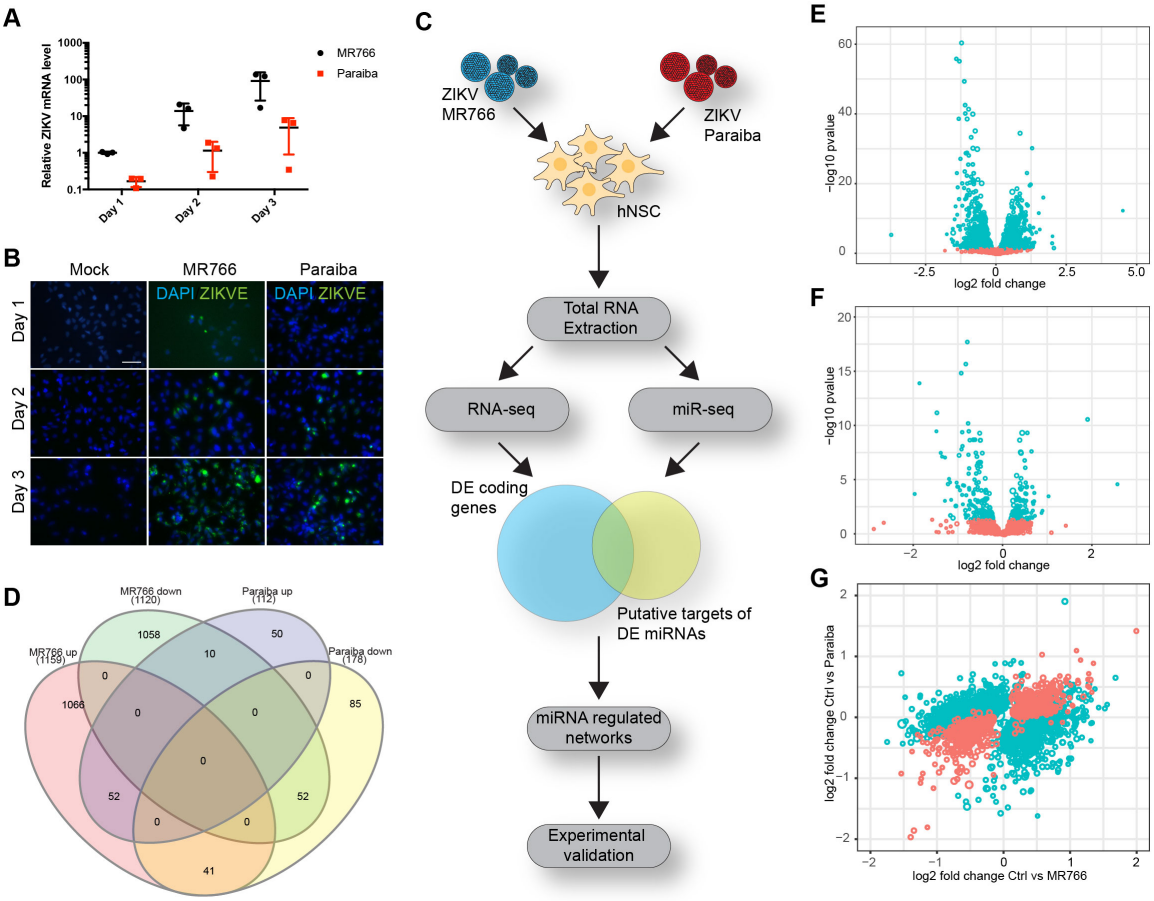
A
Relative ZIKV mRNA level
1000
100
10
1
0.1
MR766
Paraiba
Day 1
Day 2
Day 3
B
Mock
MR766
Paraiba
DAPI ZIKVE
DAPI ZIKVE
Day 1
Day 2
Day 3
C
ZIKV MR766
ZIKV Paraiba
hNSC
Total RNA Extraction
RNA-seq
miR-seq
DE coding genes
Putative targets of DE miRNAs
miRNA regulated networks
Experimental validation
D
MR766 down (1120)
Paraiba up (112)
MR766 up (1159)
Paraiba down (178)
1058
50
10
0
0
1066
0
0
85
0
52
52
0
0
41
E
−log10 pvalue
log2 fold change
F
−log10 pvalue
log2 fold change
G
log2 fold change Ctrl vs Paraiba
log2 fold change Ctrl vs MR766

commonly upregulated and downregulated, respectively, in both MR766-infected and Paraiba-infected cells (Figure 4.1D, G).

We next performed gene set enrichment analysis (GSEA) of the differentially expressed genes. In ZIKV MR766-infected hNSCs, the upregulated genes were enriched in functions related to chromosome organization and cell cycle processes (Figure S4.1A), whereas the downregulated genes were involved in gene expression, biosynthetic processes, and cell death (Figure S4.1B). Overall, the processes in hNSCs most affected by MR766 infection were those governing chromosome organization, metabolism, cell cycle, and cell stress (Figure S4.1C), which is consistent with previous reports(Tang et al., 2016). In contrast, both the upregulated and downregulated genes in ZIKV Paraiba-infected hNSCs were largely related to metabolism and biosynthetic processes, with additional enrichment of genes involved in tissue development and neurogenesis (Figure S4.1D–F). Collectively, these data suggest that ZIKV MR766 and Paraiba infection of hNSCs cause strain-specific dysregulation of a number of pathways likely to contribute to the microcephaly phenotype.

MicroRNAs regulate processes implicated in ZIKV-induced microcephaly

Because miRNAs are potent translational regulators, we examined their contribution to ZIKV-induced changes in the host transcriptome. We first profiled ZIKV-induced changes in miRNAs at 3 days post-infection using miR-seq. Interestingly, although ZIKV MR766 induced a more robust change in the mRNA transcriptome than did Paraiba infection (as described above), ZIKV Paraiba

Figure 4.2: Relationship between differentially expressed miRNAs and putative mRNA targets in ZIKV-infected hNSCs

(A and B) Volcano plots of differentially expressed miRNAs in (a) MR766- and (b) Paraiba-infected hNSCs at 3 days post-infection. Blue circles represent significantly (adjusted $p<0.05$) differentially expressed miRNAs. The size of each circle is proportional to the square root of the base mean expression of the gene.
(C) Comparative dot plot of differentially expressed miRNAs in MR766 (MR)- and Paraiba (PA)-infected hNSCs. The size of each circle is proportional to the square root of the base mean expression of the gene.
(D) Number of significantly (adjusted $p<0.05$) differentially expressed coding genes (upper) and miRNAs (lower) in ZIKV MR766- and Paraiba-infected hNSCs.
(E) Principal component analyses of significantly (adjusted $p<0.05$) differentially expressed coding genes (upper) and miRNAs (lower) in mock-, MR766- and Paraiba-infected hNSC samples in duplicate. X-axis represents PC1 and Y-axis represents PC2.
(F and G) Gene set enrichment analyses (GSEA) of putative miRNA targets differentially expressed in hNSCs during MR766 (f) and Paraiba (g) infection. Blue represents downregulated mRNAs targeted by upregulated miRNAs, red represents upregulated mRNAs targeted by downregulated miRNAs. The size of the dot is proportional to the number of genes in that enriched GSEA biological category.
(H) Integrative regulatory network analyses showing upregulated miRNAs (red circles) targeting downregulated putative mRNA targets (blue hexagons) based on TargetScan, miRANDA, and miRTarBase. The number of edges between miRNAs and mRNAs is equal to the number of algorithms predicting the miR–mRNA interaction. The blue/red color intensity is proportional to the fold change in expression during ZIKV infection (darker represents larger change).

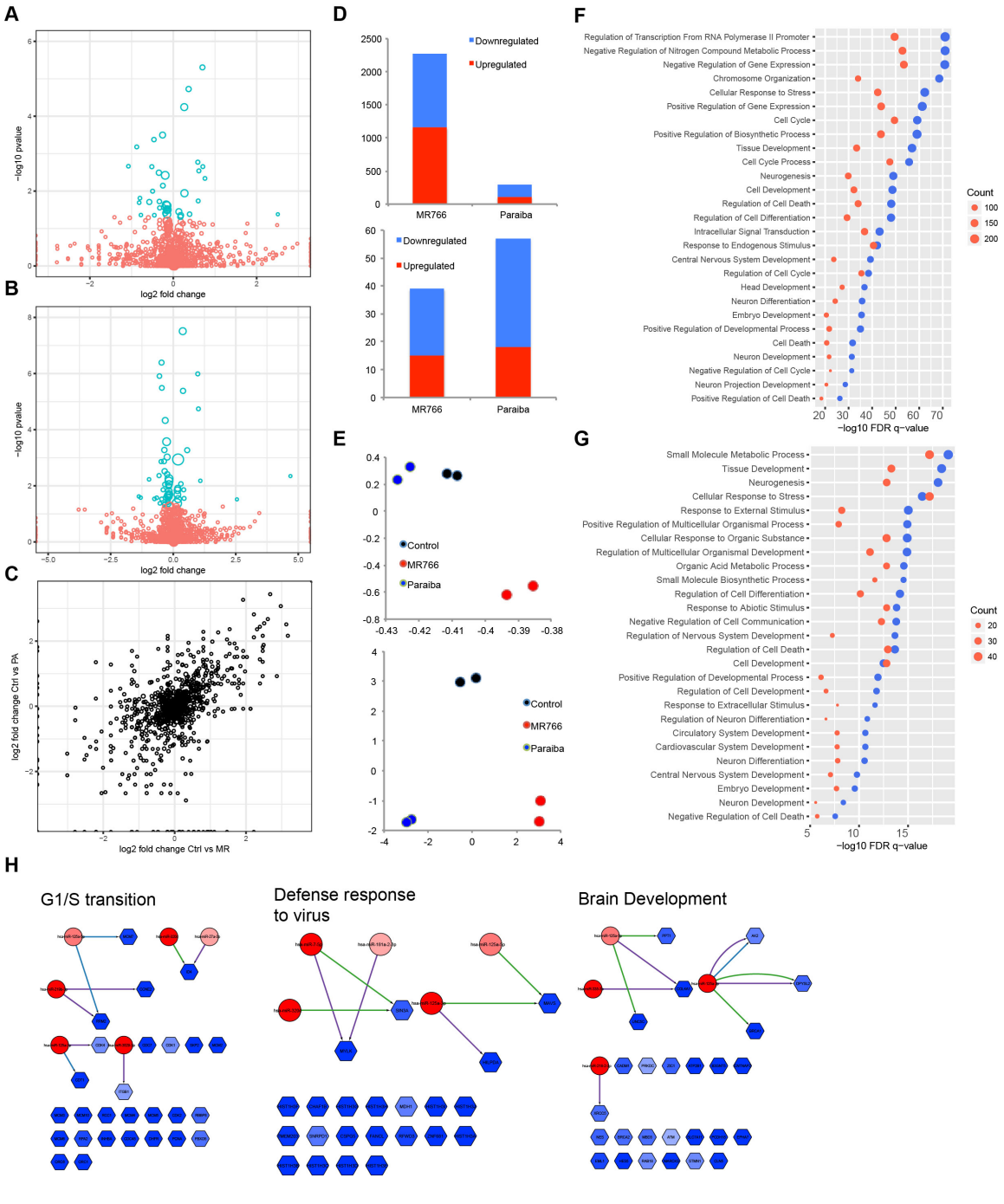
A
−log10 pvalue
log2 fold change
B
−log10 pvalue
log2 fold change
C
log2 fold change Ctrl vs PA
log2 fold change Ctrl vs MR
D
Downregulated
Upregulated
MR766
Paraiba
Downregulated
Upregulated
MR766
Paraiba
E
Control
MR766
Paraiba
Control
MR766
Paraiba
F
Regulation of Transcription From RNA Polymerase II Promoter
Negative Regulation of Nitrogen Compound Metabolic Process
Negative Regulation of Gene Expression
Chromosome Organization
Cellular Response to Stress
Positive Regulation of Gene Expression
Cell Cycle
Positive Regulation of Biosynthetic Process
Tissue Development
Cell Cycle Process
Neurogenesis
Cell Development
Regulation of Cell Death
Regulation of Cell Differentiation
Intracellular Signal Transduction
Response to Endogenous Stimulus
Central Nervous System Development
Regulation of Cell Cycle
Head Development
Neuron Differentiation
Embryo Development
Positive Regulation of Developmental Process
Cell Death
Neuron Development
Negative Regulation of Cell Cycle
Neuron Projection Development
Positive Regulation of Cell Death
−log10 FDR q−value
Count
G
Small Molecule Metabolic Process
Tissue Development
Neurogenesis
Cellular Response to Stress
Response to External Stimulus
Positive Regulation of Multicellular Organismal Process
Cellular Response to Organic Substance
Regulation of Multicellular Organismal Development
Organic Acid Metabolic Process
Small Molecule Biosynthetic Process
Regulation of Cell Differentiation
Response to Abiotic Stimulus
Negative Regulation of Cell Communication
Regulation of Nervous System Development
Regulation of Cell Death
Cell Development
Positive Regulation of Developmental Process
Regulation of Cell Development
Response to Extracellular Stimulus
Regulation of Neuron Differentiation
Circulatory System Development
Cardiovascular System Development
Neuron Differentiation
Central Nervous System Development
Embryo Development
Neuron Development
Negative Regulation of Cell Death
−log10 FDR q−value
Count
H
G1/S transition
Defense response to virus
Brain Development

induced a significantly greater change in miRNAs, in terms of both quantity and magnitude (Figure 4.2A–D, Table 4.3). Furthermore, principal component analyses revealed that the miRNA transcriptomes of mock-, Paraiba- and MR766-infected hNSCs were all markedly different from each other, whereas, as noted above, the mRNA transcriptomes of mock- and Paraiba-infected hNSCs were relatively similar (Figure 4.2E). These data highlight the strikingly disparate strain-specific effects of ZIKV MR766 and Paraiba on the coding and non-coding transcriptomes of infected hNSCs.

To understand the potential mechanistic roles of miRNAs in ZIKV infection and the associated neurodegenerative pathology, we utilized the predictive algorithms TargetScan (Agarwal et al., 2015), miRANDA (Betel et al., 2008), and miRTarBase (Chou et al., 2016) to identify putative mRNA targets of the differentially expressed miRNAs in infected hNSCs. These algorithms evaluate target seed sequence pairing, site numbers, conservation, and site context scores to predict targets with high confidence(Agarwal et al., 2015; Betel et al., 2008). We then compared the putative mRNA targets of the most differentially expressed miRNAs with the mRNAs shown to be most significantly altered by ZIKV infection to identify pathways potentially regulated by miRNAs in ZIKV-infected cells. GSEA of the dataset indicated that the common mRNAs (i.e., were directly modulated by ZIKV infection and were putative targets of differentially expressed miRNAs) were enriched in functions related to transcriptional regulation, metabolism, cellular stress response, cell cycle, tissue development, neurogenesis and nervous system development, cell death, and neuron

differentiation (Figure 4.2F). Similarly, mRNAs that were directly modulated by ZIKV Paraiba infection and were putative targets of differentially expressed miRNAs in Paraiba-infected cells were likely to be involved in processes related to metabolism, tissue development, and neurogenesis (Figure 4.2G). These data indicate that both ZIKV strains dysregulate host miRNA–mRNA networks potentially involved in the neurodegenerative phenotype associated with ZIKV infection.

To more precisely identify miRNA-regulated pathways that may contribute to ZIKV pathogenesis, we constructed integrative networks of the miRNAs and miRNA-regulated mRNAs modulated by ZIKV infection of hNSCs. First, genes that were downregulated by ZIKV infection and enriched in annotated gene ontology functions related to “cell cycle” and “G1/S transition,” “defense response to virus,” and “brain development” (Figure 4.2H, blue hexagons) were cross-referenced with potential miRNA regulators that were concomitantly upregulated upon ZIKV infection (Figure 4.2H, red circles). Likewise, genes that were upregulated by ZIKV infection and were enriched in gene ontology terms “viral process,” “apoptosis,” “NFKB signaling,” and “cell cycle arrest” were cross-referenced with potential miRNA regulators that were concomitantly downregulated by ZIKV infection (Figure S4.2A). The miRNAs identified from these analyses included many that may regulate pathways relevant to the pathogenic ZIKV phenotype, including G1/S transition, defense response to virus, brain development (Figure 4.2H) viral process, apoptosis, NFKB signaling and cell cycle arrest (Figure S4.2A). Conversely, we generated networks of

miRNA targets downregulated by ZIKV (Figure S4.2B) and grouped them based on gene ontology function (Figure S4.2C). Collectively, these miRNA–mRNA interaction networks suggest a relationship between miRNA and mRNA changes in expression and emphasize the ability of multiple dysregulated miRNAs simultaneously targeting the same transcripts to suppress biologically relevant pathways during ZIKV infection.

ZIKV infection upregulates miRNAs involved in control of the cell cycle and neuronal differentiation

To validate the miR-seq data, we selected the two miRNAs most upregulated upon infection of hNSCs with ZIKV Paraiba (miR-188-3p) and MR766 (miR-218-3p) for further analysis. RT-qPCR analysis confirmed that expression of both miRNAs was upregulated by both strains of ZIKV, but miR-188-3p was preferentially induced by Paraiba and miR-218-3p by MR766 (Figure S4.3A).

The miR-188-3p-3p sequence showed high conservation across the species examined, strongly suggesting that it has fundamentally important functions (Figure S4.3B). To investigate the role of miR-188-3p in ZIKV pathogenesis, we transfected hNSCs with either a non-targeting control sequence or a miR-188-3p mimic and analyzed their transcriptional profiles by RNA-seq (Figure S4.3C, D, E, Table 4.4). hNSCs overexpressing miR-188-3p showed significant downregulation of mRNAs predicted by TargetScan to be miR-188-3p targets, as evidenced by the divergent distribution (Figure S4.3F)

Figure 4.3: miR-218-3p regulates NSC maintenance and induces neuronal differentiation

(A) Volcano plot of differentially expressed mRNAs in miR-218-3p-overexpressing hNSCs at 3 days post-transfection. Blue circles represent significantly (adjusted $p<0.05$) differentially expressed mRNAs. The size of each circle is proportional to the square root of the base mean expression of the gene.
(B) Gene ontology analysis of significantly downregulated genes in miR-218-3p overexpressing hNSCs (from (A)).
(C) Representative images of neurospheres of NTC or miR-218-3p transfected human neurospheres 5 days post-transfection. Scale bar = 250 μm.
(D) Fluorescence immunostaining of TUJ1+ neurons after hNSC transfection with control or miR-218-3p mimics. Nuclei were stained with DAPI. Scale bar, 100 μm.
(E) RT-qPCR analysis of *NESTIN* and *PAX6* mRNA levels in hNSCs 3 days post-inoculation with ZIKV MR766 and ZIKV Paraiba at a MOI of 1. Mean ± SEM of n=3.
(F) RT-qPCR analysis of *NESTIN* and *PAX6* mRNA levels in hNSCs 3 days post-transfection with non-targeting control or miR-218-3p. Mean ± SEM of n=3.
(G) Distribution plot of log2-fold changes in mRNA expression in hNSCs transfected with non-targeting control (red) or miR-218-3p (blue) mimics. The blue curve represents putative miR-218-3p target mRNAs with total context scores of ≤ −0.1 based on TargetScan prediction, while the red curve represents all mRNAs not predicted to be targets of miR-218-3p.
(H) Cumulative distribution plot of log2-fold changes in mRNA expression in hNSCs transfected with non-targeting control (red) or miR-218-3p (blue) mimics. The blue curve represents putative miR-218-3p target mRNAs with total context scores of ≤ −0.1 based on TargetScan prediction, while the red curve represents all mRNAs not predicted to be targets of miR-218-3p.
(I) Venn diagram of putative miR-218-3p target genes, genes downregulated by MR766, genes downregulated by Paraiba and genes downregulated by hNSCs overexpressing miR-218-3p.
(J) Protein–protein interactome of putative miR-218-3p target genes commonly downregulated by miR-218-3p overexpression and ZIKV infection. The color depth is proportional to the magnitude of the log2-fold change (darker representing greater downregulation). The size of the nodes is proportional to the TargetScan context score, with larger nodes representing targets with higher confidence.
(K) Gene ontology analysis of the miR-218-3p–target interactome in ZIKV-infected hNSCs (from (e)).

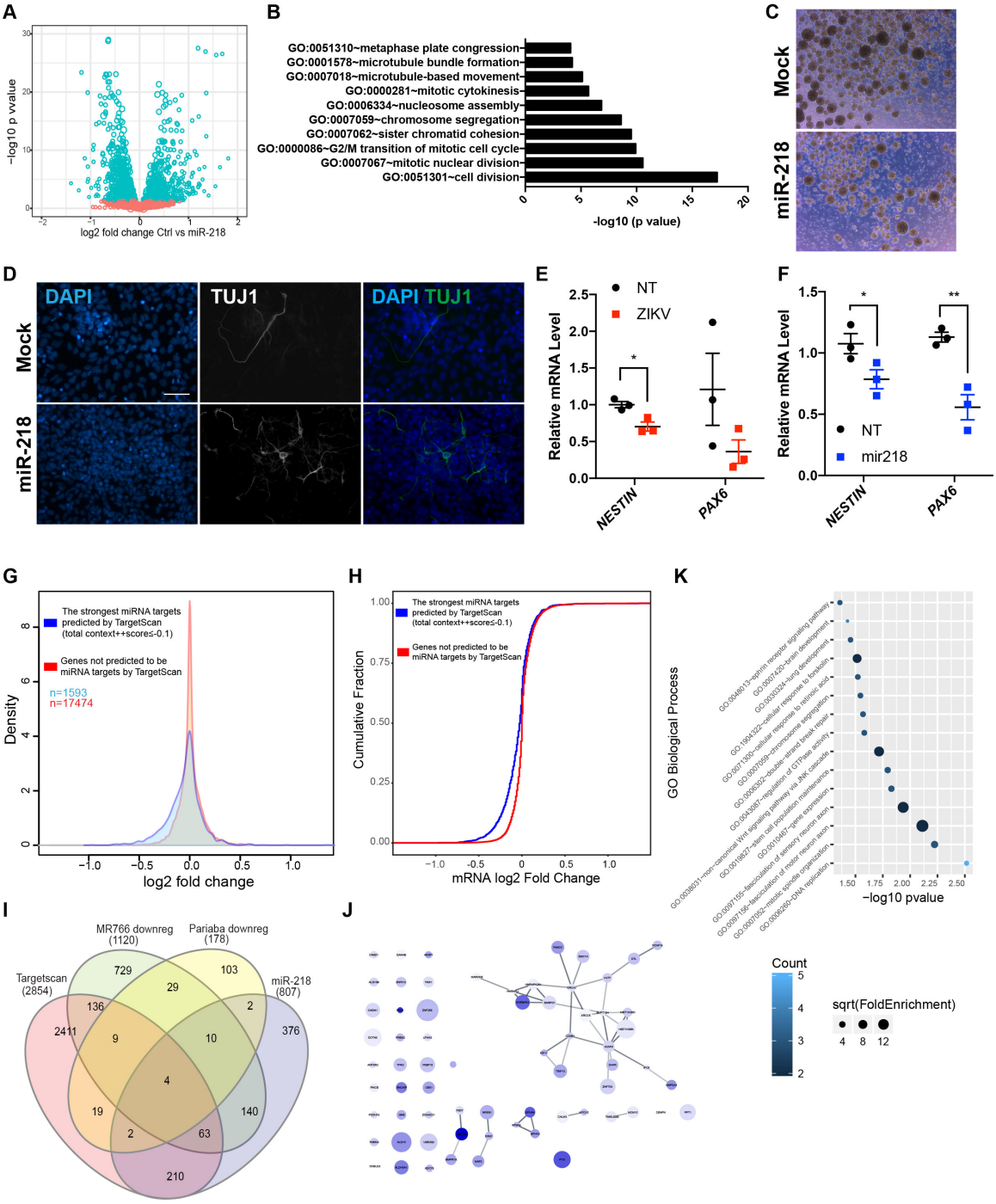
A
−log10 p value
log2 fold change Ctrl vs miR-218
B
GO:0051310~metaphase plate congression
GO:0001578~microtubule bundle formation
GO:0007018~microtubule-based movement
GO:0000281~mitotic cytokinesis
GO:0006334~nucleosome assembly
GO:0007059~chromosome segregation
GO:0007062~sister chromatid cohesion
GO:0000086~G2/M transition of mitotic cell cycle
GO:0007067~mitotic nuclear division
GO:0051301~cell division
-log10 (p value)
C
Mock
miR-218
D
DAPI
TUJ1
DAPI TUJ1
Mock
miR-218
E
NT
ZIKV
Relative mRNA Level
NESTIN
PAX6
F
NT
mir218
Relative mRNA Level
NESTIN
PAX6
G
The strongest miRNA targets predicted by TargetScan (total context++score≤-0.1)
Genes not predicted to be miRNA targets by TargetScan
n=1593
n=17474
Density
log2 fold change
H
The strongest miRNA targets predicted by TargetScan (total context++score≤-0.1)
Genes not predicted to be miRNA targets by TargetScan
Cumulative Fraction
mRNA log2 Fold Change
K
GO Biological Process
−log10 pvalue
I
MR766 downreg (1120)
Pariaba downreg (178)
Targetscan (2854)
miR-218 (807)
729
103
29
136
2
2411
9
10
376
4
19
140
2
63
210
J
Count
sqrt(FoldEnrichment)

and cumulative distribution curves (Figure S4.3G) of the fold change in expression of mRNAs with high context scores. To identify gene networks potentially regulated by miR-188-3p during ZIKV infection, we then compared the putative mRNA targets of miR-188-3p, the genes downregulated in hNSCs by expression of the miR-188-3p mimic, and the genes downregulated by ZIKV Paraiba infection (Figure S4.3H). Gene ontology analysis of the resulting datasets revealed enrichment of genes associated with cell cycle and cell division processes (Figure S4.3I), both of which have previously been implicated in ZIKV pathogenesis(Li et al., 2016; Souza et al., 2016; Tang et al., 2016)

We performed similar analyses to elucidate the function of miR-218-3p, another highly conserved miRNA, in ZIKV infection (Figure S4.4A). hNSCs were transfected with control or miR-218-3p mimics and total RNA was analyzed by RNA-seq (Figure S4.4B, Figure 4.3A, Table 4.5**)**. Gene ontology analysis of all significantly downregulated genes during miR-218-3p overexpression showed an enrichment of genes related to cell division and cell cycle progression (Figure 4.3B). To functionally validate the role of miR-218-3p in neural stem cells, miR-218-3p was overexpressed in neurospheres and neural stem cells in monolayer. Upregulation of miR-218-3p attenuated neurosphere formation, consistent with the downregulation of cell cycle related genes identified by gene ontology analyses (Figure 4.3C). To determine whether miR-218-3p attenuates neurosphere growth by perturbing stem cell maintenance processes, as suggested by RNA-seq analyses, and promoting neuronal differentiation, hNSCs were transfected with miR-218-3p mimic and cultured over 7 days. After 7 days,

we observed an increase in expression of TUJ1, a neuronal marker (Figure 4.3D), indicating that miR-218-3p does indeed promote the differentiation of hNSCs to neurons. Moreover, we examined expression of the NSC markers *NESTIN* and *Pax6* in hNSCs after infection with ZIKV MR766 or transfection with miR-218-3p mimic. Notably, both *NESTIN* and *PAX6* were downregulated in both ZIKV-infected and miR-218-3p-overexpressing hNSCs (Figure 4.3E, F). These findings are consistent with recent reports that have suggested that ZIKV infection may induce premature differentiation of hNSCs to neurons, resulting in the depletion of progenitor cells in the ventricular zone and cortical thinning (Gabriel et al., 2017; Li et al., 2016).

Next, to identify the mRNAs which are directly regulated by miR-218-3p, we compared next generation sequencing data with putative miRNA target prediction algorithms. The distribution (Figure 4.3G) and cumulative distribution (Figure 4.3H) of differentially expressed mRNAs validated bioinformatic target predictions of miR-218-3p in hNSCs. Comparison of the miR-218-3p targets predicted by TargetScan, the genes downregulated by expression of the miR-218-3p mimic in hNSCs, and the genes downregulated by ZIKV infection, identified 67 and 13 miR-218-3p-regulated target mRNAs in hNSCs infected with ZIKV MR766 and ZIKV Paraiba, respectively (Figure 4.3I). These findings are consistent with the higher expression of miR-218-3p in MR766-infected compared with Paraiba-infected hNSCs and strongly suggest that miR-218-3p upregulation is causally related to the transcriptional perturbation of the 67 and

Figure 4.4: miR-218-3p dysregulates neurogenesis by directly repressing *TFRC*

(A) RT-qPCR analysis of *EPHA4* and *TFRC* mRNA levels in hNSCs 3 days post-inoculation with ZIKV MR766 and ZIKV Paraiba at a MOI of 1. Mean ± SEM of n=5.
(B) RT-qPCR analysis of *EPHA4* and *TFRC* mRNA levels in hNSCs 3 days post-transfection with non-targeting control or miR-218-3p. Mean ± SEM of n=4.
(C) Dual luciferase assay analyzing direct repression of *EPHA4* and *TFRC* by miR-218-3p. 3'UTR fragments containing predicted miR-218-3p target sequence with or without mutated seed regions of *EPHA4* and *TFRC* were cloned into pGL3 luciferase reporters and transfected into 293FT cells together with pRL-TK. Cells were then transfected with either siNTC or miR-218-3p mimic and lysates analyzed 48 hrs post-transfection. Relative luciferase activity was calculated by the Firefly/Renilla signal and normalized to siNTC-transfected cells. Mean ± SEM of n=3.
(D) AGO2-RIP-qPCR analysis of hNSCs transfected with siNTC or miR-218-3p 48 hrs post-transfection. Lysates were pulled down by IgG control or anti-AGO2 and RNAs were analyzed by RT-qPCR. Mean ± SEM of n=2.
(E) Immunoblot analysis of TFR in hNSCs infected with ZIKV Paraiba, overexpressing miR-218-3p or transfected with siTFRC 3 days post-infection/transfection.
(F) Heatmap of RT-qPCR analysis of STAT3-FoxM1 downstream target genes in hNSCs infected with ZIKV Paraiba, overexpressing miR-218-3p or transfected with siTFRC 3 days post-infection/transfection. Mean of n=6. Color bar on right represents relative expression to siNT control.
(G) Immunostaining of neural progenitor marker SOX2 (green) and ZIKV envelope flavivirus group antigen (ZIKVE, red) in the hippocampus (top row) and SVZ (bottom row) of ZIKV Paraiba-infected *Ifnar*$^{-/-}$ mice two weeks post-infection. Nuclei were stained with DAPI (gray). Right-most column in shows enlargements of the regions. SGZ = subgranular zone, DG = dentate gyrus, LV = lateral ventricle, STR = striatum. Scale bars, 200 μM (and 50 μM in right panel only) as indicated in figure.
(H) RT-qPCR analysis of *Epha4* and *Tfrc* mRNA levels in brains of uninfected and ZIKV Paraiba-infected *Ifnar*$^{-/-}$ newborn mice. Mean ± SEM of n=3.

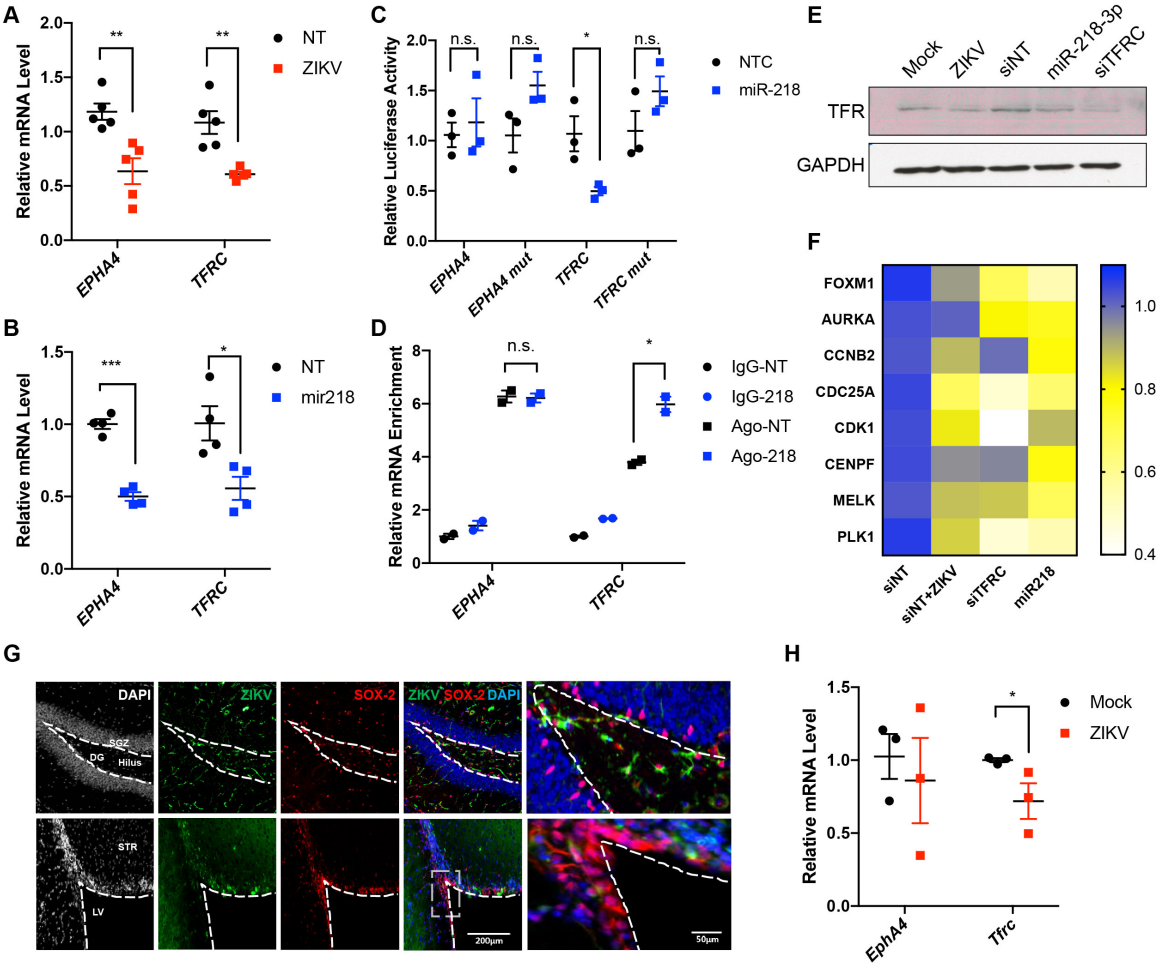
A
Relative mRNA Level
NT
ZIKV
EPHA4
TFRC
B
Relative mRNA Level
NT
mir218
EPHA4
TFRC
C
Relative Luciferase Activity
NTC
miR-218
n.s.
EPHA4
EPHA4 mut
TFRC
TFRC mut
D
Relative mRNA Enrichment
IgG-NT
IgG-218
Ago-NT
Ago-218
n.s.
EPHA4
TFRC
E
Mock
ZIKV
siNT
miR-218-3p
siTFRC
TFR
GAPDH
F
FOXM1
AURKA
CCNB2
CDC25A
CDK1
CENPF
MELK
PLK1
siNT
siNT+ZIKV
siTFRC
miR218
G
DAPI
ZIKV
SOX-2
ZIKV SOX-2 DAPI
SGZ
DG
Hilus
STR
LV
200μm
50μm
H
Relative mRNA Level
Mock
ZIKV
EphA4
Tfrc

13 genesets. Network analyses of the 67 genes revealed that miR-218-3p suppresses highly connected protein–protein interaction networks related to DNA replication, mitotic spindle organization, fasciculation of neurons, and stem cell population maintenance (Figure 4.3J, K).

Based on the gene networks downregulated by ZIKV and miR-218-3p overexpression (Figure 4.3J), we selected *EPHA4* and *TFRC* for further validation due to their roles in neurogenesis (Khodosevich et al., 2011) and stem cell self-renewal (Schonberg et al., 2015), respectively. RT-qPCR confirmed downregulation of both *EPHA4* and *TFRC* mRNA in ZIKV and miR-218-3p overexpressing hNSCs (Figure 4.4A, B). To assess whether these transcripts are directly or indirectly repressed by miR-218-3p, dual luciferase assays were utilized to analyze the extent of direct repression of miR-218-3p based on target sequence. Fragments of the *EPHA4* and *TFRC* 3' UTR containing the putative miR-218-3p target sequences with or without a mutated seed sequence region were cloned into the pGL3 luciferase vector and overexpressed in 293FT cells. Overexpression of miR-218-3p reduced luciferase signal in only *TFRC* 3' UTR expressing samples (Figure 4.4C), thus suggesting that *TFRC* is directly repressed by miR-218-3p while *EPHA4* is not. Moreover, AGO2 RNA immunopreciptiation was performed in hNSCs expressing either a non-targeting control or miR-218-3p and bound mRNAs were analyzed by RT-qPCR (Figure S4.4C). Consistent with the dual luciferase assay results, *EPHA4* showed an increased affinity to AGO2 relative to the IgG control but no enrichment when

miR-218-3p was overexpressed (Figure 4.4D). *TFRC* mRNAs, however, showed greater loading into the AGO2/RISC complex when miR-218-3p was overexpressed. Immunoblot analysis of transferrin receptor (TFR) confirmed downregulation of TFR in ZIKV infected hNSCs and hNSCs overexpressing miR-218-3p (Figure 4.4E).

Recent studies have shown that iron metabolism and TFR regulation play a role in neurogenesis and glioblastoma cancer stem cell proliferation and self-renewal (Schonberg et al., 2015; Silvestroff et al., 2013). In glioblastoma cancer stem cells, iron metabolism, regulated by TFR, governs mitotic progression through the STAT3-FoxM1 regulatory signaling loop. Attenuated iron uptake decreased FoxM1 and STAT3 expression, decreased downstream targets involved in cell cycle regulation. Similarly, both ZIKV infection and miR-218-3p overexpression in neural stem cells resulted in the downregulation of *AURKA*, *CCNB2*, *CDC25A*, *CDK1*, *CENPF*, *MELK* and *PLK1* (Figure 4.4F). In all, these results suggest that miR-218-3p downregulates TFRC, thus decreasing iron uptake and downregulating cell cycle related genes by disrupting the previously established STAT3-FoxM1 regulatory axis.

Lastly, to confirm the in vivo relevance of these findings, pregnant *Ifnar1*$^{-/-}$ mice were inoculated with ZIKV and fetal brains were isolated (Figure 4.4G and Figure S4.4D, E). RT-qPCR analysis of these samples confirmed downregulated of both *EPHA4* and *TFRC* in infected fetal tissues (Figure 4.4H). Together, these results suggest that miR-218-3p regulates neural stem cell proliferation and

stemness through direct repression of *TFRC* and indirect repression of *EPHA4*. Collectively, the results presented here shed light on the functional role of miRNAs, particularly miR-188-3p and miR-218-3p, in post-transcriptional regulation of ZIKV-infected hNSCs and the associated microcephaly phenotype.

Chapter 4.3: Discussion

Our integrative analyses of coding and non-coding transcriptomes in hNSCs revealed novel miRNA–mRNA networks that are dysregulated during ZIKV infection and may contribute to the microcephaly phenotype. Analysis of the dynamic transcriptomic landscape associated with ZIKV infection in hNSCs revealed strain-specific dysregulation of genes associated with cell cycle, neurogenesis, stem cell population maintenance, and metabolism. Interestingly, we found that, while ZIKV MR766 infection had a greater effect on coding gene expression, Paraiba had more impact on the miRNA transcriptome.

To the best of our knowledge, this is the first study to examine the miRNA–mRNA interactome in the context of ZIKV pathogenesis. In particular, we observed differential expression of miRNAs with targets strongly associated with cell cycle, neurogenesis, and stem cell population maintenance related-pathways. Previous studies have shown that ZIKV-induced perturbation of these processes contributes to the microcephaly phenotype; however, only a few mechanisms had been proposed to explain how ZIKV modulates these pathways(Dang et al., 2016; Gabriel et al., 2017; Hamel et al., 2015; Li et al.,

2016; Liang et al., 2016; Onorati et al., 2016; Tang et al., 2016). Our findings now propose miRNA regulation as a direct link between ZIKV infection of hNSCs and the microcephaly phenotype.

Analysis of the miRNA–mRNA networks provided evidence that multiple differentially expressed miRNAs regulate the same mRNA targets enriched in processes implicated in ZIKV-induced microcephaly. For instance, miRNAs miR-125a-3p and miR-125a-5p, which we found to be upregulated by ZIKV infection, are both negative regulators of *MAVS*, an essential signaling protein in the RIG-I and type I interferon response pathways of the innate immune system(Baril et al., 2009). In addition, miR-320c and miR-7-5p, also upregulated by ZIKV, target *SIN3A*. The SIN3A repressor complex is an essential element in the interferon-mediated antiviral response through its interaction with STAT3(Icardi et al., 2012). Previously, ZIKV was shown to inhibit type I interferon production through a mechanism involving ZIKV NS5 binding to STAT2 to promote its proteasomal degradation(Grant et al., 2016; Kumar et al., 2016). Thus, our findings reveal a potential mechanism by which miRNAs mediate suppression of interferon signaling in ZIKV-infected hNSCs. Taken together, these data suggest that multiple miRNAs work in concert to suppress networks of genes related to immunity and neurodegeneration during ZIKV infection.

One of the miRNAs upregulated in ZIKV-infected hNSCs was miR-188-3p. gene ontology analysis of potential miR-188-3p mRNA targets downregulated during ZIKV infection identified networks enriched in cell cycle-related functions. Our findings are consistent with previously published reports showing that miR-

188-3p suppresses the G1/S transition, cell cycle progression, and cell proliferation through post-transcriptional regulation of cyclin/CDK complexes and *SIX1* expression in nasopharyngeal carcinoma and oral squamous cell carcinoma(Wang and Liu, 2016; Wu et al., 2014). Following ZIKV infection of hNSCs, upregulation of miR-188-3p and inhibition of cell cycle progression and proliferation may contribute to the microcephaly phenotype, which is associated with dysregulation of the neural progenitor population in vivo(Cugola et al., 2016; Dang et al., 2016; Qian et al., 2016).

We also analyzed the function of putative miR-218-3p targets that were modulated by ZIKV infection, and uncovered a network of genes involved in neural stem cell maintenance and neuron fasciculation. Moreover, we confirmed that overexpression of miR-218-3p in hNSCs induced their differentiation into TUJ1+ neurons, providing a potential mechanism by which ZIKV infection leads to depletion of neural progenitors. miR-218-3p is shown to indirectly suppress expression of the receptor tyrosine kinase EPHA4, which is essential for maintaining NSCs in an undifferentiated state(Khodosevich et al., 2011), and knockdown of *EphA4* in mice results in depletion of NSCs in the subventricular zone(Khodosevich et al., 2011).

On the other hand, dual luciferase assays and AGO2 RIP-qPCR confirmed that miR-218-3p directly represses *TFRC* mRNA. *TFRC* is a regulator of cellular iron uptake and metabolism which regulates stem cell self-renewal and cell cycle (Sanchez et al., 2006; Schonberg et al., 2015; Silvestroff et al., 2013). Rat NSCs supplemented with ferric iron and apoTransferrin showed greater cell

proliferation mediated through TfRc1 (Silvestroff et al., 2013). Interestingly, *TFRC* has been shown to play a role in glioblastoma cancer stem cell self-renewal through an iron-dependent STAT3-FoxM1 regulatory mechanism (Schonberg et al., 2015). TFRC is upregulated in glioblastomas and highly upregulated in cancer stem cell populations. Schonberg et al. then showed that neurosphere formation is *TFRC*-dependent and that targeting the iron-metabolic pathways can decrease cancer stem cell growth in vitro and in vivo. Additionally, iron negatively regulates replication of the flavivirus, hepatitis C virus, by binding to the viral polymerase NS5B in the protein's Mg^{2+} binding pocket (Fillebeen and Pantopoulos, 2010; Fillebeen et al., 2005). Thus, miRNA-mediated downregulation of *TFRC* highlights a potential causal link between dysregulated cellular metabolic processes and perturbation of cell cycle during ZIKV infection as identified by RNA-seq.

Collectively, the data presented here identify novel miRNA-regulated transcriptional networks in ZIKV-infected hNSCs that regulate neural stem cell self-renewal, cell cycle progression, and neurogenesis. Interestingly, integrative analyses of the profiling data revealed that ZIKV MR766 and Paraiba strains had distinct effects on the mRNA and miRNA transcriptomes, providing a possible mechanism for virus-specific effects on neuronal damage during brain development. Lastly, functional validation of miR-188-3p and miR-218-3p provided insight into dysregulated post-transcriptional mechanisms relevant to ZIKV pathogenesis.

Chapter 4.4: Materials and Methods

Cell Lines and Culture Conditions

All cells were maintained at 37°C in a humidified 5% CO_2 atmosphere. Vero cells were maintained in Eagle's Minimum Essential Medium (EMEM; ATCC, 30-2003) supplemented with 10% fetal bovine serum (FBS; Gibco) and antibiotics. Human NSCs (ThermoFisher, A15654) were cultured in StemPro NSC SFM medium consisting of Knockout DMEM/F-12 media supplemented with 2 mM GlutaMax, 20 ng/ml basic fibroblast growth factor, 20 ng/ml epidermal growth factor, and 2% StemPro Neural Supplement (ThermoFisher, A1050901) on Matrigel- or CELLStart-coated plates following the manufacturer's instructions. Neurospheres were generated by plating single cell suspensions of hNSC in uncoated tissue culture plates.

For miRNA overexpression experiments, hNSCs were transfected using Lipofectamine 2000 (ThermoFisher, 11668019) following the manufacturer's instructions. Briefly, miRIDIAN miRNA mimics (GE Dharmacon) and Lipofectamine 2000 were each diluted in OptiMEM, incubated for 10 min at room temperature, mixed, and incubated for an additional 20 min. The mixture was then added dropwise to hNSCs to give a final concentration of miRNA mimics of 25 μM. The medium was changed the following day and total RNA was extracted at 2 days post-transfection. For the miR-218-3p mimic-induced differentiation experiments, hNSCs were transfected twice, on days 0 and 3, and harvested for experiments on day 7.

Zika Virus Propagation

ZIKV prototype MR766 and Paraiba strains were propagated in the low passage Vero cell line. Vero cells were infected with virus at a MOI of 1 in EMEM medium supplemented with 10% FBS. The medium was refreshed 4 h after infection and the viral supernatant was collected at 5 days post-infection. Viral titers were assessed using iScript One-Step RT-PCR kit (Bio-Rad). Viral copy numbers were calculated from a standard curve of in vitro-transcribed viral RNA transcripts.

Immunofluorescence Microscopy

To assess ZIKV infection, hNSCs were fixed at 24, 48, and 72 h post-infection and immunostained as described previously(Dang et al., 2016). In brief, ZIKV- and mock-infected hNSCs were fixed with 4% paraformaldehyde in PBS for 20 min at room temperature. Cells were permeabilized by incubation in 0.1% Triton X-100 for 5 min at room temperature and then blocked in 5% bovine serum albumin for 30 min. Cells were then incubated overnight at 4°C with a mouse anti-ZIKVE/anti-flavivirus group antigen (1:500, Millipore MAB10216), which is directed against the flavivirus envelope protein. Cells were washed with PBS and incubated for 1 h at room temperature with fluorescein isothiocyanate (FITC)-conjugated anti-mouse IgG. The nuclei were stained with Hoechst 33258 before analysis. To assess neuronal differentiation by expression of TUJ1, hNSCs were cultured for 7 days and then fixed and stained as described above, except the

primary antibody was specific for TUJ1 (Abcam, ab7751). Immunostained cells were imaged using a Leica fluorescence microscope (DMI 3000B).

ZIKV infection of mice

Ifnar$^{-/-}$ mice (4–5-week-old, MMRRC Jackson Laboratories) were infected with ZIKV Paraiba (5×10^4 MOI/µl) or MR766 (3.2×10^5 MOI/µl) by i.p. injection (500 µl) as previously described (Lazear et al., 2016; Zhao et al., 2016). Mice were sacrificed for immunostaining 2 weeks after ZIKV infection.

Immunohistochemistry

Mice were transcardially perfused with normal saline (0.9% NaCl) followed by ice-cold 4% paraformaldehyde (PFA, pH 7.2) under deep anesthesia, as described previously (Tiwari et al., 2014). Brains were removed and post-fixed in 10% PFA overnight at 4°C followed by cryopreservation in 10%, 20%, and 30% (w/v) sucrose in PBS. Serial coronal sections of 30 µm thickness beginning at bregma −1.50 to −3.50 mm through the dorsal hippocampus encompassing the dentate gyrus region and +0.26 to −2.5 mm through the SVZ were cut using a freezing cryostat (Leica Biosystems, CM3050s). Free-floating sections were washed, antigen retrieval was performed with citrate buffer (pH 6.2), and the sections were blocked with 3% normal goat serum, 0.1% Triton X-100, and 0.5% BSA for 2 h. Sections were then incubated with mouse anti-ZIKVE (flavivirus group antigen) antibody (1:500), rabbit anti-SOX2, or goat anti-FANCC (1:100) for 24 h at 40°C. Sections were then stained with secondary antibodies (anti-

mouse and anti-rabbit Alexa Fluor 488 at 1:200; anti-rabbit, anti-mouse, and anti-goat Alexa Fluor 594 at 1:200), washed, mounted with DAPI-containing Hard Set anti-fade mounting medium (Vectashield, Vector Laboratories, CA, USA), and stored in the dark at 4°C. Slides were analyzed using an inverted Leica fluorescence microscope (DMI 3000B) or a Leica SP5 confocal with Resonant Scanner microscope with Leica LAS Lite Software.

Dual Luciferase Assay

3' UTR fragments were cloned into pGL3-basic firefly luciferase vectors. pGL3 (Promega, E1751), pRL-TK (Renilla luciferase) (Promega, E2241) and miR-218-3p or control were transfected together using Lipofectamine 2000 (ThermoFisher, 11668019) in 293FT cells. Cells were lysed using passive lysis buffer and analyzed using the Promega Dual-luciferase Reporter Assay System (Promega, E1980) following manufacturer's instructions using a BioTek Synergy 2 plate reader.

AGO2 RNA immunoprecipitation

Cells were lysed using Pierce IP Lysis Buffer (ThermoFisher, 87787) supplemented with cOmplete Mini Protease Inhibitor Cocktail (Roche, 4693159001) and RNasin ribonuclease inhibitor (Promega, N2111) and rotate with 5ug of either control IgG (Santa Cruz Biotechnology, sc-2026) or AGO2 antibody (Sigma, SAB4200085) for 2 hours at 4°C. 50ul of washed Pierce A/G magnetic beads (ThermoFisher, 88802) were added to each sample and rotated overnight at 4°C. The

following day, samples were washed 5 times using Pierce IP lysis buffer and aliquoted for RNA extraction using TRIzol reagent and protein analyses by western blot.

RNA Extraction, cDNA Synthesis, and qRT-PCR

Total RNA was extracted from hNSCs using a miRNeasy Mini Kit (Qiagen, 217004) according to the manufacturer's instructions. RNA samples were treated with RNase-free DNase (Qiagen), and cDNA was generated from 500 ng RNA/sample using iScript Mastermix (Bio-Rad) according to the manufacturer's instructions. For miRNA RT-qPCR analyses, miRNA cDNA synthesis was performed using the MiR-X miRNA First-Strand Synthesis Kit (Clontech, 638315). qPCR of mRNA and miRNA was performed with SYBR Green PCR Master Mix (Bio-Rad) using a Roche LightCycler 480.

RNA-Seq and miR-Seq Data Analysis

RNA was extracted from hNSCs as described above and then ribo-depleted. RNA and miRNA sequencing were performed using an Illumina NextSeq 500 with an average of 20 million and 5 million reads per sample, respectively.

For RNA-seq analyses, the single-end reads that passed Illumina filters were filtered for reads aligning to tRNA, rRNA, adapter sequences, and spike-in controls. The reads were then aligned to UCSC hg19 reference genome using TopHat (v 1.4.1). DUST scores were calculated with PRINSEQ Lite (v 0.20.3), and low-complexity reads (DUST >4) were removed from the BAM files. The

alignment results were parsed using SAMtools to generate SAM files. Read counts to each genomic feature were obtained with the htseq-count program (v 0.6.0) using the “union” option. After removing absent features (zero counts in all samples), the raw counts were imported into R/Bioconductor package DESeq2 to identify genes differentially expressed between samples. DESeq2 normalizes counts by dividing each column of the count table (samples) by the size factor of the column. The size factor was calculated by dividing the samples by the geometric means of the genes. This brought the count values to a common scale suitable for comparison. P values for differential expression were calculated using a binomial test for differences between the base means of two conditions. The p values were adjusted for multiple test correction using the Benjamini–Hochberg algorithm to control the false discovery rate. Cluster analyses, including principal component analysis and hierarchical clustering, were performed using standard algorithms and metrics.

For miR-seq analyses, quality control was assessed using FastQC. Reads were aligned to the genome with bowtie2 using the following reference and annotations: Homo_sapiens.GRCh38.dna.primary_assembly.fa (NCBI) and Homo_sapiens.GRCh38.86.gtf (NCBI). Random 100 unmapped reads were generated and compared using BLAST (NCBI). Partek was utilized to generate read counts, RPKM, and the mapping summary. Genes with read count values <1 across all samples were filtered out. DESeq was utilized to calculate the fold change, p value, and adjusted p value for differentially expressed miRNAs.

Gene ontology analyses of biological processes were performed using The Database for Annotation, Visualization and Integrated Discovery (DAVID) (Huang da et al., 2009). Grouped functional pathway/gene ontology network and miR–mRNA target analyses were performed using Cytoscape with the ClueGo and CyTargetLinker add-ons(Bindea et al., 2009; Kutmon et al., 2013; Shannon et al., 2003). miRNA target predictions were performed using TargetScan, miRTarBase, and miRANDA(Agarwal et al., 2015; Betel et al., 2008; Chou et al., 2016; Kutmon et al., 2013). Density and cumulative density plots were generated in R after calculating the cumulative context scores of a given mRNA based on miRNA target sites within the 3′-UTR(Wu et al., 2016).

Western blotting

Cells were lysed in RIPA buffer containing protease inhibitor cocktail (Roche), and proteins were resolved by SDS-PAGE and transferred to PVDF membranes (Bio-Rad). Membranes were blocked with Fast Western Blot Kit blocking reagent (Thermo Scientific Pierce) and signals were detected with Supersignal West Pico Chemiluminescent Substrate (Pierce). The following antibodies were used: GAPDH (Cell Signaling Technology, 5174S), TFR (Invitrogen, 13-6800) and AGO2 (Sigma, SAB4200085).

Statistical analysis

Statistical analysis was carried out using GraphPad Prism software. Differences between group means were analyzed by Student's t test. Differentially expressed genes in the RNA-seq data were analyzed using ANOVA. A p value ≤0.5 was considered statistically significant.

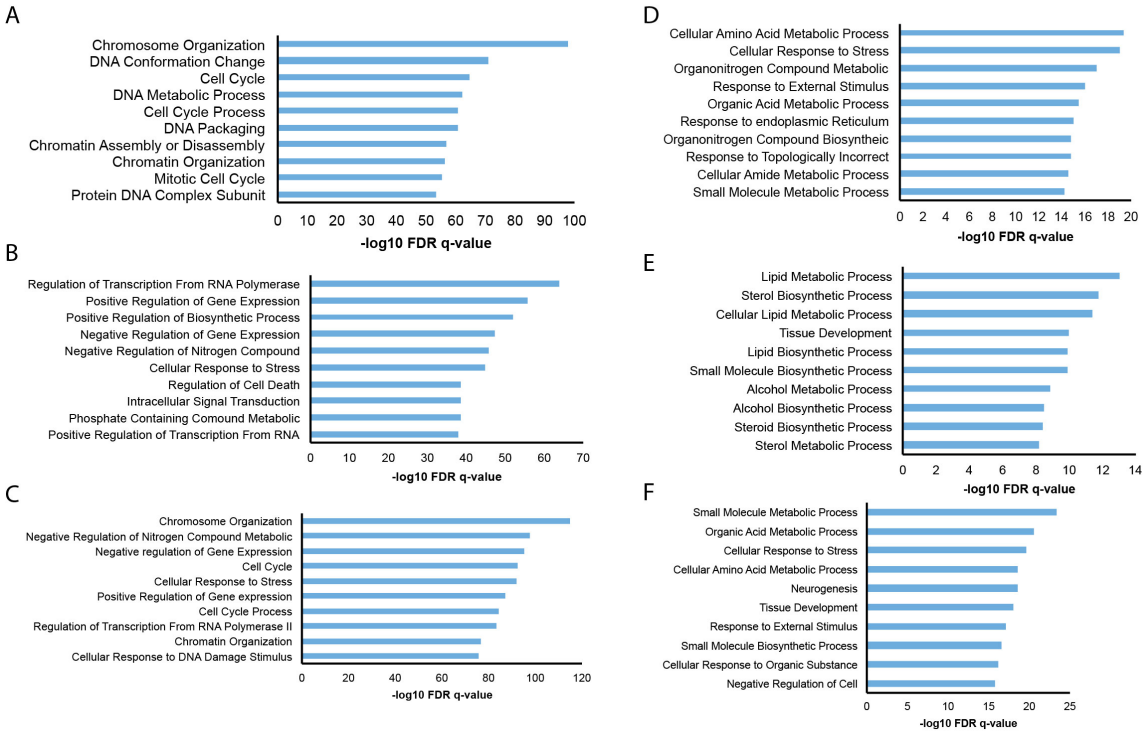

Figure S4.1: Gene set enrichment analyses of differentially expressed genes in ZIKV-infected hNSCs

(A–C) GSEA of upregulated (a), downregulated (b) or either upregulated or downregulated (c) genes in ZIKV MR766-infected hNSCs at 3 days post-infection at a MOI of 1.
(D–F) GSEA of upregulated (d), downregulated (e), or either upregulated or downregulated (f) genes in ZIKV Paraiba-infected hNSCs at 3 days post-infection at a MOI of 1.

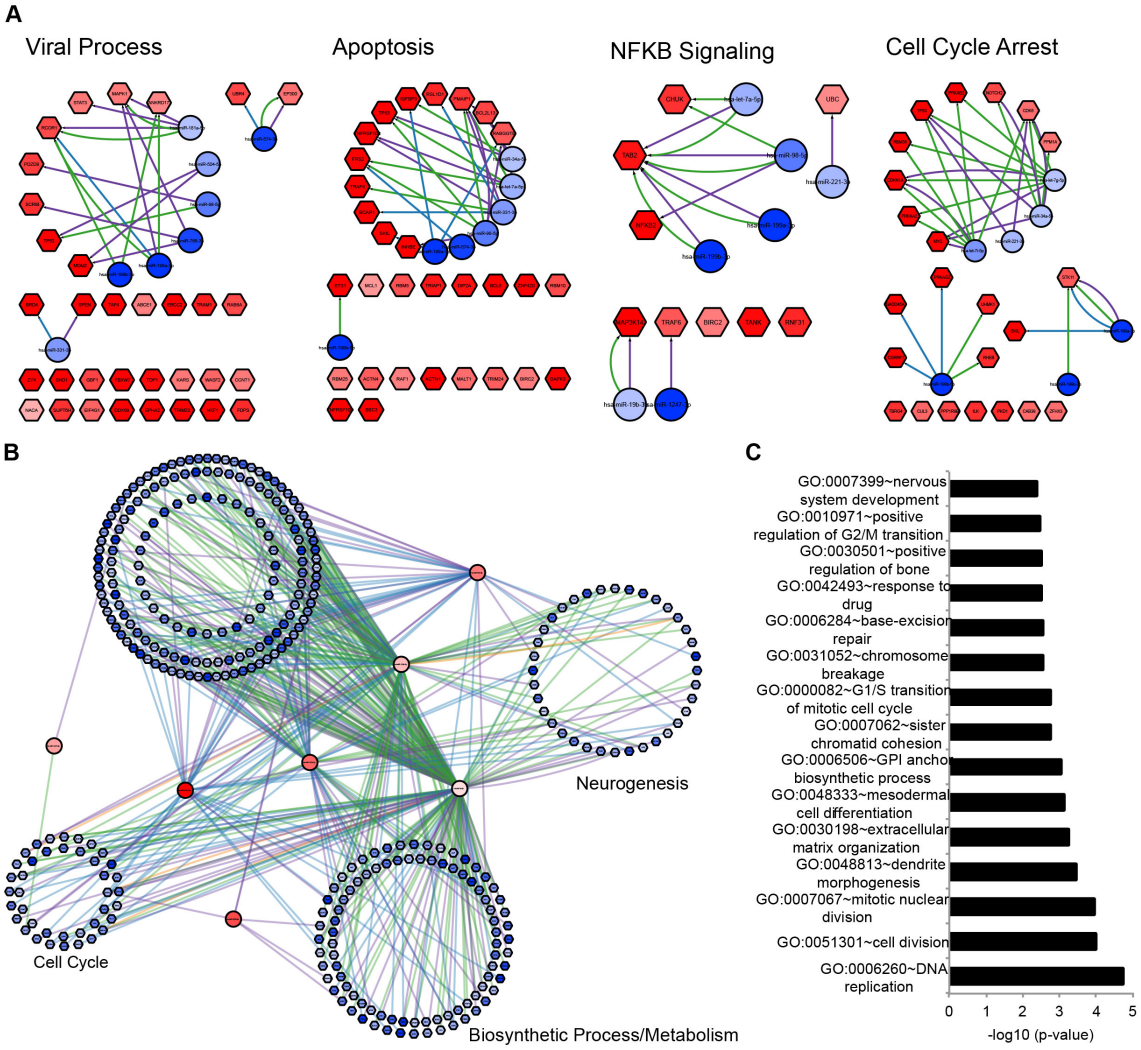

Figure S4.2: miRNA-mediated regulatory networks in ZIKV-infected hNSCs

(A) Integrative networks of mRNAs downregulated and miRNAs upregulated in ZIKV-infected hNSCs involved in “viral process,” “apoptosis,” “NFKB signaling,” and “cell cycle arrest” based on gene ontology annotation.
(B) miRNA–mRNA network of commonly upregulated miRNAs and downregulated mRNAs in ZIKV MR766- and Paraiba-infected hNSCs. Genes are clustered based on gene ontology annotation.
(C) Gene ontology analyses of putative mRNA targets of commonly upregulated miRNAs in ZIKV MR766- and Paraiba-infected hNSCs (shown in (b)).

Figure S4.3: ZIKV-induced upregulation of miR-188-3p in hNSCs targets cell cycle-related processes

(A) RT-qPCR validation of miRNAs identified in miR-seq analyses to be differentially expressed in mock-, ZIKV MR766-, and ZIKV Paraiba-infected hNSCs. Mean ± SEM of biological triplicates.
(B) Sequence conservation of miR-188-3p-3p.
(C) RT-qPCR analysis of miR-188-3p expression in hNSCs 2 days after transfection with control or miR-188-3p mimics. Mean ± SEM of biological triplicates.
(D) Experimental design. hNSCs were transfected with miR-188-3p mimic for 3 days and total RNA was analyzed by RNA-seq. Genes differentially expressed during ZIKV infection, putative miR-188-3p targets, and genes downregulated by miR-188-3p overexpression were cross-referenced to identify miRNA-regulated gene networks implicated in ZIKV pathogenesis.

(E) Volcano plot of differentially expressed mRNAs in hNSCs overexpressing miR-188-3p mimic at 3 days post-transfection. Blue circles represent significantly (adjusted $p<0.05$) differentially expressed mRNAs. The size of each circle is proportional to the square root of the base mean expression of the gene.
(F) Distribution plot of log2-fold changes in mRNA expression in hNSCs transfected with non-targeting control (red) or miR-188-3p (blue) mimics. The blue curve represents putative miR-188-3p target mRNAs with total context scores of ≤ −0.1 based on TargetScan prediction, while the red curve represents all mRNAs not predicted to be targets of miR-188-3p.
(G) Cumulative distribution plot of log2-fold changes in mRNA expression in hNSCs transfected with non-targeting control (red) or miR-188-3p (blue) mimics. The blue curve represents putative miR-188-3p target mRNAs with total context scores of ≤ −0.1 based on TargetScan prediction, while the red curve represents all mRNAs not predicted to be targets of miR-188-3p.
(H) Protein–protein interactome of putative miR-188-3p target genes commonly downregulated by miR-188-3p overexpression and ZIKV infection. The color depth is proportional to the magnitude of the log2-fold change (darker represents greater downregulation). The size of the nodes is proportional to the TargetScan context score, with larger nodes representing targets with higher confidence.
(I) Gene ontology analysis of the miR-188-3p–target interactome in ZIKV-infected hNSCs (from (h)).

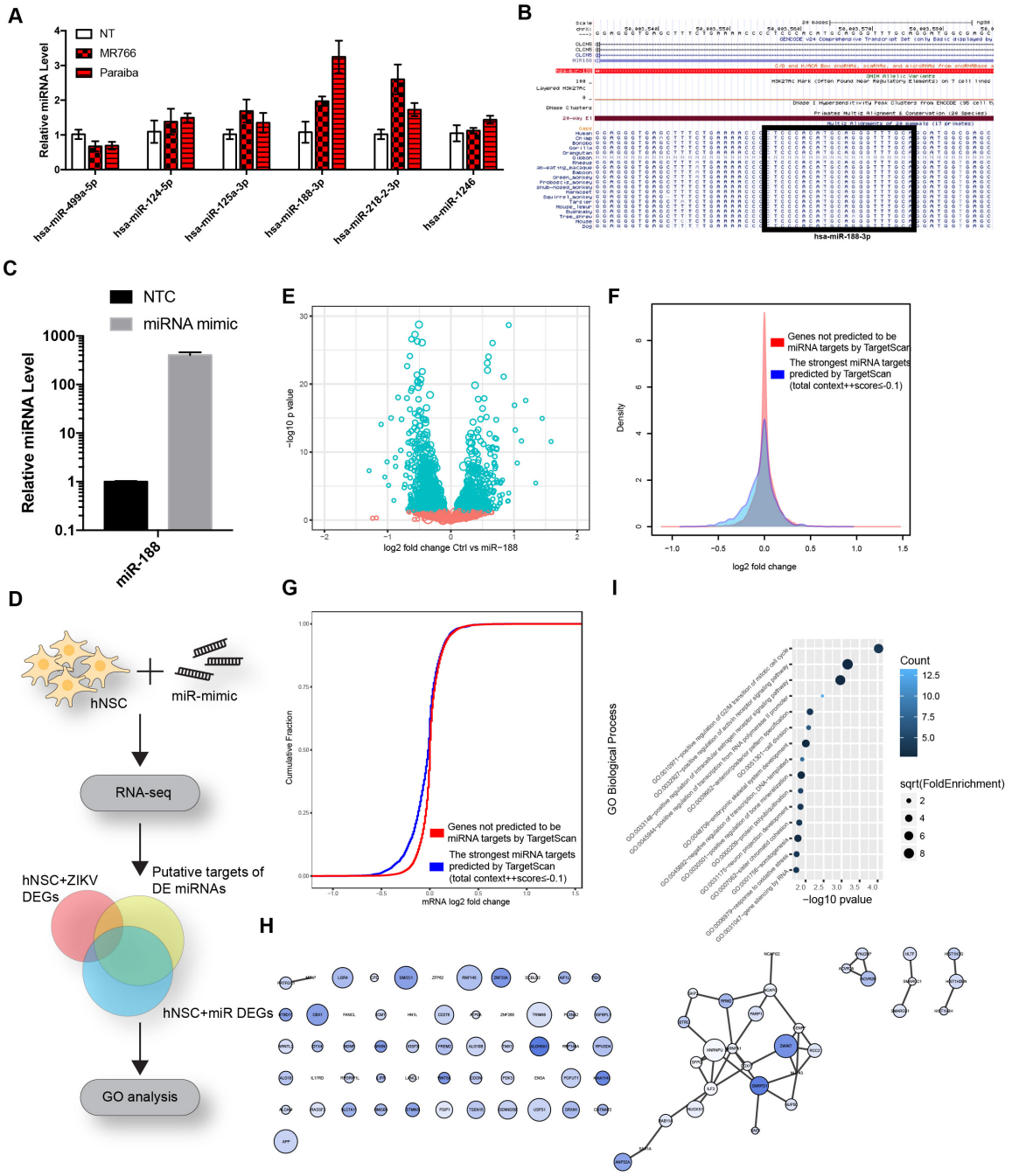
A
NT
MR766
Paraiba
Relative miRNA Level
hsa-miR-499a-5p
hsa-miR-124-5p
hsa-miR-125a-3p
hsa-miR-188-3p
hsa-miR-218-2-3p
hsa-miR-1246
B
hsa-miR-188-3p
C
NTC
miRNA mimic
Relative miRNA Level
miR-188
D
hNSC
miR-mimic
RNA-seq
Putative targets of DE miRNAs
hNSC+ZIKV DEGs
hNSC+miR DEGs
GO analysis
E
−log10 p value
log2 fold change Ctrl vs miR−188
F
Genes not predicted to be miRNA targets by TargetScan
The strongest miRNA targets predicted by TargetScan (total context++score≤-0.1)
Density
log2 fold change
G
Cumulative Fraction
mRNA log2 fold change
I
GO Biological Process
Count
sqrt(FoldEnrichment)
−log10 pvalue
H

Figure S4.4: Validation of miR-218-3p overexpression in hNSCs and miR-218-3p sequence alignment

(A) Sequence conservation of miR-218-3p-2-3p.
(B) RT-qPCR analysis of miR-218-3p expression in hNSCs 2 days after transfection with control or miR-218-3p mimics. Mean ± SEM of biological triplicates.
(C) Immunoblot analysis of input and AGO2 immunoprecipitated cell lysates from hNSCs transfected with miR-218-3p 3 days post-transfection.
(D) Immunostaining of neural progenitor marker SOX2 (green) and ZIKV envelope flavivirus group antigen (ZIKVE, red) in the hippocampus (top row) and SVZ (bottom row) of control uninfected *Ifnar*$^{-/-}$ mice. Nuclei were stained with DAPI (gray). Right-most column in shows enlargements of the regions. SGZ = subgranular zone, DG = dentate gyrus, Scale bars, 200 μM (and 50 μM in right panel only).
(E) Immunostaining of mature neuronal marker NeuN (red) and ZIKV envelope flavivirus group antigen (ZIKVE, green) in the hippocampus of uninfected (top) or ZIKV Paraiba-infected (bottom) *Ifnar*$^{-/-}$ mice two weeks post-infection. Nuclei were stained with DAPI (gray). SGZ = subgranular zone, DG = dentate gyrus, Scale bars are as indicated on image.

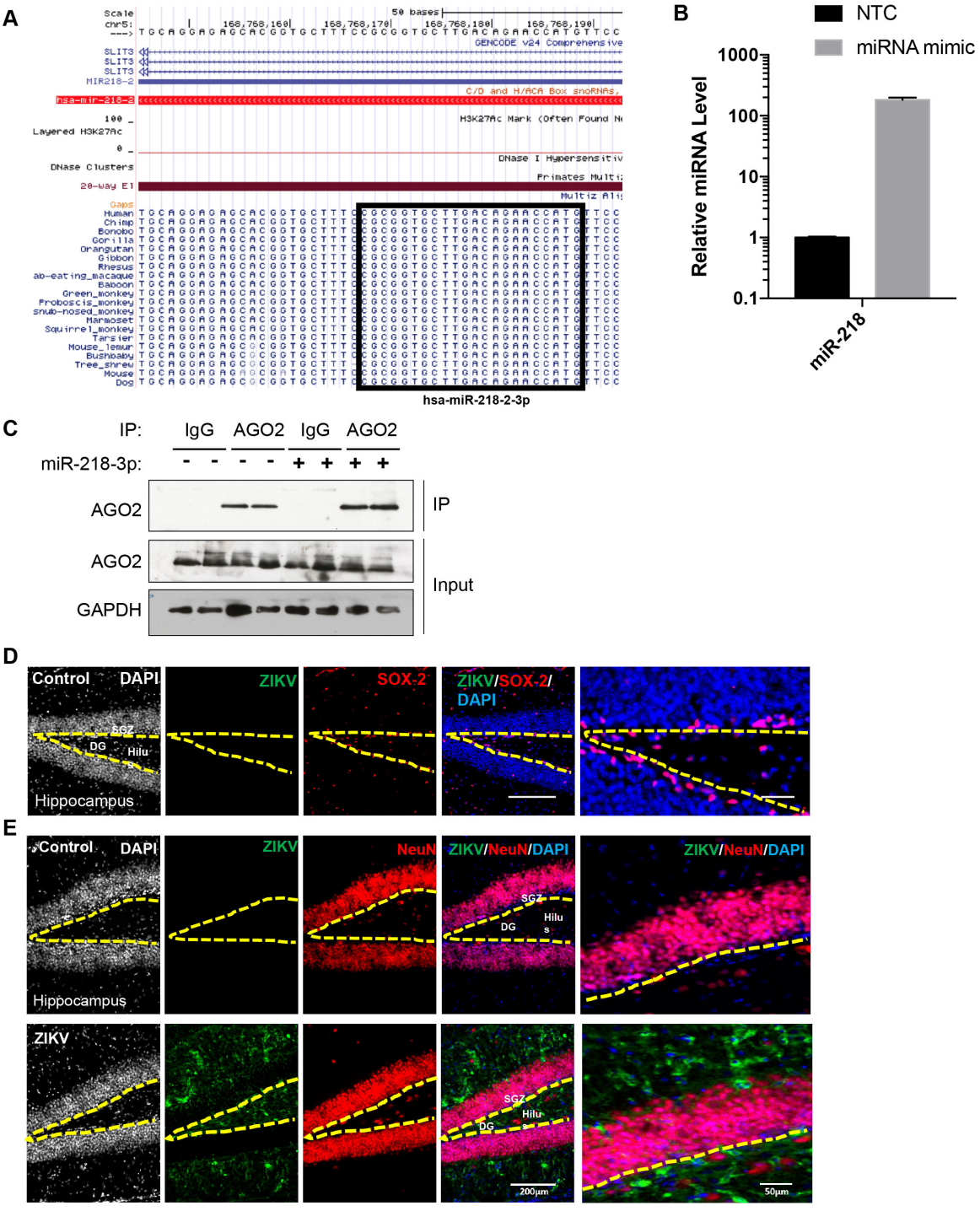
A
B
NTC
miRNA mimic
Relative miRNA Level
1000
100
10
1
0.1
miR-218
hsa-miR-218-2-3p
C
IP:
IgG
AGO2
IgG
AGO2
miR-218-3p:
AGO2
AGO2
GAPDH
IP
Input
D
Control
DAPI
ZIKV
SOX-2
ZIKV/SOX-2/
DAPI
SGZ
DG
Hilu
Hippocampus
E
Control
DAPI
ZIKV
NeuN
ZIKV/NeuN/DAPI
ZIKV/NeuN/DAPI
Hippocampus
ZIKV
SGZ
Hilu
DG
200μm
50μm

CHAPTER 5: Discussion and Future Directions

Because of the inherent morphological and functional differences between mouse and human brain development, novel stem cell-based platforms for the human brain model are required to dissect the molecular mechanisms that contribute to neurodegenerative diseases. This dissertation set out to generate human pluripotent stem cell-derived models of the brain to study neurodegenerative diseases, such as the emerging ZIKV epidemic. The first goal was to dissect the mechanisms that contribute to the stochastic nature of somatic cell reprogramming in an effort to enhance iPSC yield, the primary limitation of iPSC reprogramming. Second, this dissertation aimed to utilize pluripotent stem cells – either human embryonic stem cells or induced pluripotent stem cells – to generate human cerebral organoid models to study brain development and neurodegeneration in vitro. The last goal was to utilize these tools to explore the correlation between the increased incidence in ZIKV infection and fetal microcephaly and better study the dynamic transcriptomic response during ZIKV infection.

Chapter 5.1: miR-135b modulates ECM expression to facilitate somatic reprogramming

To study the molecular mechanisms which promote and enhance somatic cell reprogramming, we hypothesized that miRNAs may regulate barriers which inhibit iPSC maturation and/or facilitate successfully reprogramming. We profiled

miRNAs in Thy1+ and Thy1- fibroblasts with Thy1+ MEFs being highly resistant to programming as indicated by AP staining. Through gain of function and loss of function assays, miR-135b was confirmed to enhance iPSC induction through a novel extracellular matrix-driven regulation of the iPSC microenvironment. Yamanka OSKM reprogramming induced an upregulation of miR-135b expression which directly repressed *Wisp1* and *Igfbp5* expression. Further functional analyses revealed that Wisp1 is a key regulator of Tgfbi, Igfbp5, Dkk2, Nov and Ccl20 expression, possibly mediated interactions with biglycan. Thus, these data suggest that miRNA-mediated regulation of ECM components contributes to the stochasticity of somatic cell reprogramming. While previous studies have explored the dynamic transcriptome, epigenome, epitranscriptome and metabolome during somatic reprogramming, this study reveals a novel role of extracellular matrix reprogramming during iPSC induction. Moreover, this study highlights the ability of miRNAs to enhance iPSC reprogramming through downregulation of barrier genes such as Wisp1, which is highly expressed by MEF.

Previous studies have shown that iPSC reprogramming is characterized by two major stages: the initial epigenetic reprogramming induced by OSKM transduction, and the later stage of maturation in which iPSCs enter a deterministic stage (Polo et al., 2012; Soufi et al., 2012). Future work in this field of study may focus on the role of the extracellular matrix and microenvironment during the deterministic phases of iPSC induction and the biphasic nature of Wisp1 during somatic cell reprogramming. Inducible shRNA or CRISPR/Cas9-

mediated knockdown/knockout and overexpression of Wisp1 in a time course dependent manner during somatic cell reprogramming may elucidate the temporally sensitive role of Wisp1. These analyses in combination with RNA-seq will provide insight into the specific stage in which Wisp1 transitions from a positive to negative regulator of iPSC induction and the gene networks modulated by Wisp1 signaling.

In addition, the mechanistic role of Wisp1-mediated ECM regulation remains to be revealed. Does Wisp1 modulate the iPSC microenvironment and expression of ECM genes Igfbp5, Dkk2, Nov and Tgfbi through interactions with biglycan and decorin? To address these questions, FLAG-tagged Wisp1 can be overexpressed, immunoprecipitated and interacting proteins can be identified by mass spectrometry. These experiments may be performed at various timepoints during iPSC induction determine whether or not Wisp1 interacting proteins differ in a temporal manner during the reprogramming process, thus accounting for its dual role. Knockdown or knockout experiments of Wisp1 interacting proteins as well as overexpression of mutated Wisp1 can be utilized to dissect the key signaling proteins responsible for remodeling the microenvironment during reprogramming. Extracellular matrix components involved in Wisp1 signaling during reprogramming may be utilized to identify soluble media factors that may enhance reprogramming efficiency.

Chapter 5.2: 3D self-organizing cerebral organoids model ZIKV-microcephaly

The second aim of this dissertation was to examine the potential causal relationship between ZIKV and microcephaly using three-dimensional, self-organizing human cerebral organoid models. The current and ongoing ZIKV epidemic originating in Brazil showed a strong correlation between maternal ZIKV infection and microcephalic infants. Thus, organoids present a physiologically relevant human model for the developing fetal brain with which to study ZIKV pathogenesis in vitro. First, we generated stem cell-derived cerebral organoids using an “intrinsic” neural differentiation model to allow for broad regionalization. Immunohistochemistry revealed the expression of forebrain, midbrain and hippocampal markers. Calcium dye imaging was utilized to assess electrophysiology. RNA-seq of whole organoids revealed large transcriptomic changes between human embryonic stem cells and 1 and 2 month old organoids. Correlation between organoid transcriptomes and BrainSpan datasets from post-mortem fetal tissues across age and region suggested a strong correlation between early first trimester fetal brains and organoids. In addition, transcriptomic analyses showed that organoids recapitulate regions such as the developing neocortex and ganglionic eminence. Overall, this demonstrates the ability of stem cell-derived cerebral organoids to model the developing brain at the morphological, functional and transcriptomic level.

Organoids were then treated with prototype MR766 ZIKV to understand the phenotypic and transcriptomic response during early stage neural

development. Organoids treated with ZIKV showed significant decrease in the neuroepithelium and overall organoid size. This was one of the foundational studies that showed that ZIKV preferentially infects the neural stem cell population in the brain as evidenced by the colocalization of cells expressing the flavivirus envelope protein and neural stem cell marker, NESTIN, and leads to a microcephaly-like phenotype.

Because TLR3, a key antiviral component of the innate immunity, has been linked to neurodegenerative phenotypes, so we hypothesized that ZIKV may activate the TLR3 pathway in neural progenitor cells, subsequently triggering a apoptotic cascade and altered cell fate (Cameron et al., 2007; Dang et al., 2016; Hamel et al., 2015; Okun et al., 2010; Okun et al., 2011; Tsai et al., 2009; Yaddanapudi et al., 2011). Indeed, ZIKV infection of organoids and neurospheres revealed an increased activation of TLR3. 41 genes were then shown to be commonly differentially expressed during cerebral organoid formation and TLR3 activation, thus presenting a potential link between antiviral innate immune activation and neurodegenerative pathways.

These data suggest a potential link between ZIKV induced TLR3 activation and neurodegeneration. To further build upon this, gain and loss of function studies should be performed to analyze these individual genes in the context of innate immune activation and neurodegeneration. Moreover, the mechanistic link between these neurogenesis-related genes and immune activation remains unresolved.

In addition, genetic mouse models and in vivo knockdown experiments would provide insight into the ZIKV-mediate neurodegenerative phenotype in vivo. Finally, single cell RNA-seq of ZIKV infected organoids would identify which cells are in highly infected in a human brain model and the transcriptomic response in infected cells at the single cell level.

Chapter 5.3: miRNAs regulate transcriptional networks during ZIKV infection and associated neurodegeneration

Finally, the last aim of this dissertation was to analyze the coding and non-coding transcriptome in ZIKV infected neural stem cells, which were shown to be highly infected in organoid models. This study identified ZIKV dysregulated miRNA-regulated transcriptional networks involved in neural stem cell self-renewal, cell cycle progression and neurogenesis using an integrative approach analyzing RNA-seq, miR-seq and predictive algorithms. Following ZIKV infection, miR-218 was upregulated, thereby repressing a gene network involved in stem cell maintenance. Functional analyses showed the miR-218 directly represses TFRC and indirectly downregulates EPHA4, both previously shown to regulate neurogenesis.

Future studies should focus on the role of TFRC in ZIKV-mediated neurodegeneration. TFRC is a regulator of ferric iron metabolism and has been implicated in regulation of cell cycle regulation, neurogenesis and cancer stem cell stemness (Matak et al., 2016; Sanchez et al., 2006; Schonberg et al., 2015;

Silvestroff et al., 2013). In addition, TFRC has previously been shown to regulate bone resorption, which may potentially play a role in the increased incidence of brain calcifications shown in ZIKV infected fetal brains (Ishii et al., 2009). In vivo shRNA-mediated knockdown of Tfrc by adeno-associated virus in mice may provide additional insight into the role of TFRC in ZIKV pathogenesis. Moreover, these findings suggest a causal link between ZIKV induced dysregulation of metabolic process and perturbed cell cycle mediated through downregulation of TFRC. In depth analysis of TFRC's role in the STAT3-FoxM1 regulatory axis identified by Schonberg et al. may provide further insight into the causes of ZIKV-mediated neurodegeneration (Schonberg et al., 2015). Further analysis of iron uptake during ZIKV infection and its role in both cell cycle regulation and neural stem cell self-renewal may provide designs for novel ZIKV therapeutics.

miRNA biology may regulate ZIKV infection and pathogenesis in several non-canonical ways. For instance, HCV has been shown to functionally sequester miR-122 to de-repress miR-122 mRNA targets, thus acting as a miR-sponge (Luna et al., 2015). This phenomenon follows the competing endogenous RNA (ceRNA) hypothesis in which mRNAs, pseudogenes, and long non-coding RNAs may collectively compete for miRNA binding (Salmena et al., 2011; Thomson and Dinger, 2016). Essentially, if a transcript containing binding sites for a specific miRNA is overexpressed, it will, in effect, act as a miRNA-sponge and relieve miRNA-mediated repression of other mRNAs. This hypothesis has been experimentally supported by Poliseno et al. who observed that the pseudogene *PTENP1* regulated *PTEN* expression in a DICER-dependent

manner (Poliseno et al., 2010). However, the ceRNA hypothesis is quite controversial, stemming from recent analyses about the stoichiometry of miRNAs and target site abundance. Denzler et al. systematically calculated that the threshold number of transcripts for a given miRNA necessary to effectively act as a miR-sponge would be approximately $1.5x10^5$, a physiologically dubious number (Denzler et al., 2014). On the other hand, RNA viruses such as ZIKV are highly overexpressed and may indeed act as a miR-sponge. Bioinformatic analyses to predict putative miRNA binding sites within the ZIKV transcript and AGO-iCLIP-seq or CLASH-seq experiments should be performed to analyze the global de-repression by ZIKV-sponged miRNAs.

Lastly, analysis of viral-encoded miRNAs may provide insight into novel ZIKV-mediated regulatory mechanisms. While numerous studies have shown that DNA viruses are capable of encoding for miRNAs, only a few have indicated that RNA viruses are capable of generating small RNAs. The majority of known functional viral miRNAs are generated by viruses within the *Herpesviridae* family – including Herpes Simplex Virus 1 and 2, Herpes B virus and human cytomegalovirus – and regulate the latent versus lytic viral lifecycle and evade the immune response (Kincaid and Sullivan, 2012). Previously, it was discovered that RNA viruses such as Dengue, Vesicular Stomatitis, Polio, Hepatitis C, West Nile and Flock House are capable of generating viral small RNAs, some of which were able to load into Argonaute complexes (Parameswaran et al., 2010). Furthermore, Rouha et al. indicated that functional miRNAs can be generated from cytoplasmic RNA viruses through the introduction of pre-miRNA-like hairpin

structures into tick-borne encephalitis virus (Rouha et al., 2010). Together, these studies indicate that flaviviruses like ZIKV or tick-borne encephalitis virus may generate novel viral miRNAs. Use of RNA secondary-structure algorithms to identify hairpin structures coupled with miR-seq analyses may be used to identify novel ZIKV-encoded miRNAs.

REFERENCES

Adams, J.C., and Watt, F.M. (1993). Regulation of development and differentiation by the extracellular matrix. Development *117*, 1183-1198.

Agarwal, V., Bell, G.W., Nam, J.W., and Bartel, D.P. (2015). Predicting effective microRNA target sites in mammalian mRNAs. Elife *4*.

Ahmed, A.A., Mills, A.D., Ibrahim, A.E., Temple, J., Blenkiron, C., Vias, M., Massie, C.E., Iyer, N.G., McGeoch, A., Crawford, R., Nicke, B., Downward, J., Swanton, C., Bell, S.D., Earl, H.M., Laskey, R.A., Caldas, C., and Brenton, J.D. (2007). The extracellular matrix protein TGFBI induces microtubule stabilization and sensitizes ovarian cancers to paclitaxel. Cancer Cell *12*, 514-527.

Ambros, V. (2004a). The functions of animal microRNAs. Nature *431*, 6.

Ambros, V. (2004b). The functions of animal microRNAs. Nature *431*, 350-355.

Ang, Y.S., Tsai, S.Y., Lee, D.F., Monk, J., Su, J., Ratnakumar, K., Ding, J., Ge, Y., Darr, H., Chang, B., Wang, J., Rendl, M., Bernstein, E., Schaniel, C., and Lemischka, I.R. (2011). Wdr5 mediates self-renewal and reprogramming via the embryonic stem cell core transcriptional network. Cell *145*, 183-197.

Anokye-Danso, F., Trivedi, C.M., Juhr, D., Gupta, M., Cui, Z., Tian, Y., Zhang, Y., Yang, W., Gruber, P.J., Epstein, J.A., and Morrisey, E.E. (2011). Highly efficient miRNA-mediated reprogramming of mouse and human somatic cells to pluripotency. Cell Stem Cell *8*, 376-388.

Aoi, T., Yae, K., Nakagawa, M., Ichisaka, T., Okita, K., Takahashi, K., Chiba, T., and Yamanaka, S. (2008). Generation of pluripotent stem cells from adult mouse liver and stomach cells. Science *321*, 699-702.

Baek, D., Villen, J., Shin, C., Camargo, F.D., Gygi, S.P., and Bartel, D.P. (2008). The impact of microRNAs on protein output. Nature *455*, 64-71.

Banito, A., Rashid, S.T., Acosta, J.C., Li, S., Pereira, C.F., Geti, I., Pinho, S., Silva, J.C., Azuara, V., Walsh, M., Vallier, L., and Gil, J. (2009). Senescence impairs successful reprogramming to pluripotent stem cells. Genes Dev *23*, 2134-2139.

Baril, M., Racine, M.E., Penin, F., and Lamarre, D. (2009). MAVS dimer is a crucial signaling component of innate immunity and the target of hepatitis C virus NS3/4A protease. J Virol *83*, 1299-1311.

Bartel, D.P. (2009). MicroRNAs: target recognition and regulatory functions. Cell *136*, 215-233.

Bayer, A., Lennemann, N.J., Ouyang, Y., Bramley, J.C., Morosky, S., Marques, E.T., Jr., Cherry, S., Sadovsky, Y., and Coyne, C.B. (2016). Type III Interferons Produced by Human Placental Trophoblasts Confer Protection against Zika Virus Infection. Cell Host Microbe.

Beattie, J., Allan, G.J., Lochrie, J.D., and Flint, D.J. (2006). Insulin-like growth factor-binding protein-5 (IGFBP-5): a critical member of the IGF axis. Biochem J *395*, 1-19.

Bendall, S.C., Stewart, M.H., Menendez, P., George, D., Vijayaragavan, K., Werbowetski-Ogilvie, T., Ramos-Mejia, V., Rouleau, A., Yang, J., Bosse, M., Lajoie, G., and Bhatia, M. (2007). IGF and FGF cooperatively establish the regulatory stem cell niche of pluripotent human cells in vitro. Nature *448*, 1015-1021.

Berschneider, B., and Konigshoff, M. (2011). WNT1 inducible signaling pathway protein 1 (WISP1): a novel mediator linking development and disease. Int J Biochem Cell Biol *43*, 306-309.

Betel, D., Wilson, M., Gabow, A., Marks, D.S., and Sander, C. (2008). The microRNA.org resource: targets and expression. Nucleic Acids Res *36*, D149-153.

Bin, J.M., Han, D., Lai Wing Sun, K., Croteau, L.P., Dumontier, E., Cloutier, J.F., Kania, A., and Kennedy, T.E. (2015). Complete Loss of Netrin-1 Results in Embryonic Lethality and Severe Axon Guidance Defects without Increased Neural Cell Death. Cell Rep *12*, 1099-1106.

Bindea, G., Mlecnik, B., Hackl, H., Charoentong, P., Tosolini, M., Kirilovsky, A., Fridman, W.H., Pages, F., Trajanoski, Z., and Galon, J. (2009). ClueGO: a Cytoscape plug-in to decipher functionally grouped gene ontology and pathway annotation networks. Bioinformatics *25*, 1091-1093.

Bissell, M.J., and Hines, W.C. (2011). Why don't we get more cancer? A proposed role of the microenvironment in restraining cancer progression. Nat Med *17*, 320-329.

Brambrink, T., Foreman, R., Welstead, G.G., Lengner, C.J., Wernig, M., Suh, H., and Jaenisch, R. (2008). Sequential expression of pluripotency markers during direct reprogramming of mouse somatic cells. Cell Stem Cell *2*, 151-159.

Brasil, P., Calvet, G.A., de Souza, R.V., and Siqueira, A.M. (2016a). Exanthema associated with Zika virus infection. Lancet Infect Dis *16*, 866.

Brasil, P., Sequeira, P.C., Freitas, A.D., Zogbi, H.E., Calvet, G.A., de Souza, R.V., Siqueira, A.M., de Mendonca, M.C., Nogueira, R.M., de Filippis, A.M., and

Solomon, T. (2016b). Guillain-Barre syndrome associated with Zika virus infection. Lancet *387*, 1482.

Briant, L., Despres, P., Choumet, V., and Misse, D. (2014). Role of skin immune cells on the host susceptibility to mosquito-borne viruses. Virology *464-465*, 26-32.

Calvet, G., Aguiar, R.S., Melo, A.S., Sampaio, S.A., de Filippis, I., Fabri, A., Araujo, E.S., de Sequeira, P.C., de Mendonca, M.C., de Oliveira, L., Tschoeke, D.A., Schrago, C.G., Thompson, F.L., Brasil, P., Dos Santos, F.B., Nogueira, R.M., Tanuri, A., and de Filippis, A.M. (2016a). Detection and sequencing of Zika virus from amniotic fluid of fetuses with microcephaly in Brazil: a case study. Lancet Infect Dis *16*, 653-660.

Calvet, G., Aguiar, R.S., Melo, A.S.O., Sampaio, S.A., de Filippis, I., Fabri, A., Araujo, E.S.M., de Sequeira, P.C., de Mendonça, M.C.L., de Oliveira, L., Tschoeke, D.A., Schrago, C.G., Thompson, F.L., Brasil, P., dos Santos, F.B., Nogueira, R.M.R., Tanuri, A., and de Filippis, A.M.B. (2016b). Detection and sequencing of Zika virus from amniotic fluid of fetuses with microcephaly in Brazil: a case study. The Lancet Infectious Diseases.

Cameron, J.S., Alexopoulou, L., Sloane, J.A., DiBernardo, A.B., Ma, Y., Kosaras, B., Flavell, R., Strittmatter, S.M., Volpe, J., Sidman, R., and Vartanian, T. (2007). Toll-like receptor 3 is a potent negative regulator of axonal growth in mammals. J Neurosci *27*, 13033-13041.

Camp, J.G., Badsha, F., Florio, M., Kanton, S., Gerber, T., Wilsch-Brauninger, M., Lewitus, E., Sykes, A., Hevers, W., Lancaster, M., Knoblich, J.A., Lachmann, R., Paabo, S., Huttner, W.B., and Treutlein, B. (2015). Human cerebral organoids recapitulate gene expression programs of fetal neocortex development. Proc Natl Acad Sci U S A *112*, 15672-15677.

Chambers, S.M., Fasano, C.A., Papapetrou, E.P., Tomishima, M., Sadelain, M., and Studer, L. (2009). Highly efficient neural conversion of human ES and iPS cells by dual inhibition of SMAD signaling. Nat Biotechnol *27*, 275-280.

Chen, C.C., and Lau, L.F. (2009). Functions and mechanisms of action of CCN matricellular proteins. Int J Biochem Cell Biol *41*, 771-783.

Chen, H., Qian, K., Du, Z., Cao, J., Petersen, A., Liu, H., Blackbourn, L.W.t., Huang, C.L., Errigo, A., Yin, Y., Lu, J., Ayala, M., and Zhang, S.C. (2014). Modeling ALS with iPSCs reveals that mutant SOD1 misregulates neurofilament balance in motor neurons. Cell Stem Cell *14*, 796-809.

Chi, S.W., Hannon, G.J., and Darnell, R.B. (2012). An alternative mode of microRNA target recognition. Nat Struct Mol Biol *19*, 321-327.

Choi, Y.J., Lin, C.P., Ho, J.J., He, X., Okada, N., Bu, P., Zhong, Y., Kim, S.Y., Bennett, M.J., Chen, C., Ozturk, A., Hicks, G.G., Hannon, G.J., and He, L. (2011a). miR-34 miRNAs provide a barrier for somatic cell reprogramming. Nat Cell Biol *13*, 1353-1360.

Choi, Y.J., Lin, C.P., Ho, J.J., He, X., Okada, N., Bu, P., Zhong, Y., Kim, S.Y., Bennett, M.J., Chen, C., Ozturk, A., Hicks, G.G., Hannon, G.J., and He, L. (2011b). miR-34 miRNAs provide a barrier for somatic cell reprogramming. Nat Cell Biol *13*, 1353-1360.

Chong, M.M., Zhang, G., Cheloufi, S., Neubert, T.A., Hannon, G.J., and Littman, D.R. (2010). Canonical and alternate functions of the microRNA biogenesis machinery. Genes Dev *24*, 1951-1960.

Chou, C.H., Chang, N.W., Shrestha, S., Hsu, S.D., Lin, Y.L., Lee, W.H., Yang, C.D., Hong, H.C., Wei, T.Y., Tu, S.J., Tsai, T.R., Ho, S.Y., Jian, T.Y., Wu, H.Y., Chen, P.R., Lin, N.C., Huang, H.T., Yang, T.L., Pai, C.Y., Tai, C.S., Chen, W.L., Huang, C.Y., Liu, C.C., Weng, S.L., Liao, K.W., Hsu, W.L., and Huang, H.D. (2016). miRTarBase 2016: updates to the experimentally validated miRNA-target interactions database. Nucleic Acids Res *44*, D239-247.

Chronis, C., Fiziev, P., Papp, B., Butz, S., Bonora, G., Sabri, S., Ernst, J., and Plath, K. (2017). Cooperative Binding of Transcription Factors Orchestrates Reprogramming. Cell *168*, 442-459 e420.

Chu, C.Y., and Rana, T.M. (2006). Translation repression in human cells by microRNA-induced gene silencing requires RCK/p54. PLoS Biol *4*, e210.

Chu, C.Y., and Rana, T.M. (2007). Small RNAs: regulators and guardians of the genome. Journal of cellular physiology *213*, 412-419.

Chumley, M.J., Catchpole, T., Silvany, R.E., Kernie, S.G., and Henkemeyer, M. (2007). EphB receptors regulate stem/progenitor cell proliferation, migration, and polarity during hippocampal neurogenesis. J Neurosci *27*, 13481-13490.

Cugola, F.R., Fernandes, I.R., Russo, F.B., Freitas, B.C., Dias, J.L.M., Guimarães, K.P., Benazzato, C., Almeida, N., Pignatari, G.C., Romero, S., Polonio, C.M., Cunha, I., Freitas, C.L., Brandão, W.N., Rossato, C., Andrade, D.G., Faria, D.d.P., Garcez, A.T., Buchpigel, C.A., Braconi, C.T., Mendes, E., Sall, A.A., Zanotto, P.M.d.A., Peron, J.P.S., Muotri, A.R., and Beltrão-Braga, P.C.B. (2016). The Brazilian Zika virus strain causes birth defects in experimental models. Nature, 10.1038/nature18296.

D'Ortenzio, E., Matheron, S., de Lamballerie, X., Hubert, B., Piorkowski, G., Maquart, M., Descamps, D., Damond, F., Yazdanpanah, Y., and Leparc-Goffart, I. (2016). Evidence of Sexual Transmission of Zika Virus. N Engl J Med.

Dang, J., Tiwari, S., Lichinchi, G., Qin, Y., Patil, V., Eroshkin, A., and Rana, T. (2016). Zika Virus Depletes Neural Progenitors in Human Cerebral Organoids through Activation of the Innate Immune Receptor TLR3. Cell Stee *19*.

De Miranda, J., Yaddanapudi, K., Hornig, M., Villar, G., Serge, R., and Lipkin, W.I. (2010). Induction of Toll-like receptor 3-mediated immunity during gestation inhibits cortical neurogenesis and causes behavioral disturbances. MBio *1*, 10.

Denzler, R., Agarwal, V., Stefano, J., Bartel, D.P., and Stoffel, M. (2014). Assessing the ceRNA hypothesis with quantitative measurements of miRNA and target abundance. Mol Cell *54*, 766-776.

Desnoyers, L., Arnott, D., and Pennica, D. (2001). WISP-1 binds to decorin and biglycan. J Biol Chem *276*, 47599-47607.

Dick, G.W., Kitchen, S.F., and Haddow, A.J. (1952). Zika virus. I. Isolations and serological specificity. Trans R Soc Trop Med Hyg *46*, 509-520.

Djuranovic, S., Nahvi, A., and Green, R. (2011). A parsimonious model for gene regulation by miRNAs. Science *331*, 550-553.

Driggers, R.W., Ho, C.Y., Korhonen, E.M., Kuivanen, S., Jaaskelainen, A.J., Smura, T., Rosenberg, A., Hill, D.A., DeBiasi, R.L., Vezina, G., Timofeev, J., Rodriguez, F.J., Levanov, L., Razak, J., Iyengar, P., Hennenfent, A., Kennedy, R., Lanciotti, R., du Plessis, A., and Vapalahti, O. (2016a). Zika Virus Infection with Prolonged Maternal Viremia and Fetal Brain Abnormalities. N Engl J Med.

Driggers, R.W., Ho, C.Y., Korhonen, E.M., Kuivanen, S., Jaaskelainen, A.J., Smura, T., Rosenberg, A., Hill, D.A., DeBiasi, R.L., Vezina, G., Timofeev, J., Rodriguez, F.J., Levanov, L., Razak, J., Iyengar, P., Hennenfent, A., Kennedy, R., Lanciotti, R., du Plessis, A., and Vapalahti, O. (2016b). Zika Virus Infection with Prolonged Maternal Viremia and Fetal Brain Abnormalities. N Engl J Med, 10.

Duffy, M.R., Chen, T.H., Hancock, W.T., Powers, A.M., Kool, J.L., Lanciotti, R.S., Pretrick, M., Marfel, M., Holzbauer, S., Dubray, C., Guillaumot, L., Griggs, A., Bel, M., Lambert, A.J., Laven, J., Kosoy, O., Panella, A., Biggerstaff, B.J., Fischer, M., and Hayes, E.B. (2009). Zika virus outbreak on Yap Island, Federated States of Micronesia. N Engl J Med *360*, 2536-2543.

Eacker, S.M., Dawson, T.M., and Dawson, V.L. (2009). Understanding microRNAs in neurodegeneration. Nat Rev Neurosci *10*, 837-841.

Eiraku, M., Takata, N., Ishibashi, H., Kawada, M., Sakakura, E., Okuda, S., Sekiguchi, K., Adachi, T., and Sasai, Y. (2011). Self-organizing optic-cup morphogenesis in three-dimensional culture. Nature *472*, 51-56.

Eiraku, M., Watanabe, K., Matsuo-Takasaki, M., Kawada, M., Yonemura, S., Matsumura, M., Wataya, T., Nishiyama, A., Muguruma, K., and Sasai, Y. (2008). Self-organized formation of polarized cortical tissues from ESCs and its active manipulation by extrinsic signals. Cell Stem Cell *3*, 519-532.

Enright, A.J., John, B., Gaul, U., Tuschl, T., Sander, C., and Marks, D.S. (2003). MicroRNA targets in Drosophila. Genome biology *5*, R1.

Feng, B., Jiang, J., Kraus, P., Ng, J.H., Heng, J.C., Chan, Y.S., Yaw, L.P., Zhang, W., Loh, Y.H., Han, J., Vega, V.B., Cacheux-Rataboul, V., Lim, B., Lufkin, T., and Ng, H.H. (2009a). Reprogramming of fibroblasts into induced pluripotent stem cells with orphan nuclear receptor Esrrb. Nat Cell Biol *11*, 197-203.

Feng, B., Ng, J.H., Heng, J.C., and Ng, H.H. (2009b). Molecules that promote or enhance reprogramming of somatic cells to induced pluripotent stem cells. Cell Stem Cell *4*, 301-312.

Fietz, S.A., Kelava, I., Vogt, J., Wilsch-Brauninger, M., Stenzel, D., Fish, J.L., Corbeil, D., Riehn, A., Distler, W., Nitsch, R., and Huttner, W.B. (2010). OSVZ progenitors of human and ferret neocortex are epithelial-like and expand by integrin signaling. Nat Neurosci *13*, 690-699.

Fillebeen, C., and Pantopoulos, K. (2010). Iron inhibits replication of infectious hepatitis C virus in permissive Huh7.5.1 cells. J Hepatol *53*, 995-999.

Fillebeen, C., Rivas-Estilla, A.M., Bisaillon, M., Ponka, P., Muckenthaler, M., Hentze, M.W., Koromilas, A.E., and Pantopoulos, K. (2005). Iron inactivates the RNA polymerase NS5B and suppresses subgenomic replication of hepatitis C Virus. J Biol Chem *280*, 9049-9057.

Furne, C., Rama, N., Corset, V., Chedotal, A., and Mehlen, P. (2008). Netrin-1 is a survival factor during commissural neuron navigation. PNAS *105*, 6.

Gabriel, E., Ramani, A., Karow, U., Gottardo, M., Natarajan, K., Gooi, L.M., Goranci-Buzhala, G., Krut, O., Peters, F., Nikolic, M., Kuivanen, S., Korhonen, E., Smura, T., Vapalahti, O., Papantonis, A., Schmidt-Chanasit, J., Riparbelli, M., Callaini, G., Kronke, M., Utermohlen, O., and Gopalakrishnan, J. (2017). Recent Zika Virus Isolates Induce Premature Differentiation of Neural Progenitors in Human Brain Organoids. Cell Stem Cell *20*, 397-406 e395.

Gao, D., Vela, I., Sboner, A., Iaquinta, P.J., Karthaus, W.R., Gopalan, A., Dowling, C., Wanjala, J.N., Undvall, E.A., Arora, V.K., Wongvipat, J., Kossai, M., Ramazanoglu, S., Barboza, L.P., Di, W., Cao, Z., Zhang, Q.F., Sirota, I., Ran, L., MacDonald, T.Y., Beltran, H., Mosquera, J.M., Touijer, K.A., Scardino, P.T., Laudone, V.P., Curtis, K.R., Rathkopf, D.E., Morris, M.J., Danila, D.C., Slovin, S.F., Solomon, S.B., Eastham, J.A., Chi, P., Carver, B., Rubin, M.A., Scher, H.I.,

Clevers, H., Sawyers, C.L., and Chen, Y. (2014). Organoid cultures derived from patients with advanced prostate cancer. Cell *159*, 176-187.

Giorgetti, A., Montserrat, N., Aasen, T., Gonzalez, F., Rodriguez-Piza, I., Vassena, R., Raya, A., Boue, S., Barrero, M.J., Corbella, B.A., Torrabadella, M., Veiga, A., and Izpisua Belmonte, J.C. (2009). Generation of induced pluripotent stem cells from human cord blood using OCT4 and SOX2. Cell Stem Cell *5*, 353-357.

Grant, A., Ponia, S.S., Tripathi, S., Balasubramaniam, V., Miorin, L., Sourisseau, M., Schwarz, M.C., Sanchez-Seco, M.P., Evans, M.J., Best, S.M., and Garcia-Sastre, A. (2016). Zika Virus Targets Human STAT2 to Inhibit Type I Interferon Signaling. Cell Host Microbe *19*, 882-890.

Grimson, A., Farh, K.K., Johnston, W.K., Garrett-Engele, P., Lim, L.P., and Bartel, D.P. (2007). MicroRNA targeting specificity in mammals: determinants beyond seed pairing. Mol Cell *27*, 91-105.

Hafner, M., Landthaler, M., Burger, L., Khorshid, M., Hausser, J., Berninger, P., Rothballer, A., Ascano, M., Jr., Jungkamp, A.C., Munschauer, M., Ulrich, A., Wardle, G.S., Dewell, S., Zavolan, M., and Tuschl, T. (2010). Transcriptome-wide identification of RNA-binding protein and microRNA target sites by PAR-CLIP. Cell *141*, 129-141.

Hajra, A., Bandyopadhyay, D., and Hajra, S.K. (2016). Zika Virus: A Global Threat to Humanity: A Comprehensive Review and Current Developments. N Am J Med Sci *8*, 123-128.

Hamel, R., Dejarnac, O., Wichit, S., Ekchariyawat, P., Neyret, A., Luplertlop, N., Perera-Lecoin, M., Surasombatpattana, P., Talignani, L., Thomas, F., Cao-Lormeau, V.M., Choumet, V., Briant, L., Despres, P., Amara, A., Yssel, H., and Misse, D. (2015). Biology of Zika Virus Infection in Human Skin Cells. J Virol *89*, 8880-8896.

Hanna, J., Saha, K., Pando, B., van Zon, J., Lengner, C.J., Creyghton, M.P., van Oudenaarden, A., and Jaenisch, R. (2009). Direct cell reprogramming is a stochastic process amenable to acceleration. Nature *462*, 595-601.

Hanna, J., Wernig, M., Markoulaki, S., Sun, C.W., Meissner, A., Cassady, J.P., Beard, C., Brambrink, T., Wu, L.C., Townes, T.M., and Jaenisch, R. (2007). Treatment of sickle cell anemia mouse model with iPS cells generated from autologous skin. Science *318*, 1920-1923.

Hansen, D.V., Lui, J.H., Parker, P.R., and Kriegstein, A.R. (2010). Neurogenic radial glia in the outer subventricular zone of human neocortex. Nature *464*, 554-561.

Hayes, E.B. (2009). Zika virus outside Africa. Emerg Infect Dis *15*, 1347-1350.

Henzler, C.M., Li, Z., Dang, J., Arcila, M.L., Zhou, H., Liu, J., Chang, K.Y., Bassett, D.S., Rana, T.M., and Kosik, K.S. (2013). Staged miRNA re-regulation patterns during reprogramming. Genome biology *14*, R149.

Herculano-Houzel, S. (2009). The human brain in numbers: a linearly scaled-up primate brain. Front Hum Neurosci *3*, 31.

Hong, H., Takahashi, K., Ichisaka, T., Aoi, T., Kanagawa, O., Nakagawa, M., Okita, K., and Yamanaka, S. (2009). Suppression of induced pluripotent stem cell generation by the p53-p21 pathway. Nature *460*, 1132-1135.

Huang da, W., Sherman, B.T., and Lempicki, R.A. (2009). Systematic and integrative analysis of large gene lists using DAVID bioinformatics resources. Nat Protoc *4*, 44-57.

Huntzinger, E., and Izaurralde, E. (2011). Gene silencing by microRNAs: contributions of translational repression and mRNA decay. Nature reviews Genetics *12*, 99-110.

Hutvagner, G., McLachlan, J., Pasquinelli, A.E., Balint, E., Tuschl, T., and Zamore, P.D. (2001). A cellular function for the RNA-interference enzyme Dicer in the maturation of the let-7 small temporal RNA. Science *293*, 834-838.

Icardi, L., Mori, R., Gesellchen, V., Eyckerman, S., De Cauwer, L., Verhelst, J., Vercauteren, K., Saelens, X., Meuleman, P., Leroux-Roels, G., De Bosscher, K., Boutros, M., and Tavernier, J. (2012). The Sin3a repressor complex is a master regulator of STAT transcriptional activity. Proc Natl Acad Sci U S A *109*, 12058-12063.

Ichida, J.K., Blanchard, J., Lam, K., Son, E.Y., Chung, J.E., Egli, D., Loh, K.M., Carter, A.C., Di Giorgio, F.P., Koszka, K., Huangfu, D., Akutsu, H., Liu, D.R., Rubin, L.L., and Eggan, K. (2009a). A Small-Molecule Inhibitor of Tgf-beta Signaling Replaces Sox2 in Reprogramming by Inducing Nanog. Cell stem cell.

Ichida, J.K., Blanchard, J., Lam, K., Son, E.Y., Chung, J.E., Egli, D., Loh, K.M., Carter, A.C., Di Giorgio, F.P., Koszka, K., Huangfu, D., Akutsu, H., Liu, D.R., Rubin, L.L., and Eggan, K. (2009b). A small-molecule inhibitor of tgf-Beta signaling replaces sox2 in reprogramming by inducing nanog. Cell Stem Cell *5*, 491-503.

Ishii, K.A., Fumoto, T., Iwai, K., Takeshita, S., Ito, M., Shimohata, N., Aburatani, H., Taketani, S., Lelliott, C.J., Vidal-Puig, A., and Ikeda, K. (2009). Coordination of PGC-1beta and iron uptake in mitochondrial biogenesis and osteoclast activation. Nat Med *15*, 259-266.

Itzhaki, I., Maizels, L., Huber, I., Zwi-Dantsis, L., Caspi, O., Winterstern, A., Feldman, O., Gepstein, A., Arbel, G., Hammerman, H., Boulos, M., and Gepstein, L. (2011). Modelling the long QT syndrome with induced pluripotent stem cells. Nature *471*, 225-229.

Jiao, J., Dang, Y., Yang, Y., Gao, R., Zhang, Y., Kou, Z., Sun, X.F., and Gao, S. (2013). Promoting reprogramming by FGF2 reveals that the extracellular matrix is a barrier for reprogramming fibroblasts to pluripotency. Stem cells *31*, 729-740.

Judson, R.L., Babiarz, J.E., Venere, M., and Blelloch, R. (2009a). Embryonic stem cell-specific microRNAs promote induced pluripotency. Nature biotechnology *27*, 459-461.

Judson, R.L., Babiarz, J.E., Venere, M., and Blelloch, R. (2009b). Embryonic stem cell-specific microRNAs promote induced pluripotency. Nat Biotechnol *27*, 459-461.

Jun, J.I., and Lau, L.F. (2011). Taking aim at the extracellular matrix: CCN proteins as emerging therapeutic targets. Nat Rev Drug Discov *10*, 945-963.

Kadoshima, T., Sakaguchi, H., Nakano, T., Soen, M., Ando, S., Eiraku, M., and Sasai, Y. (2013). Self-organization of axial polarity, inside-out layer pattern, and species-specific progenitor dynamics in human ES cell-derived neocortex. Proc Natl Acad Sci U S A *110*, 20284-20289.

Kang, H.J., Kawasawa, Y.I., Cheng, F., Zhu, Y., Xu, X., Li, M., Sousa, A.M., Pletikos, M., Meyer, K.A., Sedmak, G., Guennel, T., Shin, Y., Johnson, M.B., Krsnik, Z., Mayer, S., Fertuzinhos, S., Umlauf, S., Lisgo, S.N., Vortmeyer, A., Weinberger, D.R., Mane, S., Hyde, T.M., Huttner, A., Reimers, M., Kleinman, J.E., and Sestan, N. (2011). Spatio-temporal transcriptome of the human brain. Nature *478*, 483-489.

Katakowski, M., Zhang, Z., deCarvalho, A.C., and Chopp, M. (2005). EphB2 induces proliferation and promotes a neuronal fate in adult subventricular neural precursor cells. Neurosci Lett *385*, 204-209.

Kawamata, T., and Tomari, Y. (2010). Making RISC. Trends Biochem Sci *35*, 368-376.

Kawamura, T., Suzuki, J., Wang, Y.V., Menendez, S., Morera, L.B., Raya, A., Wahl, G.M., and Belmonte, J.C. (2009). Linking the p53 tumour suppressor pathway to somatic cell reprogramming. Nature *460*, 1140-1144.

Kawano, Y., and Kypta, R. (2003). Secreted antagonists of the Wnt signalling pathway. J Cell Sci *116*, 2627-2634.

Kessenbrock, K., Plaks, V., and Werb, Z. (2010). Matrix metalloproteinases: regulators of the tumor microenvironment. Cell *141*, 52-67.

Khodosevich, K., Watanabe, Y., and Monyer, H. (2011). EphA4 preserves postnatal and adult neural stem cells in an undifferentiated state in vivo. J Cell Sci *124*, 1268-1279.

Kim, K.S., Seu, Y.B., Baek, S.H., Kim, M.J., Kim, K.J., Kim, J.H., and Kim, J.R. (2007). Induction of cellular senescence by insulin-like growth factor binding protein-5 through a p53-dependent mechanism. Mol Biol Cell *18*, 4543-4552.

Kincaid, R.P., and Sullivan, C.S. (2012). Virus-encoded microRNAs: an overview and a look to the future. PLoS Pathog *8*, e1003018.

Knight, S.W., and Bass, B.L. (2001). A role for the RNase III enzyme DCR-1 in RNA interference and germ line development in Caenorhabditis elegans. Science *293*, 2269-2271.

Koehler, K.R., and Hashino, E. (2014). 3D mouse embryonic stem cell culture for generating inner ear organoids. Nat Protoc *9*, 1229-1244.

Konigshoff, M., Kramer, M., Balsara, N., Wilhelm, J., Amarie, O.V., Jahn, A., Rose, F., Fink, L., Seeger, W., Schaefer, L., Gunther, A., and Eickelberg, O. (2009). WNT1-inducible signaling protein-1 mediates pulmonary fibrosis in mice and is upregulated in humans with idiopathic pulmonary fibrosis. J Clin Invest *119*, 772-787.

Kumar, A., Hou, S., Airo, A.M., Limonta, D., Mancinelli, V., Branton, W., Power, C., and Hobman, T.C. (2016). Zika virus inhibits type-I interferon production and downstream signaling. EMBO Rep *17*, 1766-1775.

Kutmon, M., Kelder, T., Mandaviya, P., Evelo, C.T., and Coort, S.L. (2013). CyTargetLinker: a cytoscape app to integrate regulatory interactions in network analysis. PLoS One *8*, e82160.

Kuzmichev, A., Nishioka, K., Erdjument-Bromage, H., Tempst, P., and Reinberg, D. (2002). Histone methyltransferase activity associated with a human multiprotein complex containing the Enhancer of Zeste protein. Genes Dev *16*, 2893-2905.

Lancaster, M.A., and Knoblich, J.A. (2014). Organogenesis in a dish: modeling development and disease using organoid technologies. Science *345*, 1247125.

Lancaster, M.A., Renner, M., Martin, C.A., Wenzel, D., Bicknell, L.S., Hurles, M.E., Homfray, T., Penninger, J.M., Jackson, A.P., and Knoblich, J.A. (2013). Cerebral organoids model human brain development and microcephaly. Nature *501*, 373-379.

Lanford, R.E., Hildebrandt-Eriksen, E.S., Petri, A., Persson, R., Lindow, M., Munk, M.E., Kauppinen, S., and Orum, H. (2010). Therapeutic silencing of microRNA-122 in primates with chronic hepatitis C virus infection. Science *327*, 198-201.

Lathia, J.D., Okun, E., Tang, S.C., Griffioen, K., Cheng, A., Mughal, M.R., Laryea, G., Selvaraj, P.K., ffrench-Constant, C., Magnus, T., Arumugam, T.V., and Mattson, M.P. (2008). Toll-like receptor 3 is a negative regulator of embryonic neural progenitor cell proliferation. J Neurosci *28*, 13978-13984.

Lazear, H.M., and Diamond, M.S. (2016). Zika Virus: New Clinical Syndromes and Its Emergence in the Western Hemisphere. J Virol *90*, 4864-4875.

Lazear, H.M., Govero, J., Smith, A.M., Platt, D.J., Fernandez, E., Miner, J.J., and Diamond, M.S. (2016). A Mouse Model of Zika Virus Pathogenesis. Cell Host Microbe, 10.1016/j.chom.2016.1003.1010.

Lee, Y., Ahn, C., Han, J., Choi, H., Kim, J., Yim, J., Lee, J., Provost, P., Radmark, O., Kim, S., and Kim, V.N. (2003). The nuclear RNase III Drosha initiates microRNA processing. Nature *425*, 415-419.

Lewis, B.P., Burge, C.B., and Bartel, D.P. (2005). Conserved seed pairing, often flanked by adenosines, indicates that thousands of human genes are microRNA targets. Cell *120*, 15-20.

Li, C., Xu, D., Ye, Q., Hong, S., Jiang, Y., Liu, X., Zhang, N., Shi, L., Qin, C.F., and Xu, Z. (2016). Zika Virus Disrupts Neural Progenitor Development and Leads to Microcephaly in Mice. Cell Stem Cell, 10.1016/j.stem.2016.1004.1017.

Li, H., Collado, M., Villasante, A., Strati, K., Ortega, S., Canamero, M., Blasco, M.A., and Serrano, M. (2009). The Ink4/Arf locus is a barrier for iPS cell reprogramming. Nature *460*, 1136-1139.

Li, H., and Durbin, R. (2009). Fast and accurate short read alignment with Burrows-Wheeler transform. Bioinformatics *25*, 1754-1760.

Li, M.A., and He, L. (2012). microRNAs as novel regulators of stem cell pluripotency and somatic cell reprogramming. Bioessays *34*, 670-680.

Li, R., Liang, J., Ni, S., Zhou, T., Qing, X., Li, H., He, W., Chen, J., Li, F., Zhuang, Q., Qin, B., Xu, J., Li, W., Yang, J., Gan, Y., Qin, D., Feng, S., Song, H., Yang, D., Zhang, B., Zeng, L., Lai, L., Esteban, M.A., and Pei, D. (2010). A mesenchymal-to-epithelial transition initiates and is required for the nuclear reprogramming of mouse fibroblasts. Cell Stem Cell *7*, 51-63.

Li, Z., and Rana, T. (2012a). Molecular Mechanisms of RNA-Triggered Gene Silencing Machineries. Accounts of Chemical Research *45*, 10.

Li, Z., and Rana, T.M. (2012b). A kinase inhibitor screen identifies small-molecule enhancers of reprogramming and iPS cell generation. Nat Commun *3*, 1085.

Li, Z., Yang, C.S., Nakashima, K., and Rana, T.M. (2011a). Small RNA-mediated regulation of iPS cell generation. Embo J *30*, 823-834.

Li, Z., Yang, C.S., Nakashima, K., and Rana, T.M. (2011b). Small RNA-mediated regulation of iPS cell generation. EMBO J *30*, 823-834.

Liang, Q., Luo, Z., Zeng, J., Chen, W., Foo, S.S., Lee, S.A., Ge, J., Wang, S., Goldman, S.A., Zlokovic, B.V., Zhao, Z., and Jung, J.U. (2016). Zika Virus NS4A and NS4B Proteins Deregulate Akt-mTOR Signaling in Human Fetal Neural Stem Cells to Inhibit Neurogenesis and Induce Autophagy. Cell Stem Cell.

Liao, B., Bao, X., Liu, L., Feng, S., Zovoilis, A., Liu, W., Xue, Y., Cai, J., Guo, X., Qin, B., Zhang, R., Wu, J., Lai, L., Teng, M., Niu, L., Zhang, B., Esteban, M.A., and Pei, D. (2011a). MicroRNA cluster 302-367 enhances somatic cell reprogramming by accelerating a mesenchymal-to-epithelial transition. J Biol Chem *286*, 17359-17364.

Liao, B., Bao, X., Liu, L., Feng, S., Zovoilis, A., Liu, W., Xue, Y., Cai, J., Guo, X., Qin, B., Zhang, R., Wu, J., Lai, L., Teng, M., Niu, L., Zhang, B., Esteban, M.A., and Pei, D. (2011b). MicroRNA cluster 302-367 enhances somatic cell reprogramming by accelerating a mesenchymal-to-epithelial transition. J Biol Chem *286*, 17359-17364.

Lipchina, I., Elkabetz, Y., Hafner, M., Sheridan, R., Mihailovic, A., Tuschl, T., Sander, C., Studer, L., and Betel, D. (2011). Genome-wide identification of microRNA targets in human ES cells reveals a role for miR-302 in modulating BMP response. Genes Dev *25*, 2173-2186.

Liu, J., Carmell, M.A., Rivas, F.V., Marsden, C.G., Thomson, J.M., Song, J.J., Hammond, S.M., Joshua-Tor, L., and Hannon, G.J. (2004). Argonaute2 is the catalytic engine of mammalian RNAi. Science *305*, 1437-1441.

Liu, N., Landreh, M., Cao, K., Abe, M., Hendriks, G.J., Kennerdell, J.R., Zhu, Y., Wang, L.S., and Bonini, N.M. (2012). The microRNA miR-34 modulates ageing and neurodegeneration in Drosophila. Nature *482*, 519-523.

Loeb, G.B., Khan, A.A., Canner, D., Hiatt, J.B., Shendure, J., Darnell, R.B., Leslie, C.S., and Rudensky, A.Y. (2012). Transcriptome-wide miR-155 binding map reveals widespread noncanonical microRNA targeting. Mol Cell *48*, 760-770.

Loh, Y.H., Agarwal, S., Park, I.H., Urbach, A., Huo, H., Heffner, G.C., Kim, K., Miller, J.D., Ng, K., and Daley, G.Q. (2009). Generation of induced pluripotent stem cells from human blood. Blood *113*, 5476-5479.

Lowry, W.E., Richter, L., Yachechko, R., Pyle, A.D., Tchieu, J., Sridharan, R., Clark, A.T., and Plath, K. (2008). Generation of human induced pluripotent stem cells from dermal fibroblasts. Proc Natl Acad Sci U S A *105*, 2883-2888.

Luna, J.M., Scheel, T.K., Danino, T., Shaw, K.S., Mele, A., Fak, J.J., Nishiuchi, E., Takacs, C.N., Catanese, M.T., de Jong, Y.P., Jacobson, I.M., Rice, C.M., and Darnell, R.B. (2015). Hepatitis C virus RNA functionally sequesters miR-122. Cell *160*, 1099-1110.

Lund, E., Guttinger, S., Calado, A., Dahlberg, J.E., and Kutay, U. (2004). Nuclear export of microRNA precursors. Science *303*, 95-98.

Macnamara, F.N. (1954). Zika virus: a report on three cases of human infection during an epidemic of jaundice in Nigeria. Trans R Soc Trop Med Hyg *48*, 139-145.

Maherali, N., and Hochedlinger, K. (2009a). Tgfbeta Signal Inhibition Cooperates in the Induction of iPSCs and Replaces Sox2 and cMyc. Curr Biol.

Maherali, N., and Hochedlinger, K. (2009b). Tgfbeta signal inhibition cooperates in the induction of iPSCs and replaces Sox2 and cMyc. Curr Biol *19*, 1718-1723.

Marchetto, M.C., Carromeu, C., Acab, A., Yu, D., Yeo, G.W., Mu, Y., Chen, G., Gage, F.H., and Muotri, A.R. (2010). A model for neural development and treatment of Rett syndrome using human induced pluripotent stem cells. Cell *143*, 527-539.

Mariani, J., Coppola, G., Zhang, P., Abyzov, A., Provini, L., Tomasini, L., Amenduni, M., Szekely, A., Palejev, D., Wilson, M., Gerstein, M., Grigorenko, E.L., Chawarska, K., Pelphrey, K.A., Howe, J.R., and Vaccarino, F.M. (2015). FOXG1-Dependent Dysregulation of GABA/Glutamate Neuron Differentiation in Autism Spectrum Disorders. Cell *162*, 375-390.

Marson, A., Foreman, R., Chevalier, B., Bilodeau, S., Kahn, M., Young, R.A., and Jaenisch, R. (2008). Wnt signaling promotes reprogramming of somatic cells to pluripotency. Cell Stem Cell *3*, 132-135.

Martines, R.B., Bhatnagar, J., de Oliveira Ramos, A.M., Davi, H.P., Iglezias, S.D., Kanamura, C.T., Keating, M.K., Hale, G., Silva-Flannery, L., Muehlenbachs, A., Ritter, J., Gary, J., Rollin, D., Goldsmith, C.S., Reagan-Steiner, S., Ermias, Y., Suzuki, T., Luz, K.G., de Oliveira, W.K., Lanciotti, R., Lambert, A., Shieh, W.J.,

and Zaki, S.R. (2016). Pathology of congenital Zika syndrome in Brazil: a case series. Lancet, 10.1016/S0140-6736(1016)30883-30882.

Matak, P., Matak, A., Moustafa, S., Aryal, D.K., Benner, E.J., Wetsel, W., and Andrews, N.C. (2016). Disrupted iron homeostasis causes dopaminergic neurodegeneration in mice. Proc Natl Acad Sci U S A *113*, 3428-3435.

Meissner, A., Wernig, M., and Jaenisch, R. (2007). Direct reprogramming of genetically unmodified fibroblasts into pluripotent stem cells. Nat Biotechnol *25*, 1177-1181.

Melton, C., Judson, R.L., and Blelloch, R. (2010). Opposing microRNA families regulate self-renewal in mouse embryonic stem cells. Nature *463*, 621-626.

Miyoshi, N., Ishii, H., Nagano, H., Haraguchi, N., Dewi, D.L., Kano, Y., Nishikawa, S., Tanemura, M., Mimori, K., Tanaka, F., Saito, T., Nishimura, J., Takemasa, I., Mizushima, T., Ikeda, M., Yamamoto, H., Sekimoto, M., Doki, Y., and Mori, M. (2011). Reprogramming of mouse and human cells to pluripotency using mature microRNAs. Cell Stem Cell *8*, 633-638.

Mlakar, J., Korva, M., Tul, N., Popovic, M., Poljsak-Prijatelj, M., Mraz, J., Kolenc, M., Resman Rus, K., Vesnaver Vipotnik, T., Fabjan Vodusek, V., Vizjak, A., Pizem, J., Petrovec, M., and Avsic Zupanc, T. (2016). Zika Virus Associated with Microcephaly. N Engl J Med *374*, 951-958.

Moreira, J., Lamas, C.C., and Siqueira, A. (2016). Sexual Transmission of Zika Virus: Implications for Clinical Care and Public Health Policy. Clin Infect Dis.

Muguruma, K., Nishiyama, A., Kawakami, H., Hashimoto, K., and Sasai, Y. (2015). Self-organization of polarized cerebellar tissue in 3D culture of human pluripotent stem cells. Cell reports *10*, 537-550.

Nakagawa, M., Koyanagi, M., Tanabe, K., Takahashi, K., Ichisaka, T., Aoi, T., Okita, K., Mochiduki, Y., Takizawa, N., and Yamanaka, S. (2008). Generation of induced pluripotent stem cells without Myc from mouse and human fibroblasts. Nat Biotechnol *26*, 101-106.

Nathans, R., Chu, C.Y., Serquina, A.K., Lu, C.C., Cao, H., and Rana, T.M. (2009). Cellular microRNA and P bodies modulate host-HIV-1 interactions. Mol Cell *34*, 696-709.

Nichols, J., Silva, J., Roode, M., and Smith, A. (2009). Suppression of Erk signalling promotes ground state pluripotency in the mouse embryo. Development *136*, 3215-3222.

Noronha, L., Zanluca, C., Azevedo, M.L., Luz, K.G., and Santos, C.N. (2016). Zika virus damages the human placental barrier and presents marked fetal neurotropism. Mem Inst Oswaldo Cruz *111*, 287-293.

Nowakowski, Tomasz J., Pollen, Alex A., Di Lullo, E., Sandoval-Espinosa, C., Bershteyn, M., and Kriegstein, Arnold R. (2016). Expression Analysis Highlights AXL as a Candidate Zika Virus Entry Receptor in Neural Stem Cells. Cell Stem Cell.

O'Connell, R.M., Rao, D.S., Chaudhuri, A.A., and Baltimore, D. (2010). Physiological and pathological roles for microRNAs in the immune system. Nat Rev Immunol *10*, 111-122.

Okun, E., Griffioen, K., Barak, B., Roberts, N.J., Castro, K., Pita, M.A., Cheng, A., Mughal, M.R., Wan, R., Ashery, U., and Mattson, M.P. (2010). Toll-like receptor 3 inhibits memory retention and constrains adult hippocampal neurogenesis. Proc Natl Acad Sci U S A *107*, 15625-15630.

Okun, E., Griffioen, K.J., and Mattson, M.P. (2011). Toll-like receptor signaling in neural plasticity and disease. Trends Neurosci *34*, 269-281.

Oliveira Melo, A.S., Malinger, G., Ximenes, R., Szejnfeld, P.O., Alves Sampaio, S., and Bispo de Filippis, A.M. (2016). Zika virus intrauterine infection causes fetal brain abnormality and microcephaly: tip of the iceberg? Ultrasound Obstet Gynecol *47*, 6-7.

Onorati, M., Li, Z., Liu, F., Sousa, A.M., Nakagawa, N., Li, M., Dell'Anno, M.T., Gulden, F.O., Pochareddy, S., Tebbenkamp, A.T., Han, W., Pletikos, M., Gao, T., Zhu, Y., Bichsel, C., Varela, L., Szigeti-Buck, K., Lisgo, S., Zhang, Y., Testen, A., Gao, X.B., Mlakar, J., Popovic, M., Flamand, M., Strittmatter, S.M., Kaczmarek, L.K., Anton, E.S., Horvath, T.L., Lindenbach, B.D., and Sestan, N. (2016). Zika Virus Disrupts Phospho-TBK1 Localization and Mitosis in Human Neuroepithelial Stem Cells and Radial Glia. Cell Rep *16*, 2576-2592.

Ozmadenci, D., Feraud, O., Markossian, S., Kress, E., Ducarouge, B., Gibert, B., Ge, J., Durand, I., Gadot, N., Plateroti, M., Bennaceur-Griscelli, A., Scoazec, J.Y., Gil, J., Deng, H., Bernet, A., Mehlen, P., and Lavial, F. (2015). Netrin-1 regulates somatic cell reprogramming and pluripotency maintenance. Nat Commun *6*, 7398.

Panopoulos, A.D., Yanes, O., Ruiz, S., Kida, Y.S., Diep, D., Tautenhahn, R., Herrerias, A., Batchelder, E.M., Plongthongkum, N., Lutz, M., Berggren, W.T., Zhang, K., Evans, R.M., Siuzdak, G., and Izpisua Belmonte, J.C. (2012). The metabolome of induced pluripotent stem cells reveals metabolic changes occurring in somatic cell reprogramming. Cell Res *22*, 168-177.

Parameswaran, P., Sklan, E., Wilkins, C., Burgon, T., Samuel, M.A., Lu, R., Ansel, K.M., Heissmeyer, V., Einav, S., Jackson, W., Doukas, T., Paranjape, S., Polacek, C., dos Santos, F.B., Jalili, R., Babrzadeh, F., Gharizadeh, B., Grimm, D., Kay, M., Koike, S., Sarnow, P., Ronaghi, M., Ding, S.W., Harris, E., Chow, M., Diamond, M.S., Kirkegaard, K., Glenn, J.S., and Fire, A.Z. (2010). Six RNA viruses and forty-one hosts: viral small RNAs and modulation of small RNA repertoires in vertebrate and invertebrate systems. PLoS Pathog *6*, e1000764.

Park, I.H., Arora, N., Huo, H., Maherali, N., Ahfeldt, T., Shimamura, A., Lensch, M.W., Cowan, C., Hochedlinger, K., and Daley, G.Q. (2008a). Disease-specific induced pluripotent stem cells. Cell *134*, 877-886.

Park, I.H., Zhao, R., West, J.A., Yabuuchi, A., Huo, H., Ince, T.A., Lerou, P.H., Lensch, M.W., and Daley, G.Q. (2008b). Reprogramming of human somatic cells to pluripotency with defined factors. Nature *451*, 141-146.

Peerani, R., Rao, B.M., Bauwens, C., Yin, T., Wood, G.A., Nagy, A., Kumacheva, E., and Zandstra, P.W. (2007). Niche-mediated control of human embryonic stem cell self-renewal and differentiation. Embo J *26*, 4744-4755.

Pennica, D., Swanson, T.A., Welsh, J.W., Roy, M.A., Lawrence, D.A., Lee, J., Brush, J., Taneyhill, L.A., Deuel, B., Lew, M., Watanabe, C., Cohen, R.L., Melhem, M.F., Finley, G.G., Quirke, P., Goddard, A.D., Hillan, K.J., Gurney, A.L., Botstein, D., and Levine, A.J. (1998). WISP genes are members of the connective tissue growth factor family that are up-regulated in wnt-1-transformed cells and aberrantly expressed in human colon tumors. Proc Natl Acad Sci U S A *95*, 14717-14722.

Petersen, E., Wilson, M.E., Touch, S., McCloskey, B., Mwaba, P., Bates, M., Dar, O., Mattes, F., Kidd, M., Ippolito, G., Azhar, E.I., and Zumla, A. (2016a). Rapid Spread of Zika Virus in The Americas - Implications for Public Health Preparedness for Mass Gatherings at the 2016 Brazil Olympic Games. Int J Infect Dis *44*, 11-15.

Petersen, L.R., Jamieson, D.J., Powers, A.M., and Honein, M.A. (2016b). Zika Virus. N Engl J Med *374*, 1552-1563.

Pfaff, N., Fiedler, J., Holzmann, A., Schambach, A., Moritz, T., Cantz, T., and Thum, T. (2011). miRNA screening reveals a new miRNA family stimulating iPS cell generation via regulation of Meox2. EMBO Rep *12*, 1153-1159.

Picanco-Castro, V., Russo-Carbolante, E., Reis, L.C., Fraga, A.M., de Magalhaes, D.A., Orellana, M.D., Panepucci, R.A., Pereira, L.V., and Covas, D.T. (2011). Pluripotent reprogramming of fibroblasts by lentiviral mediated insertion of SOX2, C-MYC, and TCL-1A. Stem Cells Dev *20*, 169-180.

Plourde, A.R., and Bloch, E.M. (2016). A Literature Review of Zika Virus. Emerg Infect Dis *22*.

Poliak, S., Morales, D., Croteau, L.P., Krawchuk, D., Palmesino, E., Morton, S., Cloutier, J.F., Charron, F., Dalva, M.B., Ackerman, S.L., Kao, T.J., and Kania, A. (2015). Synergistic integration of Netrin and ephrin axon guidance signals by spinal motor neurons. Elife *4*.

Poliseno, L., Salmena, L., Zhang, J., Carver, B., Haveman, W.J., and Pandolfi, P.P. (2010). A coding-independent function of gene and pseudogene mRNAs regulates tumour biology. Nature *465*, 1033-1038.

Polo, J.M., Anderssen, E., Walsh, R.M., Schwarz, B.A., Nefzger, C.M., Lim, S.M., Borkent, M., Apostolou, E., Alaei, S., Cloutier, J., Bar-Nur, O., Cheloufi, S., Stadtfeld, M., Figueroa, M.E., Robinton, D., Natesan, S., Melnick, A., Zhu, J., Ramaswamy, S., and Hochedlinger, K. (2012). A molecular roadmap of reprogramming somatic cells into iPS cells. Cell *151*, 1617-1632.

Qian, X., Nguyen, H.N., Song, M.M., Hadiono, C., Ogden, S.C., Hammack, C., Yao, B., Hamersky, G.R., Jacob, F., Zhong, C., Yoon, K.J., Jeang, W., Lin, L., Li, Y., Thakor, J., Berg, D.A., Zhang, C., Kang, E., Chickering, M., Nauen, D., Ho, C.Y., Wen, Z., Christian, K.M., Shi, P.Y., Maher, B.J., Wu, H., Jin, P., Tang, H., Song, H., and Ming, G.L. (2016). Brain-Region-Specific Organoids Using Mini-bioreactors for Modeling ZIKV Exposure. Cell *165*, 1238-1254.

Rana, T.M. (2007). Illuminating the silence: understanding the structure and function of small RNAs. Nat Rev Mol Cell Biol *8*, 23-36.

Rossi, S.L., Tesh, R.B., Azar, S.R., Muruato, A.E., Hanley, K.A., Auguste, A.J., Langsjoen, R.M., Paessler, S., Vasilakis, N., and Weaver, S.C. (2016). Characterization of a Novel Murine Model to Study Zika Virus. Am J Trop Med Hyg.

Rouha, H., Thurner, C., and Mandl, C.W. (2010). Functional microRNA generated from a cytoplasmic RNA virus. Nucleic Acids Res *38*, 8328-8337.

Rozario, T., and DeSimone, D.W. (2010). The extracellular matrix in development and morphogenesis: a dynamic view. Dev Biol *341*, 126-140.

Sakaguchi, H., Kadoshima, T., Soen, M., Narii, N., Ishida, Y., Ohgushi, M., Takahashi, J., Eiraku, M., and Sasai, Y. (2015). Generation of functional hippocampal neurons from self-organizing human embryonic stem cell-derived dorsomedial telencephalic tissue. Nat Commun *6*, 8896.

Salmena, L., Poliseno, L., Tay, Y., Kats, L., and Pandolfi, P.P. (2011). A ceRNA hypothesis: the Rosetta Stone of a hidden RNA language? Cell *146*, 353-358.

Salzman, J. (2016). Circular RNA Expression: Its Potential Regulation and Function. Trends Genet *32*, 309-316.

Samavarchi-Tehrani, P., Golipour, A., David, L., Sung, H.K., Beyer, T.A., Datti, A., Woltjen, K., Nagy, A., and Wrana, J.L. (2010). Functional genomics reveals a BMP-driven mesenchymal-to-epithelial transition in the initiation of somatic cell reprogramming. Cell Stem Cell *7*, 64-77.

Sanchez, M., Galy, B., Dandekar, T., Bengert, P., Vainshtein, Y., Stolte, J., Muckenthaler, M.U., and Hentze, M.W. (2006). Iron regulation and the cell cycle: identification of an iron-responsive element in the 3'-untranslated region of human cell division cycle 14A mRNA by a refined microarray-based screening strategy. J Biol Chem *281*, 22865-22874.

Sanes, J.R. (1989). Extracellular matrix molecules that influence neural development. Annu Rev Neurosci *12*, 491-516.

Sarno, M., Sacramento, G.A., Khouri, R., do Rosario, M.S., Costa, F., Archanjo, G., Santos, L.A., Nery, N., Jr., Vasilakis, N., Ko, A.I., and de Almeida, A.R. (2016). Zika Virus Infection and Stillbirths: A Case of Hydrops Fetalis, Hydranencephaly and Fetal Demise. PLoS Negl Trop Dis *10*, e0004517.

Sato, T., Vries, R.G., Snippert, H.J., van de Wetering, M., Barker, N., Stange, D.E., van Es, J.H., Abo, A., Kujala, P., Peters, P.J., and Clevers, H. (2009). Single Lgr5 stem cells build crypt-villus structures in vitro without a mesenchymal niche. Nature *459*, 262-265.

Schonberg, D.L., Miller, T.E., Wu, Q., Flavahan, W.A., Das, N.K., Hale, J.S., Hubert, C.G., Mack, S.C., Jarrar, A.M., Karl, R.T., Rosager, A.M., Nixon, A.M., Tesar, P.J., Hamerlik, P., Kristensen, B.W., Horbinski, C., Connor, J.R., Fox, P.L., Lathia, J.D., and Rich, J.N. (2015). Preferential Iron Trafficking Characterizes Glioblastoma Stem-like Cells. Cancer Cell *28*, 441-455.

Selbach, M., Schwanhausser, B., Thierfelder, N., Fang, Z., Khanin, R., and Rajewsky, N. (2008). Widespread changes in protein synthesis induced by microRNAs. Nature *455*, 58-63.

Shannon, P., Markiel, A., Ozier, O., Baliga, N.S., Wang, J.T., Ramage, D., Amin, N., Schwikowski, B., and Ideker, T. (2003). Cytoscape: a software environment for integrated models of biomolecular interaction networks. Genome Res *13*, 2498-2504.

Sharma, N., Verma, R., Kumawat, K.L., Basu, A., and Singh, S.K. (2015). miR-146a suppresses cellular immune response during Japanese encephalitis virus JaOArS982 strain infection in human microglial cells. J Neuroinflammation *12*, 30.

Shimakami, T., Yamane, D., Jangra, R.K., Kempf, B.J., Spaniel, C., Barton, D.J., and Lemon, S.M. (2012). Stabilization of hepatitis C virus RNA by an Ago2-miR-122 complex. Proc Natl Acad Sci U S A *109*, 941-946.

Shinagawa, T., Takagi, T., Tsukamoto, D., Tomaru, C., Huynh, L.M., Sivaraman, P., Kumarevel, T., Inoue, K., Nakato, R., Katou, Y., Sado, T., Takahashi, S., Ogura, A., Shirahige, K., and Ishii, S. (2014). Histone variants enriched in oocytes enhance reprogramming to induced pluripotent stem cells. Cell Stem Cell *14*, 217-227.

Shiose, S., Chen, Y., Okano, K., Roy, S., Kohno, H., Tang, J., Pearlman, E., Maeda, T., Palczewski, K., and Maeda, A. (2011). Toll-like receptor 3 is required for development of retinopathy caused by impaired all-trans-retinal clearance in mice. J Biol Chem *286*, 15543-15555.

Silva, J., Barrandon, O., Nichols, J., Kawaguchi, J., Theunissen, T.W., and Smith, A. (2008). Promotion of reprogramming to ground state pluripotency by signal inhibition. PLoS Biol *6*, e253.

Silvestroff, L., Franco, P.G., and Pasquini, J.M. (2013). Neural and oligodendrocyte progenitor cells: transferrin effects on cell proliferation. ASN Neuro *5*, e00107.

Simonin, Y., Loustalot, F., Desmetz, C., Foulongne, V., Constant, O., Fournier-Wirth, C., Leon, F., Moles, J.P., Goubaud, A., Lemaitre, J.M., Maquart, M., Leparc-Goffart, I., Briant, L., Nagot, N., Van de Perre, P., and Salinas, S. (2016). Zika Virus Strains Potentially Display Different Infectious Profiles in Human Neural Cells. EBioMedicine *12*, 161-169.

Sips, G.J., Wilschut, J., and Smit, J.M. (2012). Neuroinvasive flavivirus infections. Rev Med Virol *22*, 69-87.

Soufi, A., Donahue, G., and Zaret, K.S. (2012). Facilitators and impediments of the pluripotency reprogramming factors' initial engagement with the genome. Cell *151*, 994-1004.

Souza, B.S., Sampaio, G.L., Pereira, C.S., Campos, G.S., Sardi, S.I., Freitas, L.A., Figueira, C.P., Paredes, B.D., Nonaka, C.K., Azevedo, C.M., Rocha, V.P., Bandeira, A.C., Mendez-Otero, R., Dos Santos, R.R., and Soares, M.B. (2016). Zika virus infection induces mitosis abnormalities and apoptotic cell death of human neural progenitor cells. Sci Rep *6*, 39775.

Sridharan, R., Tchieu, J., Mason, M.J., Yachechko, R., Kuoy, E., Horvath, S., Zhou, Q., and Plath, K. (2009). Role of the murine reprogramming factors in the induction of pluripotency. Cell *136*, 364-377.

Stadtfeld, M., Maherali, N., Breault, D.T., and Hochedlinger, K. (2008). Defining molecular cornerstones during fibroblast to iPS cell reprogramming in mouse. Cell Stem Cell *2*, 230-240.

Stiles, J., and Jernigan, T.L. (2010). The basics of brain development. Neuropsychol Rev *20*, 327-348.

Subramanyam, D., Lamouille, S., Judson, R.L., Liu, J.Y., Bucay, N., Derynck, R., and Blelloch, R. (2011a). Multiple targets of miR-302 and miR-372 promote reprogramming of human fibroblasts to induced pluripotent stem cells. Nat Biotechnol *29*, 443-448.

Subramanyam, D., Lamouille, S., Judson, R.L., Liu, J.Y., Bucay, N., Derynck, R., and Blelloch, R. (2011b). Multiple targets of miR-302 and miR-372 promote reprogramming of human fibroblasts to induced pluripotent stem cells. Nature biotechnology *29*, 443-448.

Sullivan, C.S., and Ganem, D. (2005). MicroRNAs and viral infection. Mol Cell *20*, 3-7.

Taganov, K.D., Boldin, M.P., Chang, K.J., and Baltimore, D. (2006). NF-kappaB-dependent induction of microRNA miR-146, an inhibitor targeted to signaling proteins of innate immune responses. Proc Natl Acad Sci U S A *103*, 12481-12486.

Takahashi, K., Tanabe, K., Ohnuki, M., Narita, M., Ichisaka, T., Tomoda, K., and Yamanaka, S. (2007). Induction of pluripotent stem cells from adult human fibroblasts by defined factors. Cell *131*, 861-872.

Takahashi, K., and Yamanaka, S. (2006). Induction of pluripotent stem cells from mouse embryonic and adult fibroblast cultures by defined factors. Cell *126*, 663-676.

Tang, H., Hammack, C., Ogden, S.C., Wen, Z., Qian, X., Li, Y., Yao, B., Shin, J., Zhang, F., Lee, E.M., Christian, K.M., Didier, R.A., Jin, P., Song, H., and Ming, G.L. (2016). Zika Virus Infects Human Cortical Neural Progenitors and Attenuates Their Growth. Cell Stem Cell *18*, 587-590.

Thomson, D.W., and Dinger, M.E. (2016). Endogenous microRNA sponges: evidence and controversy. Nat Rev Genet *17*, 272-283.

Thomson, J.A., Itskovitz-Eldor, J., Shapiro, S.S., Waknitz, M.A., Swiergiel, J.J., Marshall, V.S., and Jones, J.M. (1998). Embryonic stem cell lines derived from human blastocysts. Science *282*, 1145-1147.

Tiwari, M., Sharma, L.K., Vanegas, D., Callaway, D.A., Bai, Y., Lechleiter, J.D., and Herman, B. (2014). A nonapoptotic role for CASP2/caspase 2: modulation of autophagy. Autophagy *10*, 1054-1070.

Tsai, Y.T., Chang, S.Y., Lee, C.N., and Kao, C.L. (2009). Human TLR3 recognizes dengue virus and modulates viral replication in vitro. Cell Microbiol *11*, 604-615.

Utikal, J., Polo, J.M., Stadtfeld, M., Maherali, N., Kulalert, W., Walsh, R.M., Khalil, A., Rheinwald, J.G., and Hochedlinger, K. (2009). Immortalization eliminates a roadblock during cellular reprogramming into iPS cells. Nature *460*, 1145-1148.

van de Wetering, M., Francies, H.E., Francis, J.M., Bounova, G., Iorio, F., Pronk, A., van Houdt, W., van Gorp, J., Taylor-Weiner, A., Kester, L., McLaren-Douglas, A., Blokker, J., Jaksani, S., Bartfeld, S., Volckman, R., van Sluis, P., Li, V.S., Seepo, S., Sekhar Pedamallu, C., Cibulskis, K., Carter, S.L., McKenna, A., Lawrence, M.S., Lichtenstein, L., Stewart, C., Koster, J., Versteeg, R., van Oudenaarden, A., Saez-Rodriguez, J., Vries, R.G., Getz, G., Wessels, L., Stratton, M.R., McDermott, U., Meyerson, M., Garnett, M.J., and Clevers, H. (2015). Prospective derivation of a living organoid biobank of colorectal cancer patients. Cell *161*, 933-945.

Venkatachalam, K., Venkatesan, B., Valente, A.J., Melby, P.C., Nandish, S., Reusch, J.E., Clark, R.A., and Chandrasekar, B. (2009). WISP1, a pro-mitogenic, pro-survival factor, mediates tumor necrosis factor-alpha (TNF-alpha)-stimulated cardiac fibroblast proliferation but inhibits TNF-alpha-induced cardiomyocyte death. J Biol Chem *284*, 14414-14427.

Venkatesan, B., Prabhu, S.D., Venkatachalam, K., Mummidi, S., Valente, A.J., Clark, R.A., Delafontaine, P., and Chandrasekar, B. (2010). WNT1-inducible signaling pathway protein-1 activates diverse cell survival pathways and blocks doxorubicin-induced cardiomyocyte death. Cell Signal *22*, 809-820.

Ventura, C.V., Maia, M., Ventura, B.V., Linden, V.V., Araujo, E.B., Ramos, R.C., Rocha, M.A., Carvalho, M.D., Belfort, R., Jr., and Ventura, L.O. (2016). Ophthalmological findings in infants with microcephaly and presumable intra-uterus Zika virus infection. Arq Bras Oftalmol *79*, 1-3.

Wang, L., and Liu, H. (2016). microRNA-188 is downregulated in oral squamous cell carcinoma and inhibits proliferation and invasion by targeting SIX1. Tumour Biol *37*, 4105-4113.

Wang, T., Chen, K., Zeng, X., Yang, J., Wu, Y., Shi, X., Qin, B., Zeng, L., Esteban, M.A., Pan, G., and Pei, D. (2011). The histone demethylases Jhdm1a/1b enhance somatic cell reprogramming in a vitamin-C-dependent manner. Cell Stem Cell *9*, 575-587.

Wang, X.H., Aliyari, R., Li, W.X., Li, H.W., Kim, K., Carthew, R., Atkinson, P., and Ding, S.W. (2006). RNA interference directs innate immunity against viruses in adult Drosophila. Science *312*, 452-454.

Wang, Y., Medvid, R., Melton, C., Jaenisch, R., and Blelloch, R. (2007). DGCR8 is essential for microRNA biogenesis and silencing of embryonic stem cell self-renewal. Nat Genet *39*, 380-385.

Warren, L., Manos, P.D., Ahfeldt, T., Loh, Y.H., Li, H., Lau, F., Ebina, W., Mandal, P.K., Smith, Z.D., Meissner, A., Daley, G.Q., Brack, A.S., Collins, J.J., Cowan, C., Schlaeger, T.M., and Rossi, D.J. (2010). Highly efficient reprogramming to pluripotency and directed differentiation of human cells with synthetic modified mRNA. Cell Stem Cell *7*, 618-630.

Watanabe, K., Kamiya, D., Nishiyama, A., Katayama, T., Nozaki, S., Kawasaki, H., Watanabe, Y., Mizuseki, K., and Sasai, Y. (2005). Directed differentiation of telencephalic precursors from embryonic stem cells. Nat Neurosci *8*, 288-296.

Wernig, M., Meissner, A., Foreman, R., Brambrink, T., Ku, M., Hochedlinger, K., Bernstein, B.E., and Jaenisch, R. (2007). In vitro reprogramming of fibroblasts into a pluripotent ES-cell-like state. Nature *448*, 318-324.

Wu, J., Lv, Q., He, J., Zhang, H., Mei, X., Cui, K., Huang, N., Xie, W., Xu, N., and Zhang, Y. (2014). MicroRNA-188 suppresses G1/S transition by targeting multiple cyclin/CDK complexes. Cell Commun Signal *12*, 66.

Wu, S., He, L., Li, Y., Wang, T., Feng, L., Jiang, L., Zhang, P., and Huang, X. (2013). miR-146a facilitates replication of dengue virus by dampening interferon induction by targeting TRAF6. J Infect *67*, 329-341.

Wu, Y.E., Parikshak, N.N., Belgard, T.G., and Geschwind, D.H. (2016). Genome-wide, integrative analysis implicates microRNA dysregulation in autism spectrum disorder. Nat Neurosci *19*, 1463-1476.

Xu, L., Corcoran, R.B., Welsh, J.W., Pennica, D., and Levine, A.J. (2000). WISP-1 is a Wnt-1- and beta-catenin-responsive oncogene. Genes Dev *14*, 585-595.

Yaddanapudi, K., De Miranda, J., Hornig, M., and Lipkin, W.I. (2011). Toll-like receptor 3 regulates neural stem cell proliferation by modulating the Sonic Hedgehog pathway. PLoS One *6*, e26766.

Yamanaka, S. (2012). Induced pluripotent stem cells: past, present, and future. Cell Stem Cell *10*, 678-684.

Yang, C.-S., and Rana, T.M. (2013). Learning the molecular mechanisms of the reprogramming factors: let's start from microRNAs. Molecular bioSystems *9*, 10-17.

Yang, C.S., Li, Z., and Rana, T.M. (2011a). microRNAs modulate iPS cell generation. Rna *17*, 1451-1460.

Yang, C.S., Lopez, C.G., and Rana, T.M. (2011b). Discovery of nonsteroidal anti-inflammatory drug and anticancer drug enhancing reprogramming and induced pluripotent stem cell generation. Stem cells *29*, 1528-1536.

Ying, Q.L., Stavridis, M., Griffiths, D., Li, M., and Smith, A. (2003). Conversion of embryonic stem cells into neuroectodermal precursors in adherent monoculture. Nat Biotechnol *21*, 183-186.

Ying, Q.L., Wray, J., Nichols, J., Batlle-Morera, L., Doble, B., Woodgett, J., Cohen, P., and Smith, A. (2008). The ground state of embryonic stem cell self-renewal. Nature *453*, 519-523.

Yoon, I.K., Kim, H.K., Kim, Y.K., Song, I.H., Kim, W., Kim, S., Baek, S.H., Kim, J.H., and Kim, J.R. (2004). Exploration of replicative senescence-associated genes in human dermal fibroblasts by cDNA microarray technology. Exp Gerontol *39*, 1369-1378.

Yu, J., Vodyanik, M.A., Smuga-Otto, K., Antosiewicz-Bourget, J., Frane, J.L., Tian, S., Nie, J., Jonsdottir, G.A., Ruotti, V., Stewart, R., Slukvin, II, and Thomson, J.A. (2007). Induced pluripotent stem cell lines derived from human somatic cells. Science *318*, 1917-1920.

Zecevic, N., Chen, Y., and Filipovic, R. (2005). Contributions of cortical subventricular zone to the development of the human cerebral cortex. J Comp Neurol *491*, 109-122.

Zhang, S.C., Wernig, M., Duncan, I.D., Brustle, O., and Thomson, J.A. (2001). In vitro differentiation of transplantable neural precursors from human embryonic stem cells. Nat Biotechnol *19*, 1129-1133.

Zhang, Y., Wen, G., Shao, G., Wang, C., Lin, C., Fang, H., Balajee, A.S., Bhagat, G., Hei, T.K., and Zhao, Y. (2009). TGFBI deficiency predisposes mice to spontaneous tumor development. Cancer Res *69*, 37-44.

Zhao, H., Fernandez, E., Dowd, K.A., Speer, S.D., Platt, D.J., Gorman, M.J., Govero, J., Nelson, C.A., Pierson, T.C., Diamond, M.S., and Fremont, D.H. (2016). Structural Basis of Zika Virus-Specific Antibody Protection. Cell *166*, 1016-1027.

Zhu, S., Wei, W., and Ding, S. (2011). Chemical strategies for stem cell biology and regenerative medicine. Annu Rev Biomed Eng *13*, 73-90.